

Washington University in St. Louis

Washington University Open Scholarship

Arts & Sciences Electronic Theses and
Dissertations

Arts & Sciences

Winter 12-15-2022

Fructose Promotes the Growth of Tumors through Metabolite Exchange with Non-malignant Tissues

Ronald Joseph Fowle-Grider
Washington University in St. Louis

Follow this and additional works at: https://openscholarship.wustl.edu/art_sci_etds



Part of the [Biochemistry Commons](#)

Recommended Citation

Fowle-Grider, Ronald Joseph, "Fructose Promotes the Growth of Tumors through Metabolite Exchange with Non-malignant Tissues" (2022). *Arts & Sciences Electronic Theses and Dissertations*. 2772.
https://openscholarship.wustl.edu/art_sci_etds/2772

This Dissertation is brought to you for free and open access by the Arts & Sciences at Washington University Open Scholarship. It has been accepted for inclusion in Arts & Sciences Electronic Theses and Dissertations by an authorized administrator of Washington University Open Scholarship. For more information, please contact digital@wumail.wustl.edu.

WASHINGTON UNIVERSITY IN ST. LOUIS

Division of Biology and Biomedical Sciences
Biochemistry, Biophysics, and Structure Biology

Dissertation Examination Committee:

Gary Patti, Chair
Brian Finck, Co-Chair
Milan Chheda
Richard Gross
Natalie Niemi

Fructose Promotes the Growth of Tumors through Metabolite Exchange with Non-malignant
Tissues

by
Ronald Joseph Fowle-Grider

A dissertation presented to
The Graduate School
of Washington University in
partial fulfillment of the
requirements for the degree
of Doctor of Philosophy

August 2022

St. Louis, Missouri

© Ronald Joseph Fowle-Grider

Table of Contents

List of Figures	iv
Acknowledgements	vi
Abstract of the dissertation	x
Chapter 1: Introduction	1
1.1.1 Overview of cancer metabolism as a discipline	1
1.1.2 Glucose metabolism in cancer cells.....	3
1.1.3 Fructose metabolism in cancer cells	7
1.2 Metabolomics	10
1.2.1 Overview	10
1.2.2 Liquid-chromatography/mass spectrometry	11
1.2.2 Stable Isotope Tracing	12
2.1 Introduction	15
Elevated consumption of dietary fructose promotes tumor growth	15
2.3 Discussion	16
Figures	18
Chapter 3: Fructose does not directly support cancer cell metabolism <i>in vitro</i>	20
3.1 Introduction	20
3.2 Results	21
Fructose does not directly support the growth of cancer cells <i>in vitro</i>	21
Ketoheokinase does not support fructolysis in transformed cell lines	23
Administration of clinical candidate PF-06835919 does not alter cell growth <i>in vitro</i>	24
Translation to human cervical cancer patients	25
Hepatocytes transfer fructose-derived nutrients to CaSki cells to promote their growth.....	26
3.3 Discussion	27
Figures	29
Extended Data Figures	33
Chapter 4: Organismal metabolism of fructose drives tumor growth.....	49

4.1 Introduction	49
4.2 Results	51
Fructose requires organismal metabolism to promote the growth of mouse cervical xenografts	51
Administration of clinical candidate PF-06835919 impairs fructose-mediated growth.....	52
Fructose requires organismal metabolism to promote the growth of melanoma tumors in zebrafish.....	53
4.3 Discussion	55
Figures.....	57
Extended Data Figures	58
Chapter 5: Conclusions	65
Chapter 6: Future directions for completed work	68
Colon cancer metastases express KHK-C.....	68
The role of fructose metabolism in intrahepatic tumors	70
Figures.....	73
Chapter 7: Materials and Methods	76
Mouse xenograft model.....	76
Zebrafish.....	77
Preparation of mouse and zebrafish serum	79
Cell culture	80
Metabolite extraction.....	81
Western blots.....	82
Silencing of sorbitol dehydrogenase	82
LC/MS.....	83
Analysis of human cervical cancer patient data	84
Statistics	84
References:.....	85

List of Figures

Figure 1.1: Metabolic priorities in quiescent and proliferating cells	1
Figure 1.2: Schematic of how biomass can be produced from glycolysis and the pentose phosphate pathway	5
Figure 1.3: Schematic of possible routes of fructose metabolism	8
Figure 1.4: Hypothetical isotopologue distribution of lactate	14
Figure 2.1: Dietary fructose supports tumor growth <i>in vivo</i>	18
Figure 2.2: Fructose does not induce insulin resistance in nude mice	19
Figure 3.1: Exogenous and endogenous fructose do not directly support growth	29
Figure 3.2: Hexokinase, not ketohexokinase, metabolizes fructose	30
Figure 3.3: Human cervical tumors exclusively express KHK-A, which is not linked to survival, recurrence, or tumor stage	31
Figure 3.4: Hepatocytes transform fructose into useable carbons for growth	32
Extended figure 3.1: CaSki cells do not efficiently metabolize fructose	33
Extended figure 3.2: Various transformed and proliferating cell lines do not efficiently metabolize fructose	34
Extended figure 3.3: Fructose does not support growth as well as glucose	35
Extended figure 3.4: Transformed and proliferative cell lines can take up fructose	36
Extended figure 3.5: Addition of fructose to glucose-containing media does not enhance growth	37
Extended figure 3.6: Fructose does not change the metabolic fate of glucose	38
Extended figure 3.7: Transformed and proliferative cell lines produce fructose from glucose	39
Extended Figure 3.8: Sorbitol dehydrogenase expression is silenced by siRNA	40
Extended Figure 3.9: Endogenous fructose has no impact on proliferation	41
Extended Figure 3.10: Fructose 1-phosphate is resolved from other hexose phosphates	42
Extended figure 3.11: Transformed and proliferative cell lines produce fructose 1-phosphate	43
Extended figure 3.12: The <i>KHK</i> gene is expressed in common human tissues	44
Extended figure 3.13: No tested cell lines express aldolase B	45

Extended figure 3.14: Proliferating 3T3-L1 cells decrease expression of KHK relative to quiescent state	46
Extended figure 3.15: Characterization of PF-06835919	47
Extended figure 3.16: KHK-A is not important for growth of CaSki or Huh7 cells	48
Figure 4.1: Organismal metabolism of fructose drives tumor growth.....	57
Extended figure 4.1: Fructose is not in metabolized by CaSki tumors directly but is readily metabolized by the organism	58
Extended figure 4.2: Single 50 mg/kg dose of PF-06835919 remains in mouse serum for over 24 hours.....	59
Extended figure 4.3: BRAF/p53 melanoma regrows faster in the presence of fructose.....	60
Extended figure 4.4: <i>BRAF/p53</i> melanoma plated <i>ex vivo</i> do not efficiently metabolize Fructose.....	61
Extended figure 4.5: <i>Ex vivo BRAF/p53</i> zebrafish melanomas produce endogenous fructose and fructose 1-phosphate	62
Extended figure 4.6: Fructose carbons enter <i>BRAF/p53</i> zebrafish melanoma via metabolite exchange	63
Extended figure 4.7: <i>BRAF/p53</i> Zebrafish metabolize fructose via KHK and aldolase B.....	64
Figure 6.1: Human colon cancers that metastasize to the liver express KHK-C.....	73
Figure 6.2: KHK-C rewires glucose metabolism via endogenous fructose.....	74
Figure 6.3: Schematic showing contribution of fructose and fructose-derived acetate to <i>de novo</i> lipogenesis in a hepatocyte.....	75

Acknowledgements

First and foremost, I would like to thank my parents, Jay and Andrea Grider, for their unwavering and unconditional love and support throughout my lifetime. You've never forced me down a pre-determined path in any sense and allowed me to explore my own peculiar interests in areas such as birdwatching and ecology as a child. Furthermore, your approach to homeschooling greatly fostered my curiosity and desire for understanding the world, which are the fundamentals of being a scientist. You encouraged me to not ignore my imagination and always to question the status quo. You also stressed the importance of ambition and hard work. I would not be who I am today without you. Thank you.

I would like to thank my mentor, Gary Patti, for the opportunity to obtain a PhD from his laboratory. I still remember the first day we met at the medical school when I showed you the library book I had checked out: "Cancer as a Metabolic Disease." You made a trip over to the med campus to meet and suffered through my ridiculous musings and hypotheses about cancer metabolism. You invested in me, nevertheless, and continued to always listen to my ideas over the years, no matter how ridiculous or absurd. I am truly grateful for that. You continued to have faith in me, even after my first project failed, and you allowed me to learn lessons from my own mistakes instead of micromanaging me toward a more productive goal. Any ability I've developed to communicate science clearly to any audience, I completely owe to you as well. Thank you. My time working in your lab has been some of the best years of my life so far. It's truly being a fun and enlightening experience. Thank you for providing it.

To my girlfriend, Meredith Stoner, I owe a big debt of gratitude. You have been incredibly understanding in dating a mad scientist with a crazy and unpredictable schedule. I realize how challenging it has been to achieve work-life balance these last few years, and I appreciate your patience in allowing me to pursue my passions. Furthermore, thank you for taking the initiative to help me manage responsibilities outside of the lab that I didn't always have the bandwidth for. You have gone above and beyond in every possible way, and your support and understanding is remarkable. Also, thanks to Porkchop for always being a constant source of warmth and comfort.

Thank you to Jonathan Spalding, for being one of the rare people sharing my obsession for science and understanding the world. Your zeal for science is contagious. I am honored that we could grow together as scientists and as individuals and that I can claim your acquaintance once you win the Nobel Prize. I have appreciated your out-of-the-box insights and iconoclastic opinions both in and out of the lab. You have definitely influenced my professional and personal development in a positive way. Also, thank you for your participation in a plethora of memorable experiences over our years of graduate school. Many of these memories will undoubtedly last a lifetime.

Thank you to Fuad Naser for being a constant source of support, understanding, and commiseration, both professionally and beyond. Thank you for your assistance with certain experiments and for helping me to navigate the complexities of intellectual property and patents. It's been great to discuss ideas about our lab projects, biotech, and life over the years. I am so impressed by how much you have developed professionally and personally and by all that you have accomplished. I am also grateful to commemorate the many experiences we had together outside the lab as well. You are an inspiration, and I glad to have gained you as a colleague and friend.

Thank you to Joe Rowles III for entering my life in the final hour of my PhD and helping me with experiments when I needed it most. I am so grateful for your bottomless patience, steadfastness, and readiness to assist. You are such a talented individual and scientist. I look forward to working more with you in the near future and beyond.

Thank you to the various technicians who have aided me over the years, including Sarah Chiang, Isabel Shen, and Alden Dunham. Your helping hands made a tremendous difference in my PhD. I am also honored to have had a hand in your professional development as well. Thank you. Isabel and Alden, thank you also for your endless entertainment and comic relief. Your ability to boost morale was unprecedented.

Thank you to all the rest of my labmates for their support, guidance, and assistance over the years. A special thanks to Conghui Yao and Yahui Wang. Many of you I claim as both my friends and my colleagues

Thank you to my thesis committee members, Brian Finck, Milan Chheda, Richard Gross, and Natalie Neimi for sticking by me over the years. I apologize profusely for how terrible my early presentations were. Thank you for not giving up on me.

Ronald Joseph Fowle-Grider

Washington University School of Medicine

August 2022

Dedicated to my mother, Andrea Grider, whose amazing sacrifices and investment in me enabled
this accomplishment

ABSTRACT OF THE DISSERTATION

Fructose Promotes the Growth of Tumors through Metabolite Exchange with Non-malignant
Tissues

by

Ronald Joseph Fowle Grider

Doctor of Philosophy in Biology and Biomedical Sciences

Biochemistry, Biophysics and Structural Biology

Washington University in St. Louis, 2021

Professor Gary Patti, Chair

The amount of dietary fructose consumed in the United States has increased considerably over the past five decades, largely due to the widespread use of high fructose corn syrup as a sweetener. The potential link between this elevated fructose intake and the development of cancer remains incompletely understood. Here we show that, even though cervical cancer cells themselves cannot directly utilize fructose carbon, diets high in fructose enhance the growth of cervical tumors by nearly threefold in mice. We demonstrate that efficient utilization of fructose carbon requires ketohexokinase-C, which was not expressed in ~100 cervical tumors that we examined from human patients or any transformed cancer cell line that we studied *in vitro*. In contrast, primary hepatocytes did express ketohexokinase-C. In a co-culture system, primary hepatocytes fed cervical cancer cells fructose-derived nutrients that drove proliferation of cancer cells through metabolite exchange. Similarly, in mice bearing cervical tumors, metabolism of fructose in ketohexokinase-C-expressing tissues enhanced tumor growth through a cell non-autonomous mechanism. We demonstrate that PF-06835919, a drug in clinical trials to inhibit ketohexokinase-C in non-alcoholic fatty liver disease, had no direct effects on cervical cancer

cells themselves. Yet, when given to mice with cervical cancer, it was sufficient to prevent diets high in fructose from promoting tumor growth by inhibiting ketohexokinase-C in non-malignant tissue. These findings suggest that PF-06835919 has anti-tumor activity and demonstrate a therapeutic paradigm where non-malignant, distal organs may be targeted as a treatment for cancer.

Chapter 1: Introduction

1.1 Cancer Metabolism

1.1.1 Overview of cancer metabolism as a discipline

Metabolism supports every cellular process in both cancerous and noncancerous cells: Cellular mobility, gene transcription, protein synthesis, ROS generation, ROS neutralization, protein trafficking, endocytosis, and exocytosis are just a few of the examples of cellular functionality that metabolism makes possible. Far from being an intransigent cellular property, however, metabolism is highly mutable, altering itself to support the demands of the cell. Thus, cells in different physiological states often have different metabolic states as well. For example, action potential-generating neurons have a different metabolic program from nutrient-absorbing enterocytes in the small intestine. A given cell type can alter its metabolism in accordance with a new functional state as well: For instance, endometrial and ovarian cells at different stages of the menstrual cycle alter their nutrient fate and turnover rate as they respond to changing levels of hormones¹⁻³

Given the importance of metabolism for supporting and enabling various functionalities of cells, one would expect that cells in a transformed, cancerous state would exhibit a different metabolic program from cells in a quiescent, somatic state. Indeed this is observed, and the field of cancer metabolism is based on this principle.

The current perspective of tumorigenesis and tumor development is that cancer is ultimately a genetic disease driven by activation of oncogenes and inactivation of tumor suppressors^{4,5}. Accordingly, cancer researchers have put forth a monumental effort over the last several decades to delineate all the genetic drivers of various tumors^{6,7}. Conversely, the study of cancer's

metabolic alterations has received considerably less attention, until more recently. These renewed investigations into tumor metabolism have revealed that oncogenic mutations and metabolism are often intimately linked: anabolic metabolism is the fundamental workhorse of genetic drivers that allows for a malignant growth phenotype. For example, several studies have revealed that activating mutations in oncogenes such as Ras, Braf, and myc result in distinctive metabolic phenotypes as compared to wildtype cells⁸⁻¹¹. Thus, by understanding the metabolic responses connected to oncogenic transformation, we can better understand how these drivers bring about cell growth.

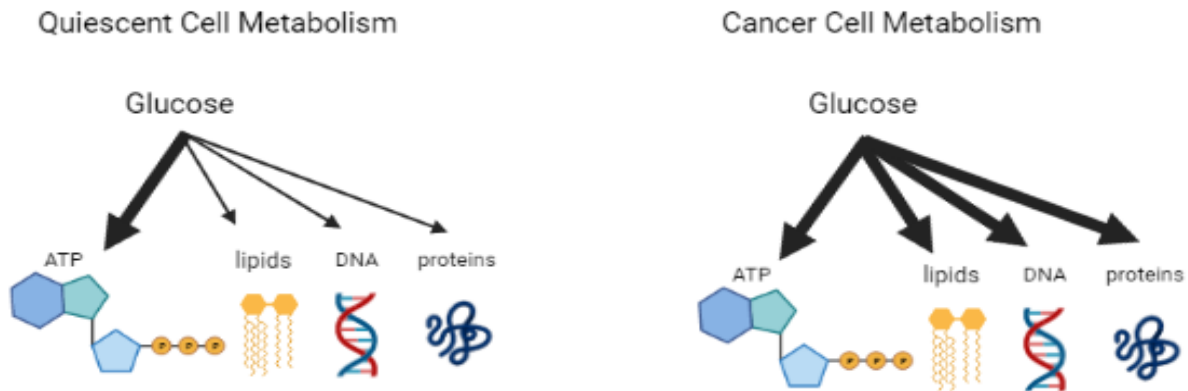


Figure 2.1 Metabolic priorities in quiescent and proliferating cells. Created with BioRender.com

So what is the metabolic phenotype of cancerous growth? To understand this, we first have to understand that the programming of cancer cells is replication. In order to replicate, a cancer cell must make copies of all of its constituent materials to produce a new cell. In other words, a cancer cell must reproduce all of its biomass, including its lipids, DNA, and proteins. Therefore, metabolism in cancer cells is programmed by oncogenes and altered tumor suppressor signaling pathways to produce biomass. This is a different metabolic goal than most non-transformed,

quiescent cells. In these cells, most of the metabolic resources are directed towards energy generation in the form of ATP and less towards biomass production. (figure 1.1). Therefore, once a cell becomes transformed and cancerous, it undergoes a metabolic rewiring from an energy-centric metabolism to a biomass-centric metabolism. Reproduction of biomass is a phenotype conserved in every type of cancer. Thus, while different cancer genotypes and tissues of origin can confer differences in metabolic fate and metabolic rate, there are many aspects of metabolism that are conserved among a diversity of malignancies. A prime example of such conservation is the dramatically enhanced rate of glucose utilization by the tumor relative to the somatic quiescent cell of origin from which it was derived¹²⁻¹⁴.

1.1.2 Glucose metabolism in cancer cells

Glucose is the most abundant nutrient in the human circulation. To capitalize on this nutrient, cancer cells alter their glucose metabolism substantially upon transformation. This is evidenced by the pervasive use of fluorodeoxyglucose (FDG) positron emission tomography (PET) to image a wide variety of tumors^{15,16}. In this technique, a radioactive analog of glucose (FDG) is administered to cancer patients. This analog of glucose cannot be metabolized but can be uptaken by glucose transporters. Imaging of the patients after FGG administration reveals a strong signal from the FDG concentrated within the tumor relative to the surrounding normal tissues. In this way, the size and extent of the tumors in a patient can be assessed. FDG accumulates in tumors to such an extent, because tumors greatly increase their glucose utilization relative to somatic tissues^{14,17}. This increase in utilization is due to increased tumor expression of glucose transporters as well as a profound increase in glucose turnover¹⁴. Several metabolic pathways drive this enhancement in tumor glucose utilization, including glycolysis, the pentose phosphate pathway, and the TCA cycle¹⁸.

Carbon flux through glycolysis is greatly increased in many cancers^{19,20}. In most somatic cells, glycolysis is fueled almost exclusively by glucose. Glucose is phosphorylated by hexokinase, which prevents it from leaving the cell and diffusing back into the extracellular environment. Glucose 6-phosphate then undergoes a series of catabolic reactions to produce a final 3-carbon product of one of two forms: pyruvate or lactate. The long-held view is that lactate is thought to be an inert “metabolic waste product” that is excreted from the cell; whereas, pyruvate can enter the mitochondria to be oxidized by the TCA cycle.

A cell’s choice to create either lactate or pyruvate from a glucose molecule has important implications for how much energy can be harvested from that molecule. If the cell makes lactate, only a net production of 2 ATP’s is obtained from glucose. If a cell makes pyruvate, then that pyruvate can be oxidized in the TCA cycle to produce a total of over 30 ATP. Most somatic cell types have the metabolic goal of producing as much energy as possible. Indeed, humans produce their body weight in ATP per day²¹. Therefore, it would seem prudent for a cell to send glucose carbons into the TCA cycle to extract maximal ATP for energy.

However, oxidation of glucose comes with a prerequisite: the availability of oxygen. Under hypoxic or anaerobic conditions, TCA cycle activity decrease significantly. For example, in a muscle that is undergoing heavy exertion, oxygen demand increases dramatically. This increased demand outpaces oxygen supply, and the tissue enters an anaerobic state. This anaerobic state results in most of the glucose carbons being fermented to lactic acid, thus precluding entry into the TCA cycle. Thus, the canonical picture of sugar metabolism is that cells prefer to send most of their glycolytic carbons into the TCA cycle in the presence of oxygen and to lactic acid as a necessary evil in oxygen-deprived conditions.

competitive advantage over the surrounding stroma cell in the tumor microenvironment¹⁸.

Another more recently proposed model is that biomass production creates an increased reliance on NAD⁺ regeneration over ATP synthesis²⁶. In this model, production of lactate helps a biomass-centric cell maintain adequate NAD⁺ levels, because the generation of lactate is accompanied by production of NAD⁺.

Regardless of the driving force for the Warburg Effect, it is accompanied by a profound increase in flux through glycolysis^{19,20}. Many biosynthetic reactions for important components of the cancer cell's biomass are fed from glycolysis (see figure 1.2). These include the hexosamine pathway for membrane glycosylation, the production of glycerol for the head groups of membrane phospholipids, the production of serine and glycine for participation in one-carbon metabolism for production of DNA precursors²⁷⁻²⁹ (see figure 1.2). Thus, glycolysis is one of the main drivers for increased glucose utilization and consumption in cancer. This increased glycolytic flux helps to fuel the growing cell with biomass precursors.

There are other pathways that glucose uses to provide biosynthetic precursors as well. The pentose phosphate pathway provides the cell with *de novo* synthesis of the ribose ring for the production of nucleotides. Furthermore, the oxidative arm of the pentose phosphate pathway is the largest source of NADPH in the cell³⁰. This NADPH is essential for oxidative stress neutralization and a necessary cofactor for fatty acid synthesis and 1-carbon metabolism aiding in the synthesis of nucleotides. Carbons from glucose that enter the TCA cycle also feed a variety of biosynthetic pathways. *De novo* lipogenesis, which begins with mitochondrial citrate, is a very important anabolic pathway for cancer cells. This pathway is a major contributor to the production of fatty acids for membrane phospholipid biosynthesis.

All in all, glucose utilization is greatly increased in a proliferative cancer cell, and this property is exploited by FDG-PET imaging. Increased glucose utilization is mostly a result of increased glycolytic flux and Warburg metabolism. Other pathways anabolic for biomass draw on glucose as well, including the pentose phosphate pathway and certain pathways fed by the TCA cycle. These pathways supply both direct carbons from glucose as well as cofactors such as NADPH for the construction of new cellular components.

1.1.3 Fructose metabolism in cancer cells

Glucose is the primary sugar that is maintained in the circulation to fuel the cells of the body. But glucose is not the only sugar that the human body is exposed to. Fructose is a dietary sugar that most Americans consume in significant quantities every day and is the second most abundant dietary sugar found in humans³¹. The amount of dietary fructose consumed in the United States has increased considerably over the past five decades, largely due to the widespread use of sucrose and high fructose corn syrup as a sweetener³²⁻³⁴. In 2008, fructose consumption in the United States accounted for over 10% of daily caloric intake in adults with over a quarter of adolescents consuming over 15% of their daily calories from fructose³⁵. The potential link between this elevated fructose intake and metabolic disorders such as obesity, insulin resistance, hyperlipidemia, and non-alcoholic fatty liver disease has been the subject of intense investigation³⁶⁻³⁹. The potential effect of high fructose consumption on the development of cancer, on the other hand, has received much less attention.

Fructose can be metabolized by two different routes by cells. The primary way fructose is thought to be metabolized is via ketohexokinase. Ketohexokinase can phosphorylate fructose to produce fructose 1-phosphate. This fructose 1-phosphate can then be metabolized by aldolase B to produce trioses, which can then enter glycolysis, glycerol synthesis, or the pentose phosphate

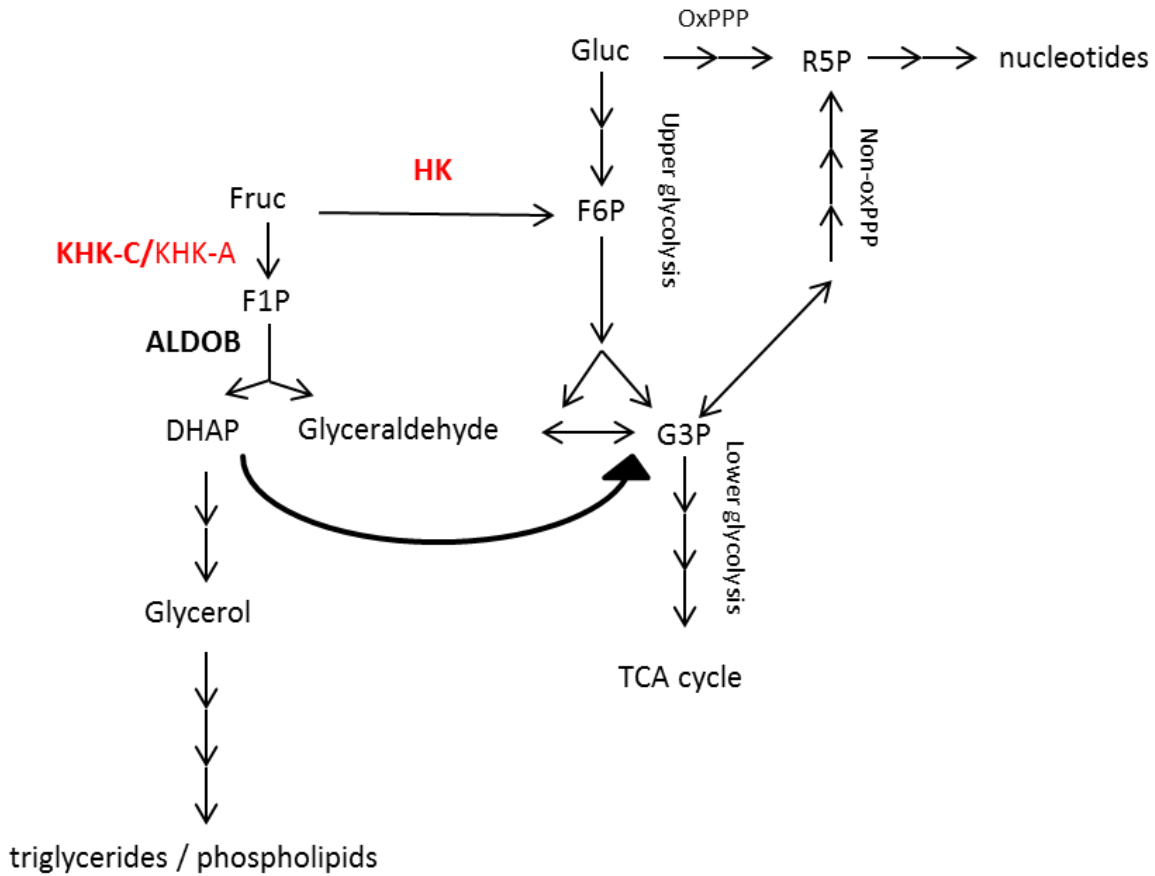


Figure 1.3 Schematic of possible routes of fructose metabolism. gluc, glucose; F6P, fructose 6-phosphate; HK, hexokinase; Fruc, fructose; KHK-C, ketohexokinase-C; KHK-A, ketohexokinase-A; F1P, fructose 1-phosphate; ALDOB, aldolase B; DHAP, dihydroxyacetone phosphate; G3P, glyceraldehyde 3-phosphate; R5P, ribose 5-phosphate; OxPPP, oxidative pentose phosphate pathway; Non-oxPPP, non oxidative pentose phosphate pathway

pathway (see figure 1.3). There are two functional isoforms of ketohexokinase: KHK-A and KHK-C. KHK-C is expressed only in the liver, small intestine, and kidney. It is the isoform that robustly metabolizes fructose, producing very high levels of fructose 1-phosphate in a short period of time^{40,41}. In contrast, KHK-A does not metabolize fructose well, having a much higher K_m for fructose than KHK-C. KHK-A is more ubiquitously expressed in various tissue types and is thought to have other primary substrates besides fructose⁴²⁻⁴⁴. Aldolase B, like KHK-C, is also only expressed in the liver, kidney, and small intestine. Thus, due to the presence of fructolytic enzymes in these organs, they are thought to be the primary sites of fructose metabolism. The second route that fructose enters central carbon metabolism is via hexokinase. Hexokinase

directly phosphorylates fructose to produce fructose 6-phosphate, which can enter glycolysis or the pentose phosphate pathway (see figure 1.3). Hexokinase is ubiquitously expressed in most cell types. Consequently, most cell types are thought to possess a hexokinase-dependent capability for fructose metabolism. However, this pathway is generally thought to be less productive for fructose turnover due to competition from glucose, which is the primary substrate for hexokinase⁴⁰.

To understand how cancer cells might productively use fructose to fuel their growth and proliferative programs, we would need to understand cancer cells capacity to metabolize fructose via either hexokinase or ketohexokinase. Several studies have reported that fructose is metabolized via ketohexokinase in certain cancers, primarily colon cancer. In one genetic model of intestinal cancer in which the adenomatous polyposis coli (APC) gene was deleted in intestinal stem cells, fructose stimulated tumor growth in a cell autonomous fashion⁴⁵. This growth stimulation was due to these tumors expressing ketohexokinase and aldolase B, allowing for intracellular fructolysis⁴⁶. However, most of the tumors studied in this model arose in the small intestine as opposed to the colon⁴⁶. Unlike the colon, the small intestine expresses high levels of ketohexokinase and aldolase b. Therefore, it is questionable how relevant these results might be to colon cancer. It has also been reported that colon cancer liver metastases increase their expression of aldolase b upon metastasizing to the liver, supporting the direct use of fructose carbons to support their growth in the liver environment⁴⁷. In hepatocellular carcinoma, it was shown that tumors predominantly expressed KHK-A unlike the liver tissue which expresses high levels of KHK-C⁴⁴. This isoform switch as a result of carcinogenesis of the liver tissue was associated with decreased fructose metabolism⁴⁴. Conversion to KHK-A in tumors

was shown to promote nucleotide biosynthesis via activation of phosphoribosyl pyrophosphate synthetase 1⁴⁴.

Several other studies have implicated fructose in supporting growth via direct utilization of fructose in certain cancer cell types. Fructose has been reported to increase the synthesis of nucleotides in pancreatic cancer cell lines⁴⁸. However, the metabolic mechanism for this phenotype was not determined. In acute myeloid leukemia, administration of fructose resulted in an increased NAD⁺/NADH ratio, which promoted carbon flux to serine biosynthesis⁴⁹. Yet, the metabolic mechanism leading to this observation was not determined. In several lung cancer cell lines, knockout of glut5, a transporter that can allow for fructose transport was associated with decreased growth *in vitro* and *in vivo*⁵⁰. In these studies, determination of how fructose gave rise to the observed metabolic phenotype was not determined.

Literature on tumor fructose metabolism and effect on tumor growth is quite sparse, especially in comparison to the vast quantity of literature that exists for glucose metabolism in cancer cells. Thus, there are many tumor types in which the effects of fructose metabolism are not known. It is possible that there is conservation in fructose metabolism among various cancer types. Or the response could be varied depending on the tissue of origin. Thus, given the how ubiquitous fructose is in the western diet, there is a need to understand how fructose might contribute to tumor growth.

1.2 Metabolomics

1.2.1 Overview

Genomics is the study of the genome. Proteomics is the study of the proteome. Metabolomics is the study of the metabolome. The metabolome is the comprehensive set of metabolites in a

biological sample. Note that the term “metabolites” is often defined in the field to include all the small molecules in the sample, not just those that have been transformed by metabolic processes. Thus, metabolomics is the comprehensive evaluation of small molecules in a sample. By “small molecules” we generally mean molecules less than 1,500 daltons. Metabolomics approaches can be either targeted or untargeted. In a targeted approach, we are intentional in the metabolites and pathways that we wish to study from a metabolomics dataset. This approach is often hypothesis-driven. In an untargeted approach, we assess all the metabolites in a sample in an unbiased manner. This approach is often hypothesis-generating. For either approach, sophisticated analytical instrumentation is needed to generate the data. The most common setup used is liquid-chromatography/mass spectrometry (LC/MS).

1.2.2 Liquid-chromatography/mass spectrometry

Frequently in a metabolomics experiment we want to assess the relative levels of a metabolite under one or more experimental conditions (i.e. wild type vs knockout). To do this, we need to 1) separate the mixture of metabolites into individual metabolites and then 2) determine the amount of each metabolite that was resolved. Liquid chromatography/mass spectrometry is the most common method to accomplish both of these aims. Liquid chromatography allows us to resolve metabolites from a biological mixture, and mass spectrometry allows us to quantify those metabolites.

Liquid chromatography separates a mixture of metabolites by chemical separation on column chromatography. The stationary phase is the solid part of the column. The mobile phase is the solvent that runs over it. Different combinations of stationary and mobile phases allow for separation of different polarities of compounds. Hydrophilic interaction chromatography (HILIC) allows for separation of polar metabolites such as sugars and amino acids. Reverse

phase chromatography allows for separate of nonpolar metabolites such as lipids. Thus, comprehensive analysis of the entire metabolome by LC/MS often requires at least two different columns.

Once metabolites are resolved, they enter the mass spectrometer where their exact mass is measured. The time at which each metabolite leaves the column and enters the mass spectrometer is characteristic to that metabolite and is known as the retention time. The putative identity of a given metabolite can be determined from a combination of its exact mass and its retention time. The intensity of the mass spectrometry signal for a given metabolite can also be determined. This signal intensity is proportional to the amount of that metabolite present. The total amount of metabolite that is measured in a sample is called the pooled size. Thus, in a conventional metabolomics experiment, the relative differences in pools sizes under various experimental conditions can be assessed. In this way, metabolic information about the experimental systems under study can be obtained by assessing the accumulation and depletion of various metabolite pools.

1.2.2 Stable Isotope Tracing

As a result of metabolism, the carbons of a given nutrient are often disseminated to dozens if not hundreds or thousands of downstream metabolites. Often we wish to understand the fate of one or several nutrients under one or more experimental conditions. Metabolomics allows us to assess all the metabolites that a given nutrient might give rise to. In order to track the carbons coming from a nutrient, we isotopically label the carbons in that nutrient, most commonly replacing them with carbon-13 (^{13}C). Most of the carbon (over 98.9%) on earth is carbon-12 (^{12}C). ^{13}C is approximately one mass unit heavier than ^{12}C due to an extra neutron. ^{13}C makes up less than 1.1% of carbon. Thus, a vast majority of the carbons in biomolecules are ^{12}C . Replacing

the ^{12}C with ^{13}C results in a molecule that is heavier than the naturally-occurring version; however, this heavier molecule is otherwise indistinguishable from the ^{12}C version, undergoing the same metabolic processes with equal efficiency. Therefore, we can track the fate of ^{13}C -labeled nutrients in mass spectrometry by determining the downstream metabolites that undergo a mass shift consistent with incorporation of ^{13}C carbon. This allows us to determine the metabolic rate and fate of a given nutrient under one or more experimental conditions.

One common way to understand ^{13}C labeling in various metabolites is through determination of isotopologue distribution. Isotopologues are molecules that differ only in their isotopic composition⁵¹. For instance, a glucose molecule containing one ^{13}C carbon is a different isotopologue than a glucose molecule with two ^{13}C carbons. Note that the term “isotopologue” does not provide any information about the connectivity of the ^{13}C carbons: if one molecule of glucose is ^{13}C -labeled at carbon 1 and another molecule of glucose ^{13}C -labeled at carbon 6, they are not distinguished in isotopologue analysis. A hypothetical presentation of the isotopologues of lactate under two different experimental conditions after administration of some ^{13}C -labeled nutrient is shown in (figure 1.4). Note M+0 represents the unlabeled metabolite and M+1, M+2, and M+3 represents one ^{13}C carbons, two ^{13}C carbons, or three ^{13}C carbons respectively within lactate, a three carbon molecule. Essentially, the data is a histogram of the carbon isotope distribution within the entire pool of lactate in each experimental condition. By studying these isotopologue distributions in metabolites downstream of the ^{13}C -labeled nutrient of interest, we can gain information concerning the metabolic fate and rate of that nutrient in the experimental conditions with wish to study. The use of ^{13}C -labeled nutrients is a recurring theme in this dissertation.

Lactate

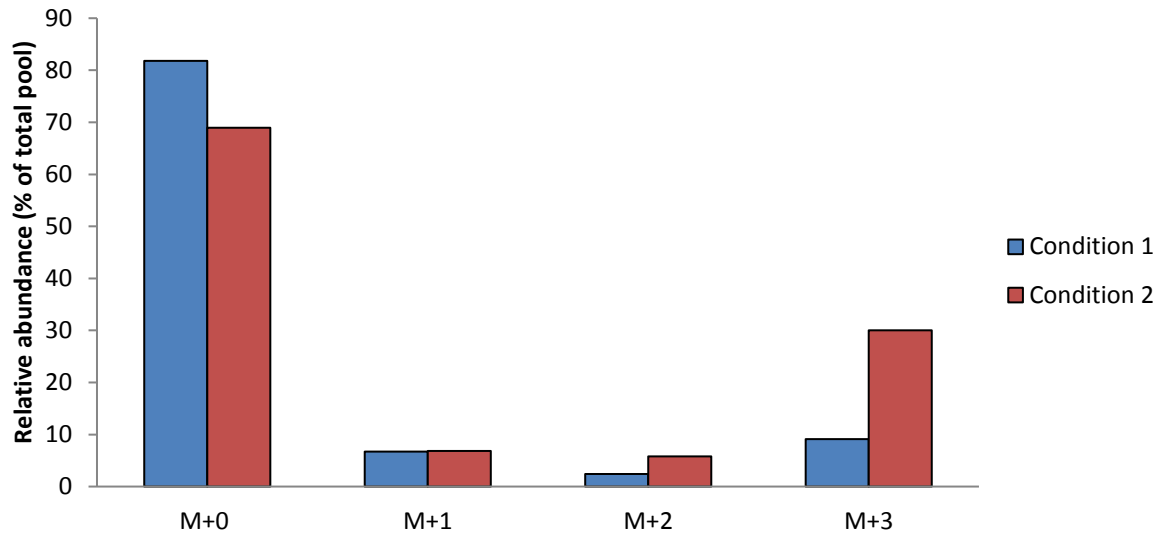


Figure 1.4 Hypothetical isotopologue distribution of lactate.

Chapter 2: Dietary fructose supports tumor growth

2.1 Introduction

It is well established that cancer cells have a high avidity for glucose relative to most other healthy tissues. Increased uptake of glucose supports an elevated glycolytic flux, which is typically assumed to be a requirement of cell proliferation²². Fructose has the same molecular formula as glucose and can be fed into glycolysis by two independent enzymes: hexokinase and ketohexokinase (KHK). Thus, it seems plausible that fructose could support the proliferation of cancer cells. Indeed, previous work has already demonstrated that fructose promotes the growth of intestinal cancers by directly activating central carbon metabolism within the intestinal cancer cell^{45,48}. Considering the availability of fructose in the microenvironment of the cervix, we aimed to determine whether dietary fructose could be utilized by cervical cancer cells to promote their growth^{52,53}.

2.2 Results

Elevated consumption of dietary fructose promotes tumor growth

To determine whether high fructose consumption increases cervical tumor growth *in vivo*, we placed nude mice with subcutaneous CaSki tumors on a high-fructose diet or a calorie-matched control diet that did not contain sugar but still contained complex carbohydrates. After 4 weeks on these respective diets, we observed a significant increase in tumor size in the high-fructose group relative to the control (figure 2.1A).

Given that fructose is most commonly consumed in combination with glucose, we also evaluated the effect of both glucose and fructose on tumor growth. For mice on a normal chow diet, replacement of water with a 10% high fructose corn syrup (HFCS) solution resulted in increased tumor growth (figure 2.1B). CaSki tumors similarly grew faster on a high sucrose diet relative to

control diet (figure 2.1C). Therefore, fructose by itself increased CaSki tumor growth and fructose in combination with glucose increased growth. To understand the mechanism behind these observations, we first wanted to ensure that increased growth with high fructose consumption was not due to increased total caloric consumption on the high-sugar diets. Indeed, we found that the total caloric consumption on all the diets was the same (figure 2.1D). Furthermore, the effects of the high-sugar diet were not secondary to weight gain, as there were no statistically significant differences in mouse weights (figure 2.1E). The mice also did not exhibit changes consistent with the onset of insulin resistance on the high fructose diet after 6 weeks of dietary consumption. This was revealed by comparable fasting glucose levels among the control and high fructose diet groups (figure 2.2A). Furthermore, there was no difference in glucose tolerance test or the rate of gluconeogenesis from [U-13C] alanine administration between the high fructose diet and control (figure 2.2B-C). Therefore, the observed increases in tumor growth rate did not appear to be secondary to obesity, caloric consumption or insulin resistance. These observations suggest that the compositions of the diets themselves may be responsible for the increased rate of tumor growth.

2.3 Discussion

The ability of high sugar consumption to promote tumor growth in any tumor model has been poorly studied. These data represent some of first to show that high sugar intake can promote growth in a cervical xenograft model. Notably, a diet high in fructose is sufficient to promote increased tumor growth relative to a calorie-matched control diet, which resembles mouse normal chow diet in terms of macronutrient distribution. Most interesting is that this sugar-induced growth enhancement was not secondary to either obesity or increased caloric consumption. Obesity has been shown in many other studies to promote both tumor incidence

and development in certain tumor types^{54,55}. Accordingly, it has previously been proposed that high sugar diets may indirectly support tumor growth via promotion of weight gain and obesity^{56,57}. Furthermore, insulin resistance has been associated with fructose consumption⁵⁸⁻⁶⁰. However, over the timescale of the tumor growth that we observed, no insulin resistance was noted. Therefore, these results suggested that the faster growth rate with fructose feeding is not secondary to metabolic syndrome in this model and may be due to the manner in which fructose is metabolized within the organism or the tumor. The organismal and intratumor metabolic fate of fructose is furthermore explored in subsequent chapters in this dissertation.

Figures

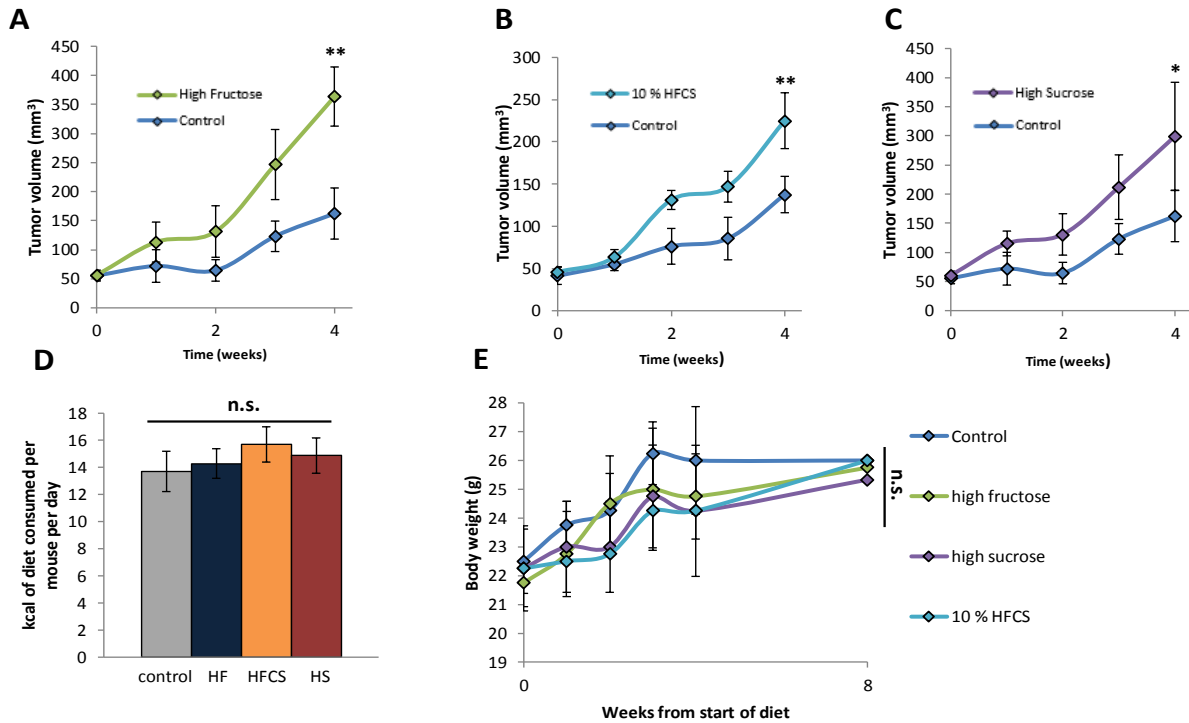


Figure 2.1 Dietary fructose supports tumor growth *in vivo*.

Tumor volume of a subcutaneous CaSki xenograft on a (A) high fructose (HF; n = 7) diet, (B) high fructose corn syrup (HFCS; n = 5) diet, or (C) high sucrose (HS; n = 7) diet compared to a control diet (n = 4-5 for each comparison) in nude mice. (D) Relative caloric intake for control, HF, HS, or HFCS diets (n=4). (E) Body weight of mice on a control, HF, HS, or HFCS diet (n = 4 for each diet). *P < 0.05, **P < 0.01, ***P < 0.001, ****P < 0.0001, and n.s. is not significant using an unpaired, two-tailed Student's *t* < 0.001, ****P < 0.0001, and n.s. is not significant

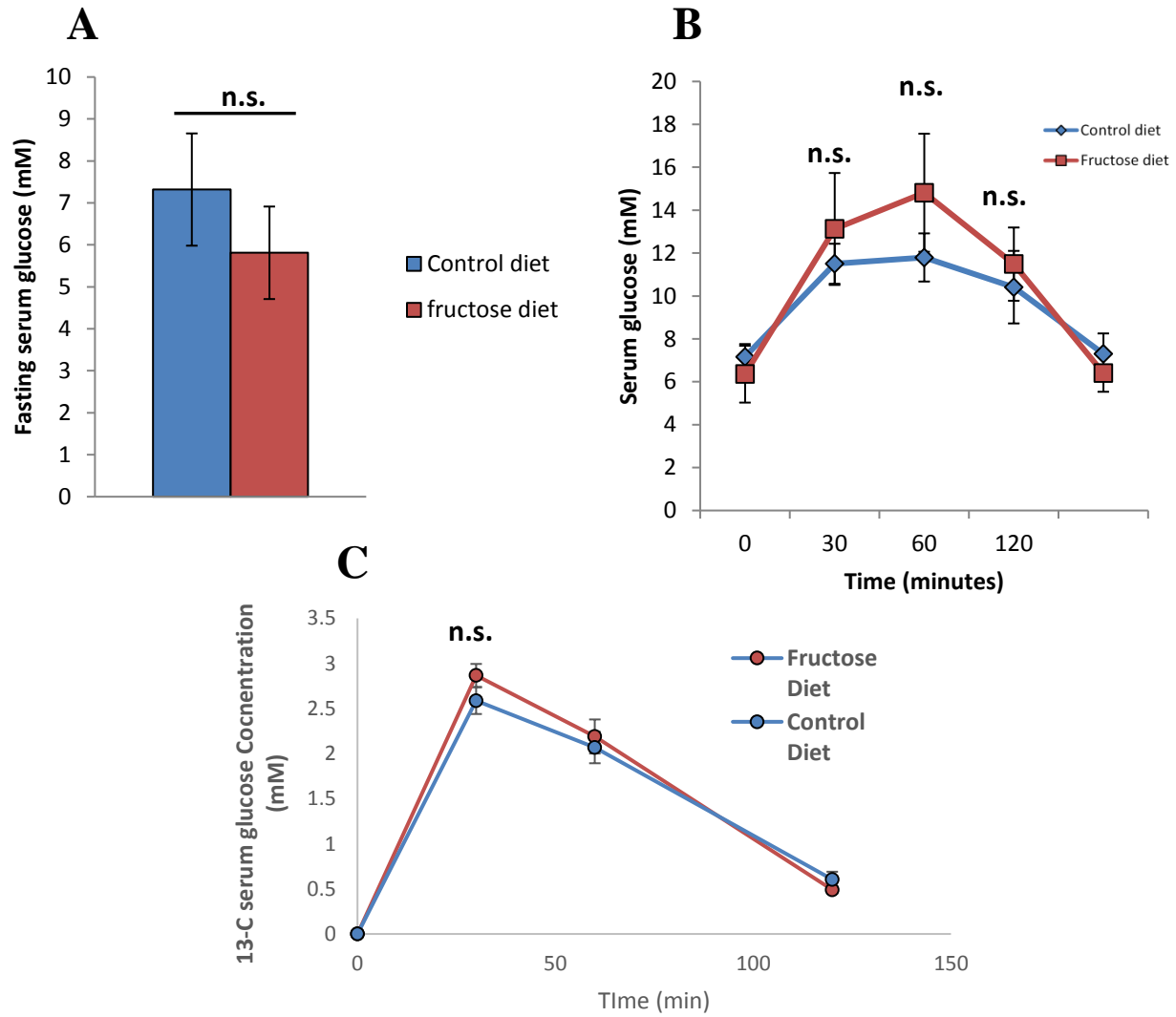


Figure 2.2 Fructose does not induce insulin resistance in nude mice

(A) Fasting glucose levels of mice after administration of a control diet (n =4) or a high fructose diet (n = 4) for 6 weeks. B) Oral glucose tolerance test with 1 g/kg of glucose gavaged into mice fed a high fructose (n = 4) or control diet (n = 4) for 6 weeks 3) alanine tolerance test with 0.5 g of alanine gavaged into mice fed a high fructose (n = 4) or control diet (n = 4) for 6 weeks. n.s. is not significant

Chapter 3: Fructose does not directly support cancer cell metabolism *in vitro*

3.1 Introduction

It is well established that cancer cells have a high avidity for glucose relative to most other healthy tissues. Increased uptake of glucose supports an elevated glycolytic flux, which is typically assumed to be a requirement of cell proliferation.²⁰ However, the role of other sugars to support tumor metabolism is less well explored. Phosphorylation of fructose by hexokinase produces the glycolytic intermediate fructose 6-phosphate. Alternatively, phosphorylation of fructose by ketohexokinase (KHK) produces fructose 1-phosphate, which can then be transformed into three-carbon glycolytic intermediates by aldolase B (figure 1.3). Thus, through the activity of hexokinase or KHK, it seems plausible that fructose could support the proliferation of cancer cells. Indeed, previous work has already demonstrated that fructose promotes the growth of pancreatic and intestinal cancers by directly activating central carbon metabolism in the cancer cells^{46,61}. However, it is not clear if the capacity for fructose catabolism is idiosyncratic to specific cancer cell types or if there is any conservation among how tumors metabolize fructose.

In this chapter one, we determined that fructose administration in the water or diet of mice could enhance the tumor growth rate of CaSki xenografts. In this chapter, we seek to understand how fructose is directly metabolized *in vitro* by CaSki cells and a variety of other cancer cell lines. We show that none of the tumor cell lines that we tested could either metabolize fructose or grow substantially *in vitro* with fructose as their only sugar source. This is due to hexokinase in these cells having a marked decreased affinity for fructose vs glucose. Furthermore, all tested cell lines expressed an isoform of ketohexokinase that did not metabolize fructose well, and none of the

cell lines expressed aldolase B. Co-culturing CaSki cells with hepatocytes, however, resulted in robust growth of CaSki cells in media containing fructose as the only sugar source. We show that CaSki growth in this context is dependent on fructose catabolism in the hepatocytes in a ketohexokinase-dependent manner. Fructose is catabolized by hepatocytes, resulting in excretion of a variety of downstream metabolites that are passaged to the cancer cell. This observation supports the idea that fructose may support cancer cell growth in a cancer cell nonautonomous manner.

3.2 Results

Fructose does not directly support the growth of cancer cells *in vitro*

Given the significant effect of high fructose supplementation on CaSki growth, we suspected that fructose was avidly metabolized by the CaSki cells. To understand fructose metabolism in CaSki, we labeled cells with [U-¹³C] fructose or [U-¹³C] glucose in culture for 4 hours. As expected, we saw extensive metabolism of the glucose label (figure 3.1A). Yet, surprisingly, we saw only minimal metabolism of the fructose label (figure 3.1A, extended data figure 3.1). To assess whether this observation was specific to CaSki cells, we repeated the labeling experiments in several other transformed and non-transformed proliferating cell lines. All cell lines that we tested produced the same results (extended data figure 3.2). Consistent with these data, CaSki cells incubated in DMEM and 10 mM fructose as the only sugar source grew poorly relative to CaSki cells grown in DMEM and 10 mM glucose as the only sugar source (figure 3.1B). Strikingly, these cells grown in fructose did not grow much better than cells in control media with no sugar added at all (figure 3.1B). Similar results were obtained for all proliferating cell lines tested (extended data figure 3.3). Furthermore, we determined that the lack of fructose

metabolism was not due to an inability of these cells to uptake fructose, as all cell lines readily took up 1-NBDF, a fluorescent fructose analog (extended data figure 3.4).

We next assessed whether the presence of glucose might allow fructose to better support the growth of cultured cancer cells. We found that the addition of fructose to glucose-containing media did not increase CaSki cell growth in our experiments (figure 3.1C). This result was replicated in all of the cell lines that we evaluated (extended data figure 3.5). Fructose also had no effect on glucose metabolism, as the fate of [U-¹³C] glucose was unaffected by the presence of fructose (figure 3.1D, extended data figure 3.6). The findings also highlight that the contribution of fructose to metabolism is undetectable in the presence of glucose, as [U-¹³C] glucose labeling is not diluted by unlabeled fructose.

For cells that express the enzymes aldose reductase and sorbitol dehydrogenase of the polyol pathway, intracellular fructose is not only derived from exogenous sources (figure 3.1E).

Fructose can be produced endogenously from conversion of glucose carbons to sorbitol, which can then form fructose via sorbitol dehydrogenase. In non-transformed cells in the retina or the kidney, this pathway is activated by hyperglycemia, as aldose reductase has a high k_m for glucose^{62,63}. We reasoned that elevated consumption of glucose in cancer cells may lead to increased levels of intracellular glucose and polyol pathway activation. Notably, we did find that CaSki cells (as well as other cell lines tested) express sorbitol dehydrogenase and thus have the capacity for endogenous fructose production (figure 3.1F). After labeling with [U-¹³C] glucose, we found evidence of fructose production in CaSki and other cell lines tested (figure 3.1G; extended data figure 3.7B-G). It is important to note that this assessment required application of a liquid chromatography method that could resolve fructose and glucose (extended data figure 3.7A). To

understand whether the fructose being produced from sorbitol dehydrogenase is important for CaSki growth, we silenced sorbitol dehydrogenase in CaSki cells grown with dialyzed FBS containing no exogenous fructose (extended data figure 3.8). Under these conditions, we observed a decrease in CaSki cell growth. Adding fructose back to the medium did not rescue this reduced cell growth (figure 3.1H). This result was similar for other tested cell lines (extended data figure 3.9). Therefore, it is unlikely that endogenously produced fructose is important for cell growth. We conclude that any impact of sorbitol dehydrogenase on cell growth is not due to its production of fructose.

Ketohexokinase does not support fructolysis in transformed cell lines

Our isotope tracer results show that a minimal amount of [U-¹³C] fructose is metabolized in CaSki cells, as well as other cell lines tested. We next sought to determine whether the minimal amount of metabolism observed was a product of hexokinase or KHK activity (figure 3.2A), which required establishing a liquid chromatography method that could resolve each product from other hexose phosphates (extended figure 3.10). We discovered that CaSki cells produce fructose 1-phosphate from both [U-¹³C] glucose and [U-¹³C] fructose, suggesting the presence of KHK in these cells (figure 3.2B). We also detected fructose 1-phosphate labeling from [U-¹³C] fructose in every cell line that we evaluated (extended figure 3.11).

It is important to point out that there are two known isoforms of ketohexokinase: KHK-A and KHK-C. In nonmalignant tissues, KHK-C is the isoform responsible for efficient metabolism of fructose. In contrast, the KHK-A isoform does not readily metabolize fructose, having a high k_m for fructose⁶⁴⁻⁶⁶. Most tissues of the body express a low level of KHK-A and no KHK-C. Only the liver, kidney, and small intestine express high amounts of KHK-C^{64,65} (extended data figure 3.12). Notably, while KHK isoform expression has been studied for normal tissues, little is

known about KHK isoform expression in tumors. Given that the presence of fructose 1-phosphate is not specific to the activity of one isoform, we assayed the levels of KHK-A and KHK-C directly in CaSki and other cell lines. None of the cell lines tested expressed KHK-C in either hypoxia or normoxia (figure 3.2C). We tested the hypoxia condition because there are several reports of hypoxia inducing expression of KHK-C in naked mole rats or human cardiomyocytes^{66,67}. On the other hand, all cell lines expressed KHK-A. These data indicate that some KHK-A activity leads to a small level of intracellular fructose 1-phosphate, but that this activity is insufficient to enable extensive metabolism of fructose (figure 3.2D). As expected, there is a striking difference in the relative pool size of fructose 1-phosphate in hepatocytes expressing KHK-C compared to CaSki cells expressing only KHK-A (figure 3.2E). Moreover, none of the cell lines expressed aldolase B (extended data figure 3.13), which is necessary to feed fructose 1-phosphate into glycolysis (figure 3.2A). We hypothesized that the lack of expression of KHK-C and aldolase-B might be due to cultured cells being chronically grown in conditions deprived of fructose. However, we determined that the FBS used in these experiments contained millimolar levels of fructose (figure 3.2F). This finding is consistent with reports that ruminants *in utero* have high blood fructose^{68,69}. Thus, cells grown in culture with 10% FBS experience physiological levels of fructose; nevertheless, this does not drive expression of fructolytic enzymes. Additionally, we determined that the relative expression of total KHK is decreased in proliferating fibroblasts compared to quiescent fibroblasts (extended data figure 3.14), suggesting that KHK may be downregulated during proliferation in some growth models.

Administration of clinical candidate PF-06835919 does not alter cell growth *in vitro*

To evaluate whether the small amount of KHK-A activity that we observed in CaSki cells contributes to proliferative metabolism, we obtained a KHK inhibitor, PF-06835919, currently in clinical trials⁷⁰(extended data figure 3.15). PF-06835919 inhibits both isoforms of KHK⁷¹. We

administered PF-06835919 to CaSki cells at doses up to 250 μ M and observed no effect on cell growth (extended data figure 3.16A). The same observation was made for immortalized Huh7 cells expressing KHK-A, even though they were derived from liver tissue expressing KHK-C (extended data figure 3.16B). At 30 μ M, fructose 1-phosphate production in CaSki and Huh7 cells was completely blocked (figure 3.2G, extended data figure 3.16C). These data suggest that KHK-A production of fructose 1-phosphate is not important for cell proliferation. Notably, administration of PF-06835919 up to 250 μ M did not reduce M+3 labeling of lactate from [U-¹³C] fructose, suggesting that the minimal amount of labeling in central carbon metabolism from [U-¹³C] fructose is not due to KHK-A activity (figure 3.2H, extended data figure 3.16D). In contrast, co-administration of 20 mM 2-deoxyglucose with [U-¹³C] fructose significantly reduced M+3 lactate labeling in CaSki cells, indicating that the minimal amount of fructose metabolism observed in these cells is a result of hexokinase rather than KHK (figure 3.2I). Given that labeling of fructose 6-phosphate in CaSki cells was small from [U-¹³C] fructose relative to [U-¹³C] glucose, it is apparent that hexokinase has a decreased capacity to use fructose as a substrate compared to glucose (extended data figure 3.16E). These observations are consistent with previous reports that hexokinase has a significantly higher k_m for fructose relative to glucose^{64,72,73}. On the basis of our results, we conclude that hexokinase cannot efficiently utilize fructose as a substrate in CaSki cells, or any of the other transformed cell lines that we investigated.

Translation to human cervical cancer patients

To examine the translational relevance of our findings of KHK isoform expression in our cervical cancer models, we used whole transcriptome sequencing (RNA-seq) data to measure KHK-A and KHK-C isoform expression in primary cervical cancer samples from a cohort of 99 patients uniformly treated with chemoradiation at Washington University School of Medicine. Overall, we observed that the relative expression of KHK-A and KHK-C from all of the human cervical tumors

were consistent with our *in vitro* data. None of the cervical tumors showed KHK-C expression, while all of the cervical tumors expressed low levels of KHK-A with a mean of 0.876 FPKM (figure 3.3A). This is also confirmed by examining read coverage of exons that are specific to KHK-A (Exon 3A) or KHK-C (Exon 3C), and splice junction reads at these exons (figure 3.3B). Although the function of KHK-A in cancer is incompletely understood, our cell-culture data indicate that KHK-A is not important for cancer cell proliferation because inhibition of KHK-A with PF-06835919 did not impact growth. Consistent with this finding, we also determined that KHK-A expression was not significantly associated with cervical cancer stage, risk of recurrence, or overall survival in this cohort of human patients (figures 3.3C-E).

Hepatocytes transfer fructose-derived nutrients to CaSki cells to promote their growth

Given that CaSki cells cannot efficiently use fructose carbon themselves, we hypothesized that fructose promotes CaSki tumor growth through its transformation in KHK-C expressing tissues. As reported by Jang et al., the small intestine and liver rapidly convert fructose into glucose and a variety of other small molecule metabolites that may support tumor growth⁷⁴. We found that isolated primary hepatocytes from C57BL/6j mice readily incorporated ¹³C-label into their metabolome after being administered [U-¹³C] fructose. In fact, the amount of [U-¹³C] lactate excreted was higher when primary hepatocytes were provided 5 mM [U-¹³C] fructose compared to when they were provided 5 mM [U-¹³C] glucose (figure 3.4A). In addition to excreting [U-¹³C] lactate, primary hepatocytes administered [U-¹³C] fructose also excreted [U-¹³C] glucose into the media (figure 3.4B). These data demonstrate that fructose supports gluconeogenesis in primary hepatocytes.

To model whether the liver can convert fructose into useable nutrients for cancer cells, we applied a transwell system to co-culture CaSki cells with primary hepatocytes isolated from

C57BL/6j mice. As a control, the same setup was used but with CaSki cells in both wells (figure 3.4C). We administered glucose and [U-¹³C] fructose to the co-cultures at a ratio of 1:1. We then harvested metabolites from both the media and from the CaSki cells. Several growth-promoting nutrients, such as lactate and aspartate, were found to be labeled in the media. The same metabolites were also found to be labeled in CaSki cells, suggesting that they were excreted by hepatocytes and taken up from the media by CaSki cells (figures 3.4D to 3.4I). Additionally, in media where the only significant source of sugar was fructose, CaSki cells co-cultured with hepatocytes proliferated significantly faster than CaSki cells alone (figure 3.4J). Taken together, these data support a nutrient-exchange model where hepatocytes transfer fructose-derived metabolites to CaSki cells to promote their cell growth.

3.3 Discussion

The data in this chapter reveals the role of direct fructose utilization in various cancer cell lines on their growth and metabolism. It was shown that fructose did not support growth as well as glucose. Furthermore, fructose was barely metabolized in contrast to glucose which was readily catabolized. Sparse fructose catabolism in these cancer cells was due to lack of expression of fructolytic enzymes and to hexokinase have a stronger preference for glucose phosphorylation vs fructose phosphorylation. Metabolism of fructose carbons by KHK-C-expressing hepatocytes, however, resulted in the passage of useable metabolites to the cancer cells that they could metabolize for growth.

This is the first report that we know of showing that fructose and glucose have remarkably different capacities for supporting tumor cell metabolism. Several other studies have shown that tumor cells express fructose transporters, and these studies often conclude that transporter

expression indicates metabolism of fructose within the cell^{50,75-77}. But as we show here, all the cancer cell lines that we studied could uptake fructose analogs comparably with glucose analogs, in spite of vastly different metabolic efficiencies with each sugar. It is also notable that there is a previous report by Goncalves et al that a mouse model of colon cancer expressed ketohexokinase and had capacity for fructolysis⁴⁵. In contrast, the HCT116 colon cancer cells that we studied did not metabolize fructose well and did not express fructolytic enzymes, though the investigators did not determine which isoform of ketohexokinase was present. In this study by Goncalves et al, a mouse deficient in APC (APC $-/-$) in the intestinal stem cells was used⁴⁵. This resulted in tumors forming all along the intestinal tract, with most tumors forming in the small intestine as opposed to the colon⁴⁵. Within the small intestine, there is very high expression of KHK-C and very little expression within the colon (figure 3.12, figure 6.1). Therefore, it is possible that the tumors in the APC $-/-$ mouse model reported by Goncalves et al expressed ketohexokinase and aldolase B because they were derived from the small intestine⁴⁵.

Figures

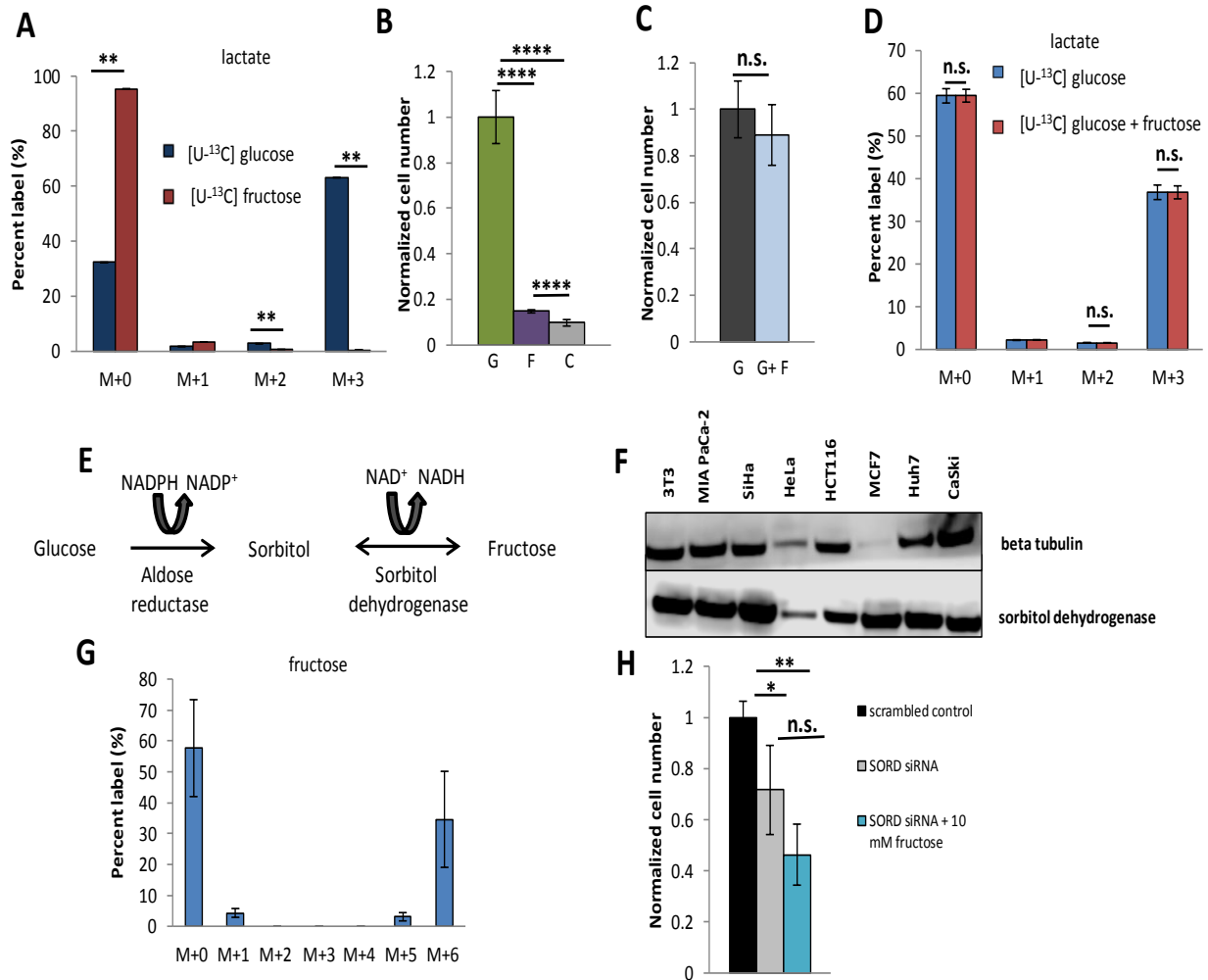


Fig 3.1. Exogenous and endogenous fructose do not directly support growth.

(A) Percent ¹³C labeling from lactate in CaSki cells after 4 hours in either 5 mM [U-¹³C] glucose (n=3) or 5 mM [U-¹³C] fructose (n=3). (B) Relative number of CaSki cells after 4 days in media containing either 10 mM glucose (G, n=5), 10 mM fructose (F, n=5), or no-sugar-added control (C, n=5). (C) Relative number of CaSki cells after 4 days in 20 mM glucose (G, n=6) or 10 mM glucose + 10 mM fructose media (G +F, n=4). (D) ¹³C-labeling of lactate after administering either 10 mM [U-¹³C] glucose ([U-¹³C] glucose, n=3) or 10 mM [U-¹³C] glucose and 10 mM fructose ([U-¹³C] glucose + fructose, n=3) for four hours. (E) Schematic depicting the polyol pathway and the generation of endogenous fructose from glucose. (F) Western blot against sorbitol dehydrogenase in 8 different cancer or proliferating cell lines (G) ¹³C labeling of fructose in CaSki cells after 4 hours of treatment with 5 mM [U-¹³C] glucose (n=3). (H) Comparing relative CaSki cell growth in response to sorbitol dehydrogenase siRNA (SORD siRNA, n=5), scrambled control (scrambled control, n=5), or sorbitol dehydrogenase silencing with exogenous fructose added to the media (SORD siRNA + 10 mM fructose, n=5). *P < 0.05, **P < 0.01, ***P < 0.001, ****P < 0.0001, and n.s. is not significant using an unpaired,

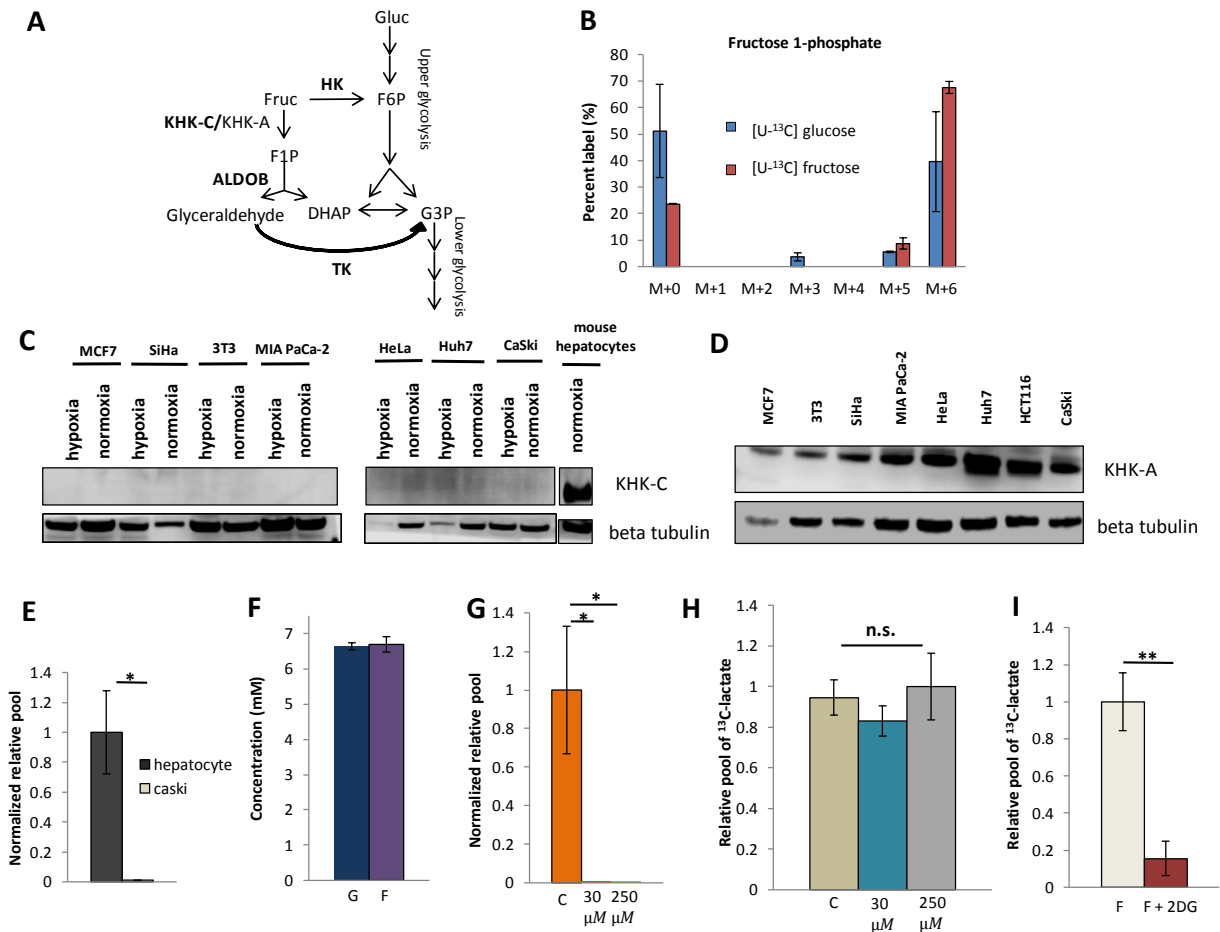


Fig 3.2 Hexokinase, not ketohexokinase, metabolizes fructose.

(A) Schematic showing fructose metabolism via hexokinase, ketohexokinase-C, or ketohexokinase-A. gluc, glucose; F6P, fructose 6-phosphate; HK, hexokinase; Fruc, fructose; KHK-C, ketohexokinase-C; KHK-A, ketohexokinase-A; F1P, fructose 1-phosphate; ALDOB, aldolase B; DHAP, dihydroxyacetone phosphate; G3P, glyceraldehyde 3-phosphate; TK, triokinase. (B) ¹³C labeling of fructose 1-phosphate in CaSki cells after labeling for 4 hours with either 5 mM [U-¹³C] glucose (n=3) or 5 mM [U-¹³C] fructose (n=3). (C) Western blot against KHK-C in the indicated cell lines. (D) Western blot against KHK-A in the indicated cell lines. (E) Relative signal of fructose 1-phosphate (F1P) per mg of cells in hepatocytes (n=3) or CaSki cells (n=3). (F) Relative concentration of glucose (G) and fructose (F) in FBS (n=3). (G) Relative pool size of fructose 1-phosphate (F1P) in CaSki after incubation with either vehicle control (C, n=3), 30 μM of PF-06835919 (n=3), or 250 μM of PF-06835919 (n=3). Experiment was performed in the presence of both 10 mM glucose and 10 mM fructose in the media. (H) Relative pool size of ¹³C-labeled lactate in cells treated with 5 mM [U-¹³C] fructose together with either vehicle control (C, n=3), 30 μM of PF-06835919 (n=3), or 250 μM of PF-06835919 (n=3). (I) Relative pool size of ¹³C-labeled lactate in CaSki cells treated with 5 mM [U-¹³C] fructose only (F, n=3) or 5 mM [U-¹³C] fructose + 20 mM 2 DG (F + 2DG, n=3). *P < 0.05, **P < 0.01, ***P < 0.001, ****P < 0.0001, and n.s. is not significant using an unpaired, two-tailed Student's *t* test. All data represent means

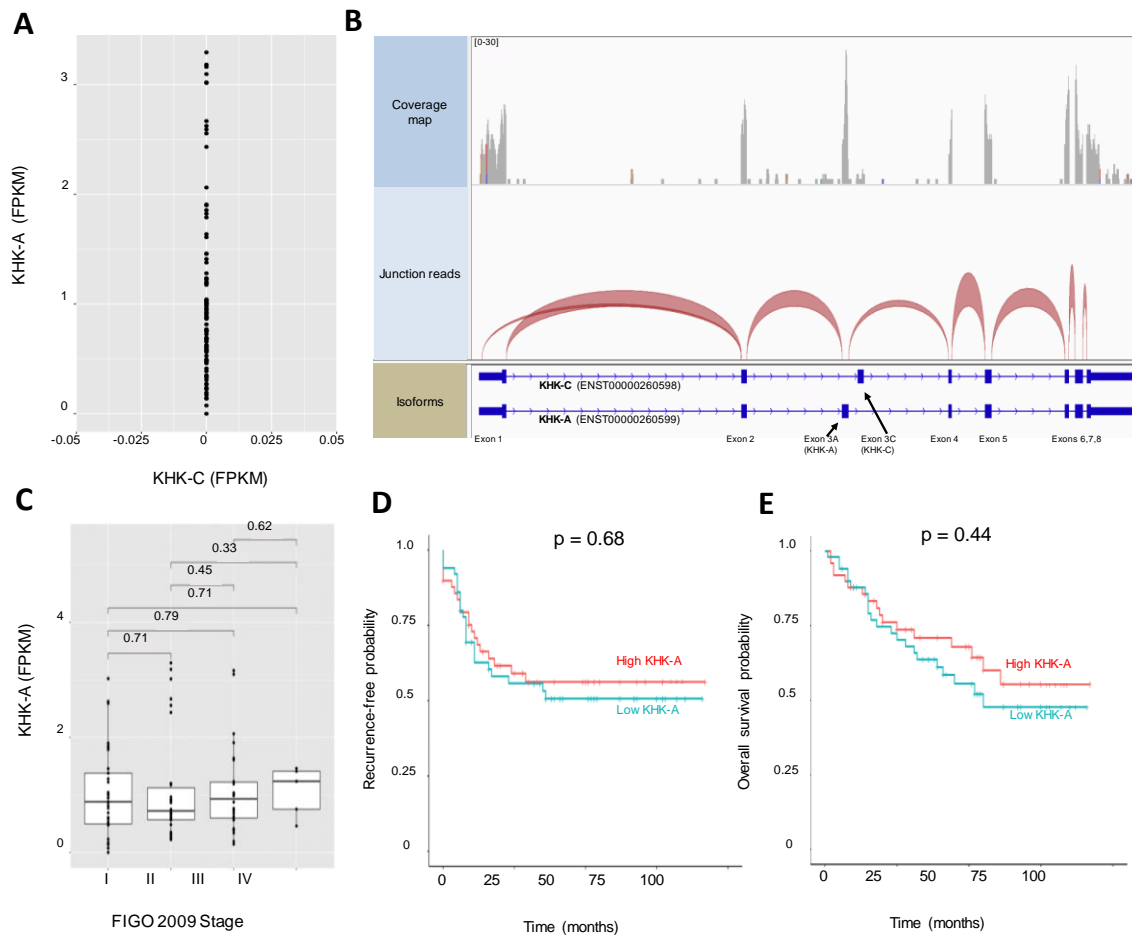


Figure 3.3. Human cervical tumors exclusively express KHK-A, which is not linked to survival, recurrence, or tumor stage.

(A) Relative isoform expression of KHK-A and KHK-C using RNA-seq data from cervical tumors of 99 patients treated at Washington University School of Medicine. (B) An IGV view of KHK gene expression in a cervical tumor shows expression of only Exon 3A that is specific to KHK-A. (C) Cervical tumor FIGO stages and KHK-A isoform expression in the 99 primary cervical cancer samples. (D) Kaplan-Meier plot of the recurrence rate of patients with pre-existing cervical cancer expressing high levels of KHK-A or low levels of KHK-A. (E) Kaplan-Meier plot of the overall survival rate of patients with cervical cancer expressing high levels of KHK-A or low levels of KHK-A.

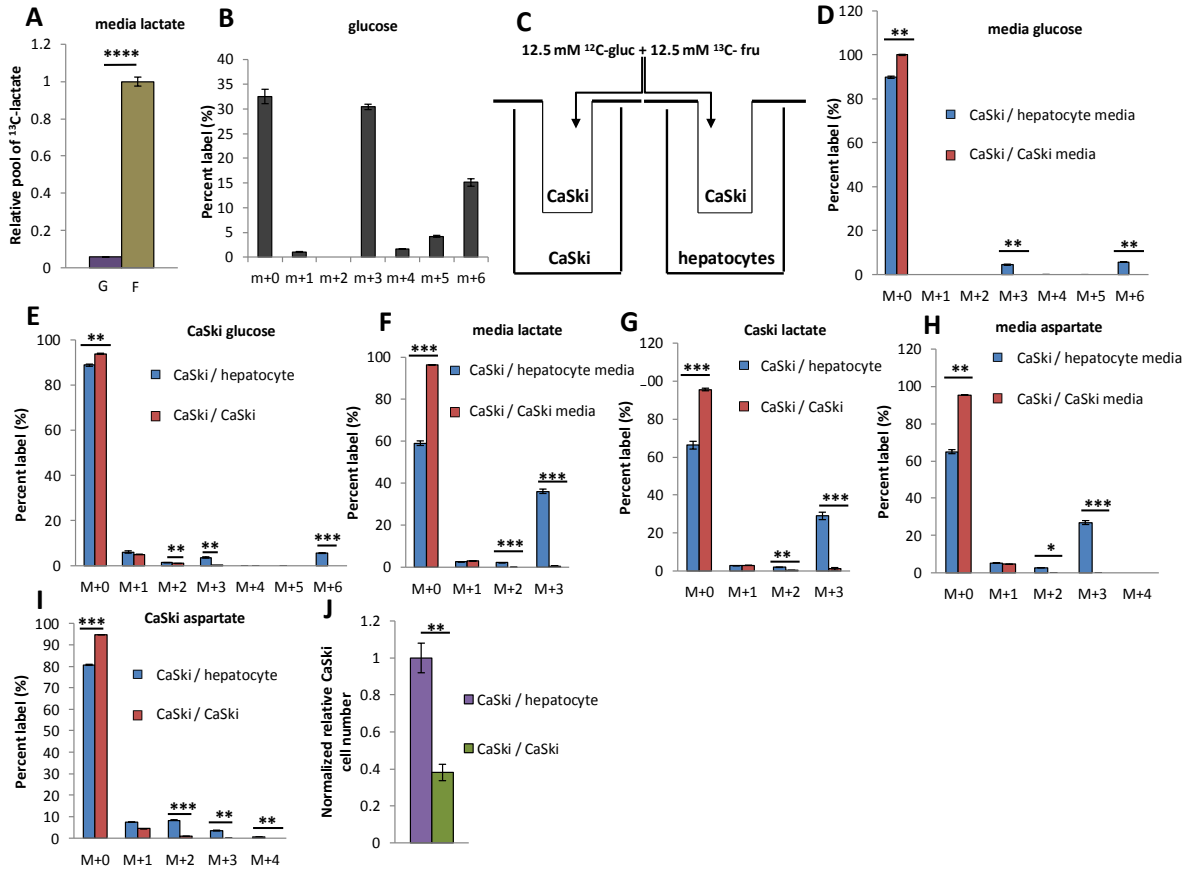
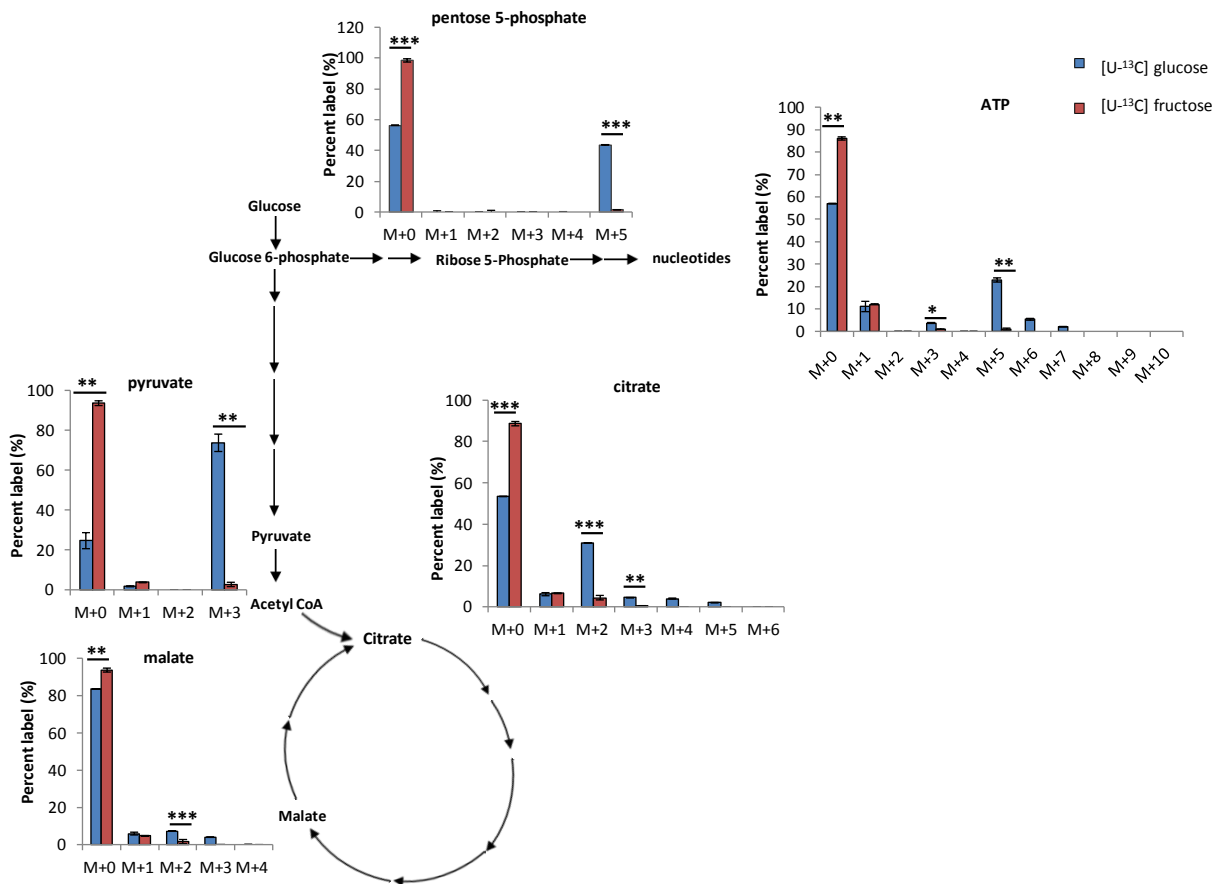


Fig 3.4. Hepatocytes transform fructose into useable carbons for growth.

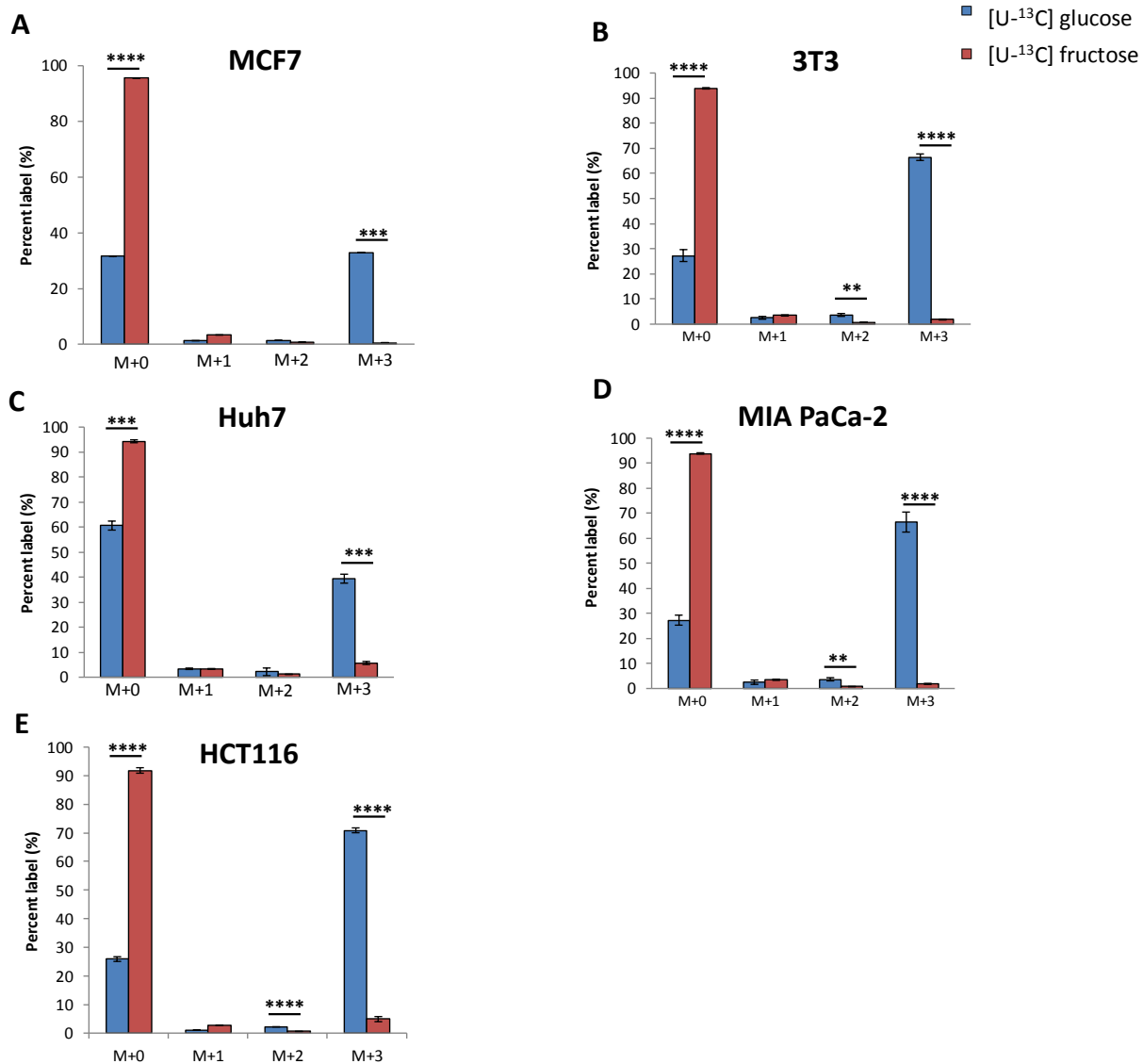
(A) Relative pool of ^{13}C -labeled lactate in the media after administering 5 mM $[\text{U-}^{13}\text{C}]$ glucose (G, $n=3$) or 5 mM $[\text{U-}^{13}\text{C}]$ fructose (F, $n=3$) to primary mouse hepatocytes for 4 hours. (B) ^{13}C labeling of media glucose after administering 5 mM $[\text{U-}^{13}\text{C}]$ fructose to primary mouse hepatocytes for 4 hours ($n=3$). (C) A schematic of a transwell coculture experiment for CaSki + hepatocytes or CaSki + CaSki. Both coculture conditions were incubated in 12.5 mM glucose + 12.5 mM $[\text{U-}^{13}\text{C}]$ fructose for 4 hours. Both the media and the CaSki cells on the upper layer of the transwell were harvested for both conditions. ^{13}C enrichment was measured in (D) media glucose ($n=3$), (E) intracellular CaSki glucose ($n=3$), (F) media lactate ($n=3$), or (G) intracellular CaSki lactate ($n=3$), (H) media aspartate ($n=3$), or (I) intracellular CaSki aspartate ($n=3$). (J) Relative CaSki cell number from the upper well of a transwell coculture of CaSki + hepatocytes ($n=3$) or CaSki + CaSki ($n=3$), each incubated for 48 hours in media containing 20 mM fructose as the only sugar source. * $P < 0.05$, ** $P < 0.01$, *** $P < 0.001$, **** $P < 0.0001$, and n.s. is not significant using an unpaired, two-tailed Student's t test. All data represent means \pm standard deviation.

Extended Data Figures



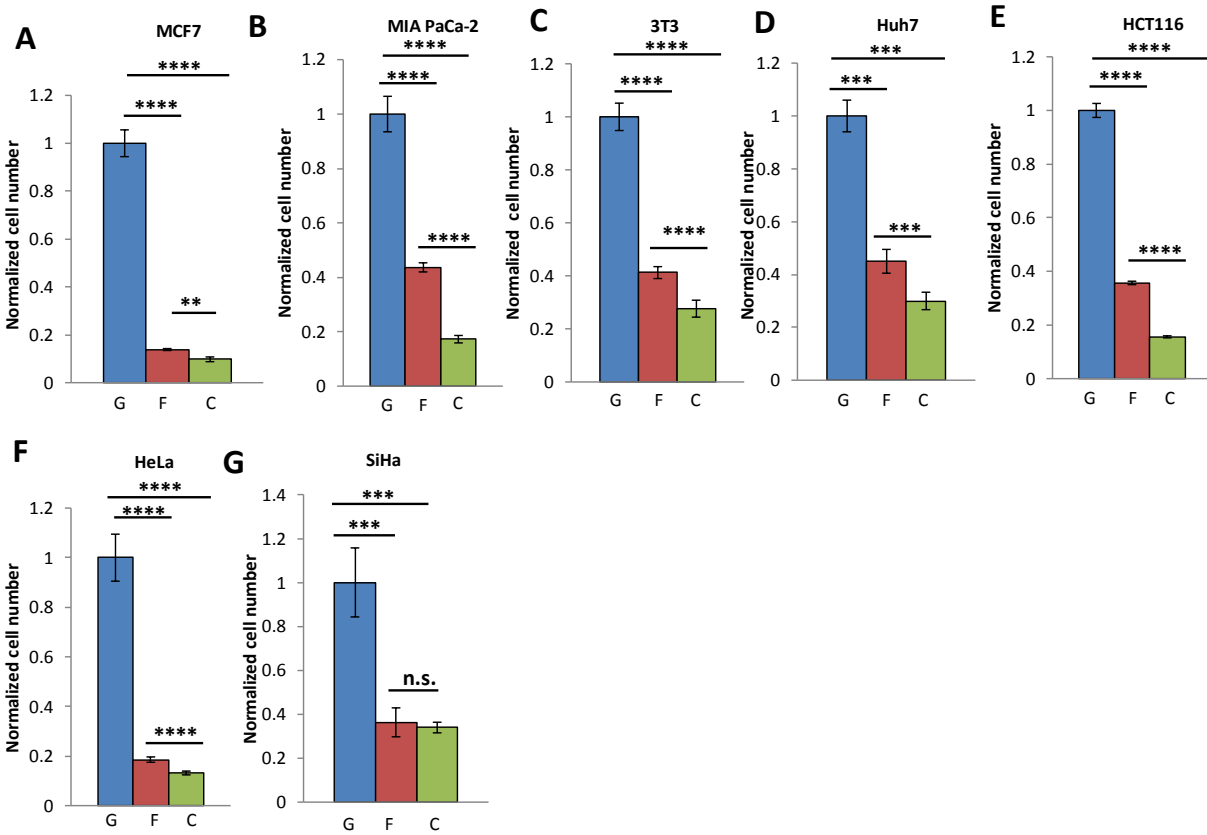
Extended figure 3.1. CaSki cells do not efficiently metabolize fructose.

¹³C enrichment in various metabolites of central carbon metabolism after 4 hours of labeling with either [U-¹³C] glucose (n=3) or [U-¹³C] fructose (n=3) in CaSki cells. *P < 0.05, **P < 0.01, ***P < 0.001, ****P < 0.0001, and n.s. is not significant using an unpaired, two-tailed Student's *t* test. All data represent means ± standard deviation



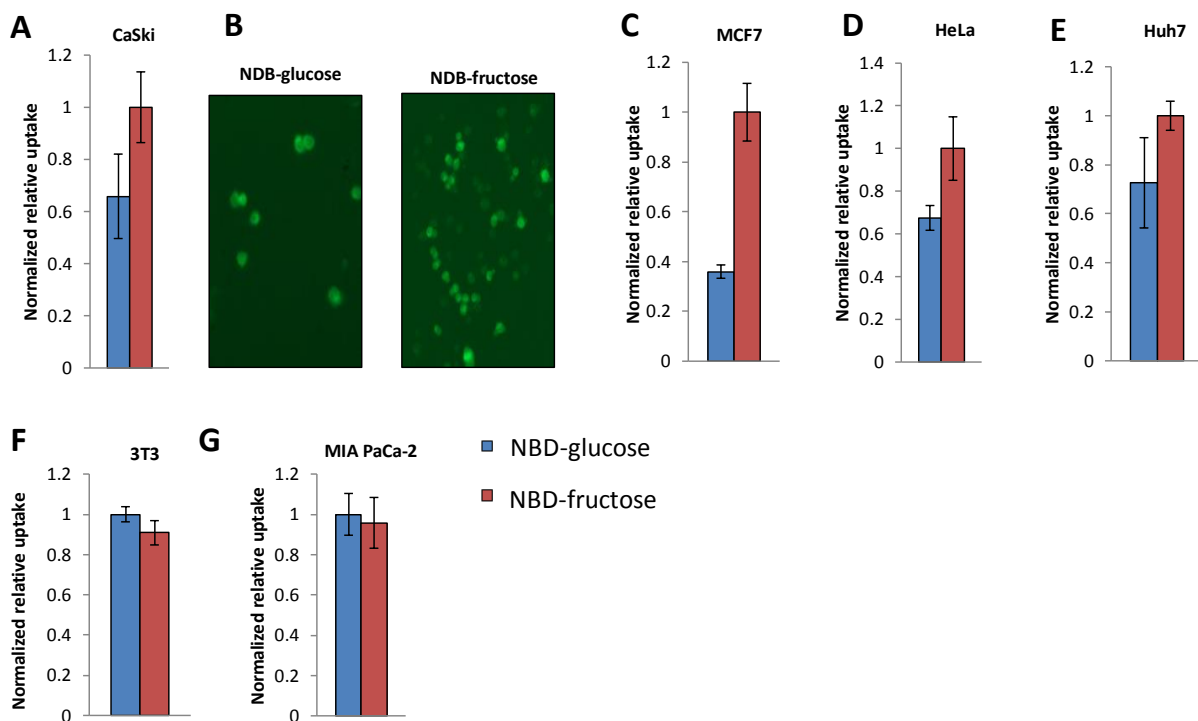
Extended figure 3.2. Various transformed and proliferating cell lines do not efficiently metabolize fructose.

(A to E) ¹³C enrichment in lactate after 4 hours of labeling the indicated cell lines with either [U-¹³C] glucose (n=3) or [U-¹³C] fructose (n=3). *P < 0.05, **P < 0.01, ***P < 0.001, ****P < 0.0001, and n.s. is not significant using an unpaired, two-tailed Student's *t* test. All data represent means ± standard deviation.



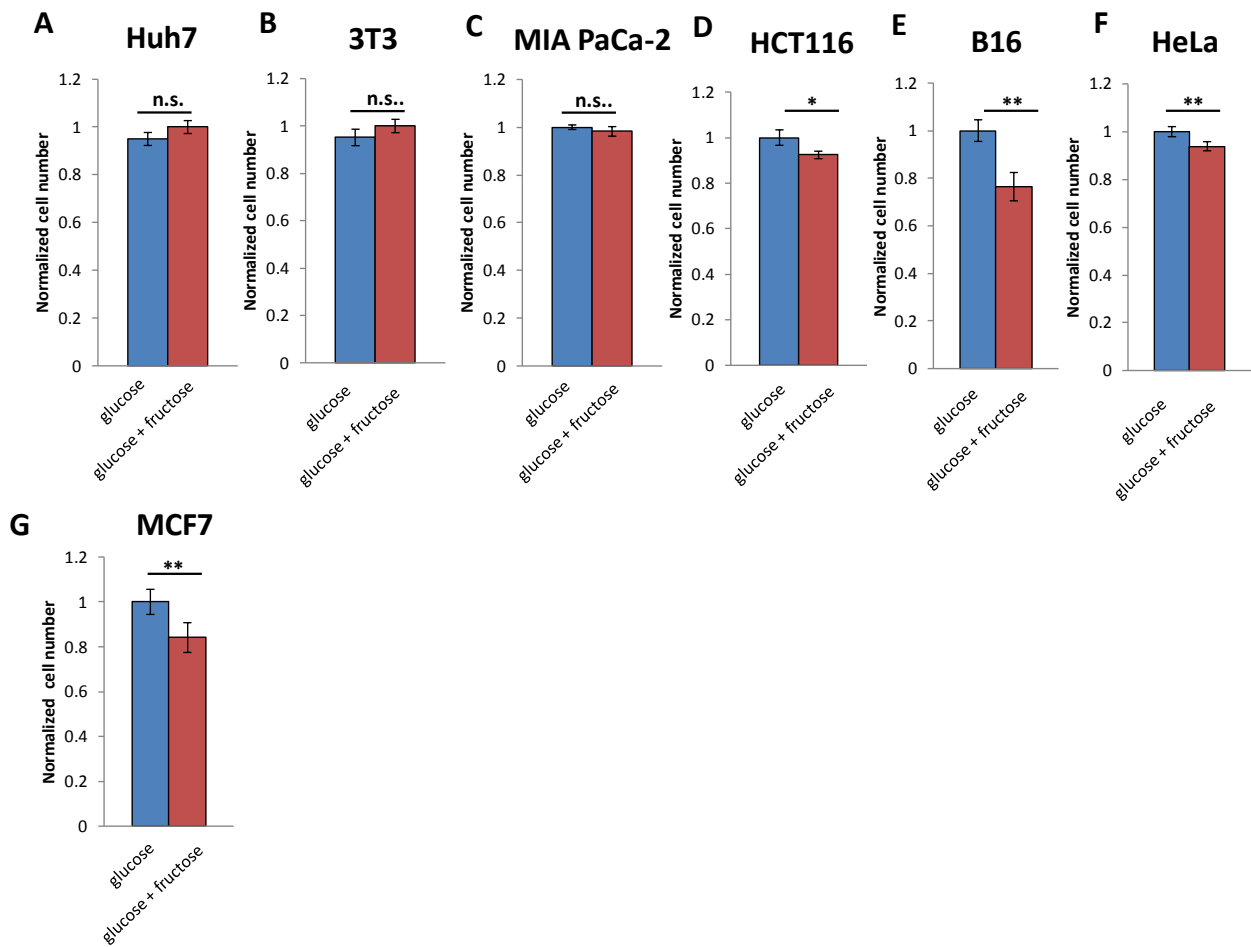
Extended figure 3.3. Fructose does not support growth as well as glucose.

Relative cell number of indicated cell lines after 4 days in media with DMEM containing 10mM glucose (G, n=4-6), 10 mM fructose (F, n=4-6), or no added sugar (C, n=4-6). Media also contains 10% FBS and 1% pen/strep. * $P < 0.05$, ** $P < 0.01$, *** $P < 0.001$, **** $P < 0.0001$, and n.s. is not significant using an unpaired, two-tailed Student's t test. All data represent means \pm standard deviation



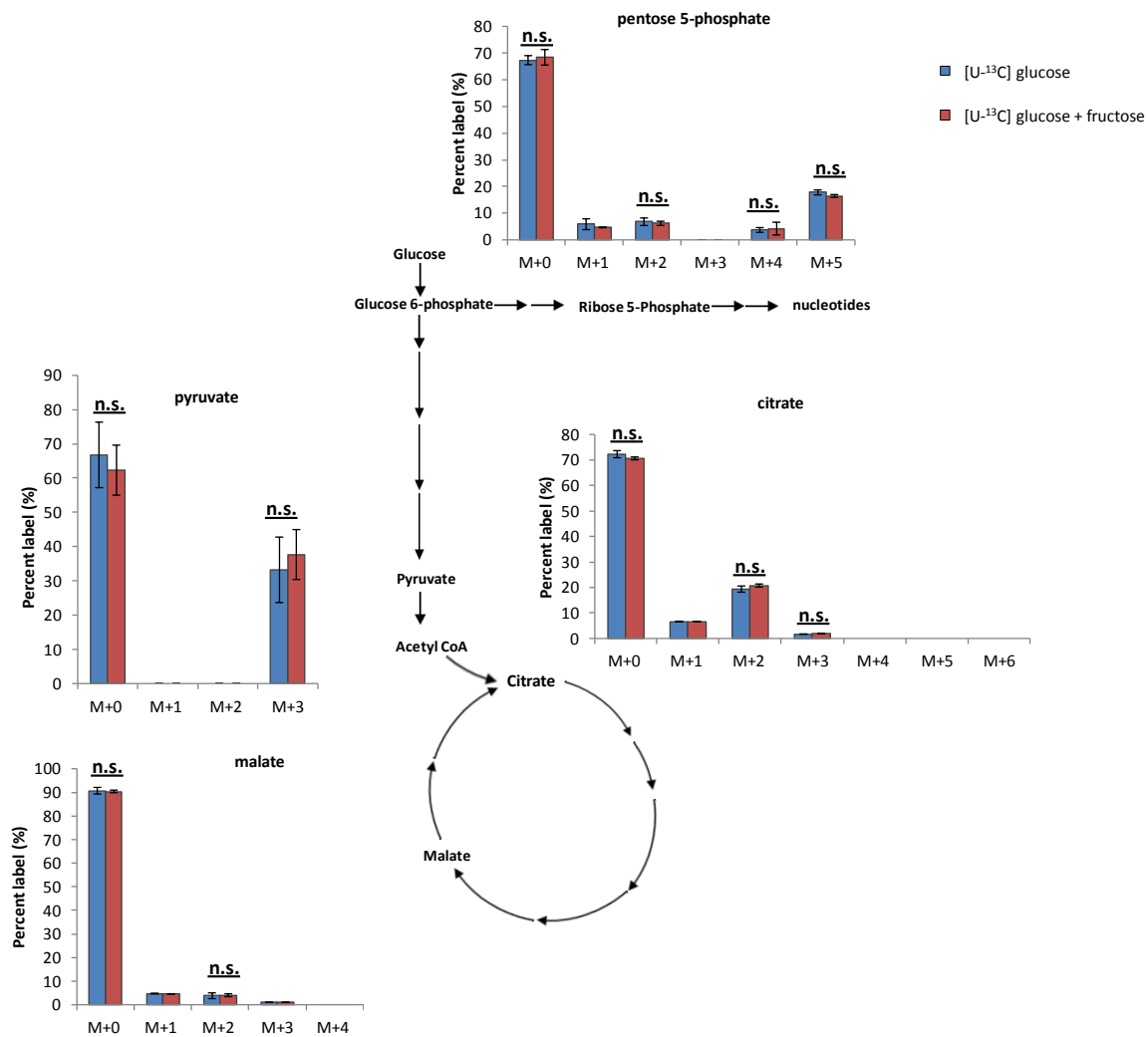
Extended figure 3.4 Transformed and proliferative cell lines can take up fructose.

(A) Relative intracellular fluorescence signal following a 30-min incubation with either 2-NBDG (n=5) or 1-NBDF (n=5) in CaSki cells. (B) Fluorescent images of CaSki cells incubated with either 2-NBDG or 1-NBDF. (C to G) Relative intracellular fluorescence signal following a 30-min incubation with either 2-NBDG (n=4-5) or 1-NBDF (n=4-5) in various cell lines. All data represent means \pm standard deviation.



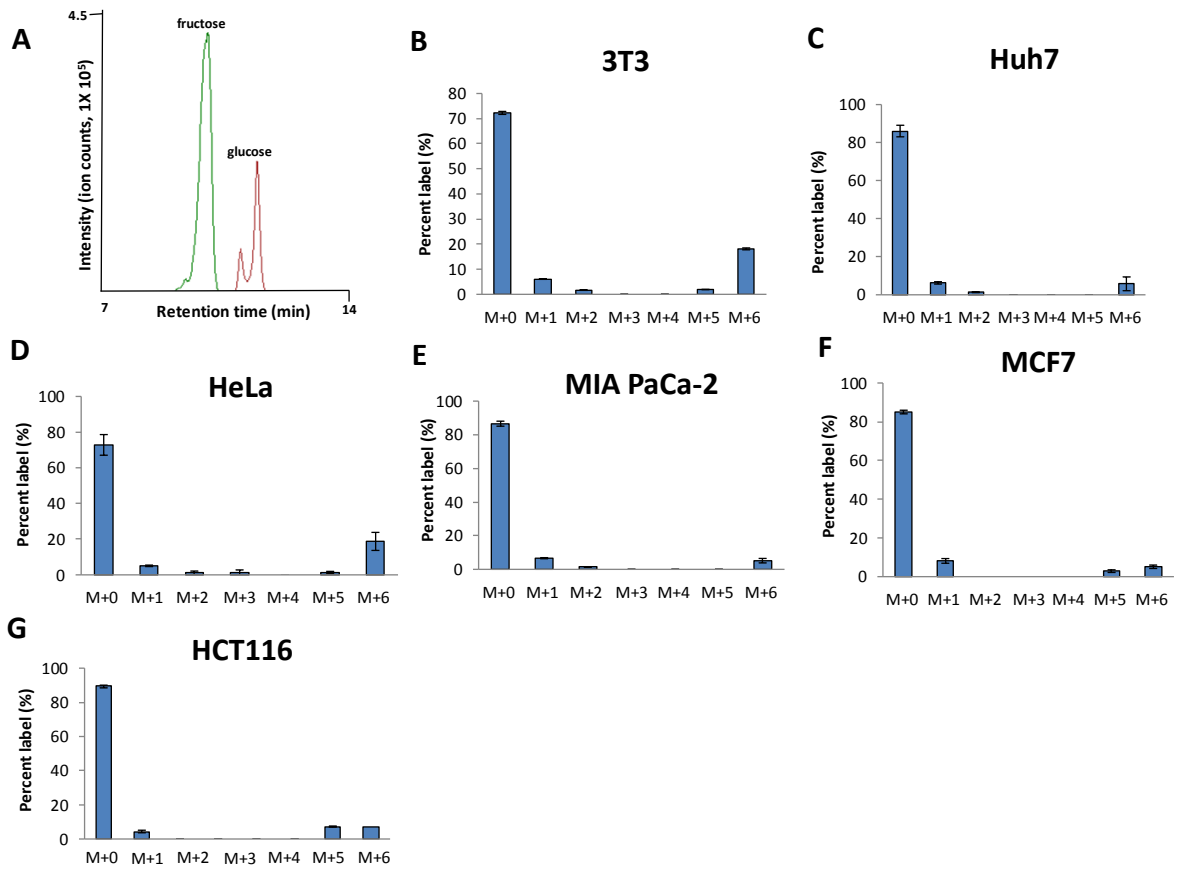
Extended figure 3.5. Addition of fructose to glucose-containing media does not enhance growth.

(A to G) Relative cell number of the indicated cell lines after 4 days in media with DMEM containing 20 mM glucose (n=4-5) or 10 mM glucose + 10 mM fructose (n=4-5). * $P < 0.05$, ** $P < 0.01$, *** $P < 0.001$, **** $P < 0.0001$, and n.s. is not significant using an unpaired, two-tailed Student's t test. All data represent means \pm standard deviation



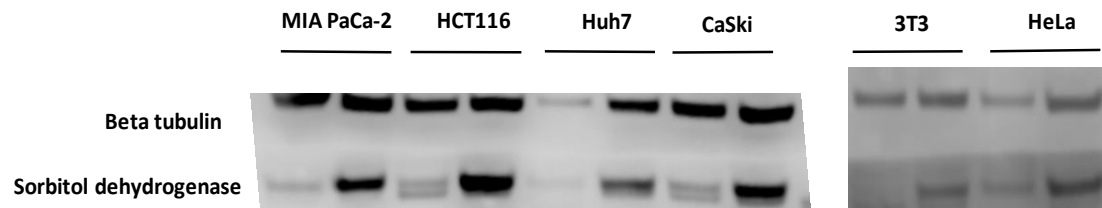
Extended figure 3.6. Fructose does not change the metabolic fate of glucose.

CaSki cells were incubated for 4 hours with either 10 mM [U-¹³C] glucose (n=3) or 10 mM [U-¹³C] glucose + 10 mM fructose (n=3). Relative labeling in various central carbon metabolites is shown. *P < 0.05, **P < 0.01, ***P < 0.001, ****P < 0.0001, and n.s. is not significant using an unpaired, two-tailed Student's *t* test. All data represent means ± standard deviation.



Extended figure 3.7. Transformed and proliferative cell lines produce fructose from glucose.

(A) Fructose and glucose can be chromatographically resolved with a pHILIC column (see Methods). (B to G) Enrichment of intracellular fructose in the indicated cell lines after labeling with 5mM $[U-^{13}C]$ glucose for 4 hours ($n=3$). All data represent means \pm standard deviation

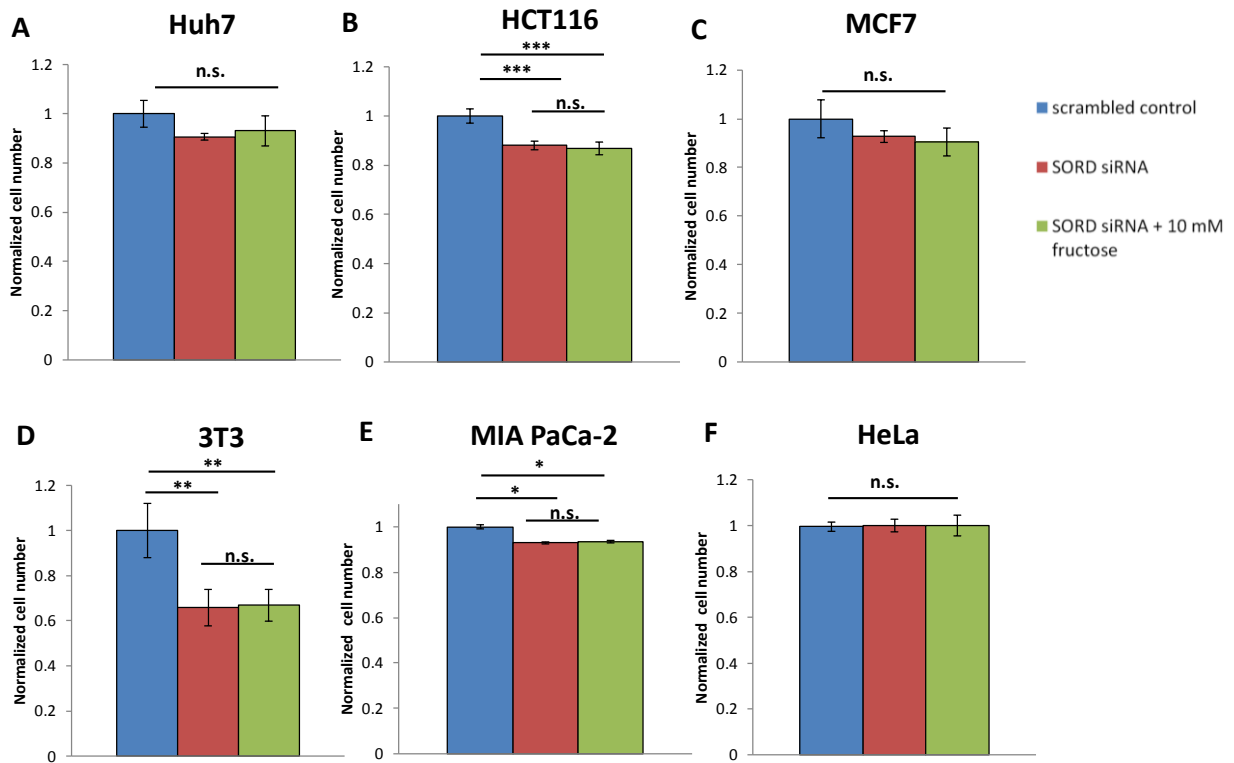


Sorbitol dehydrogenase siRNA

+ - + - + - + - + - + -

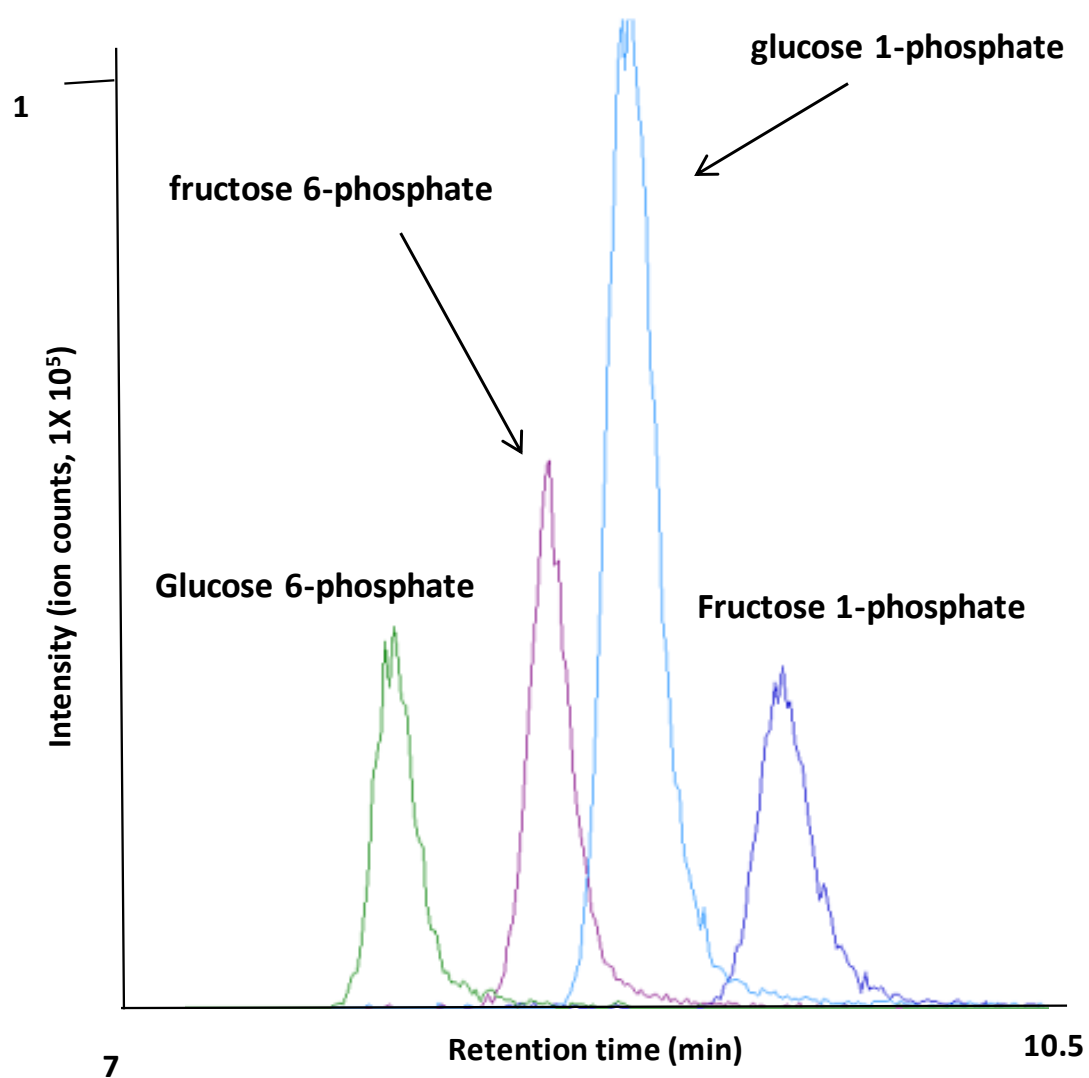
Extended figure 3.8. Sorbitol dehydrogenase expression is silenced by siRNA.

Western blot against the indicated cell lines after transfection with either sorbitol dehydrogenase siRNA (+) or scrambled control (-).



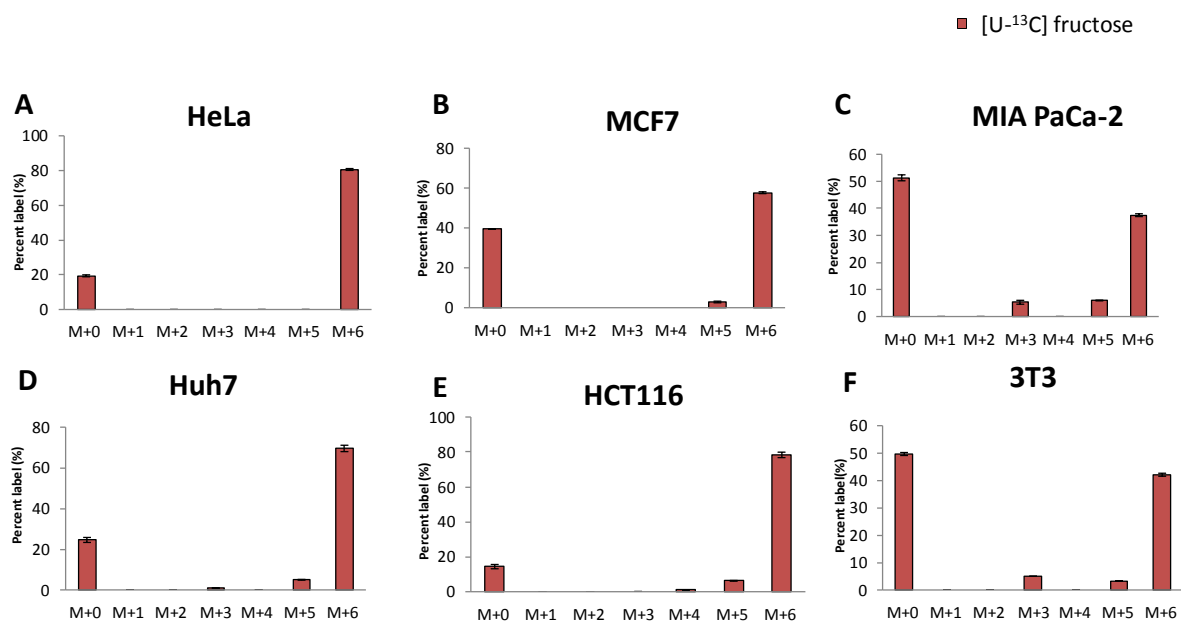
Extended figure 3.9. Endogenous fructose has no impact on proliferation.

(A to F) Relative cell number after treating the indicated cell lines for 4 days with sorbitol dehydrogenase siRNA (SORD siRNA, n=4-5), scrambled control siRNA (scrambled control, n=4-5), or sorbitol dehydrogenase siRNA and 10 mM fructose (SORD siRNA + 10 mM fructose, n=4-5). * $P < 0.05$, ** $P < 0.01$, *** $P < 0.001$, **** $P < 0.0001$, and n.s. is not significant using an unpaired, two-tailed Student's t test. All data represent means \pm standard deviation.



Extended figure 3.10. Fructose 1-phosphate is resolved from other hexose phosphates.

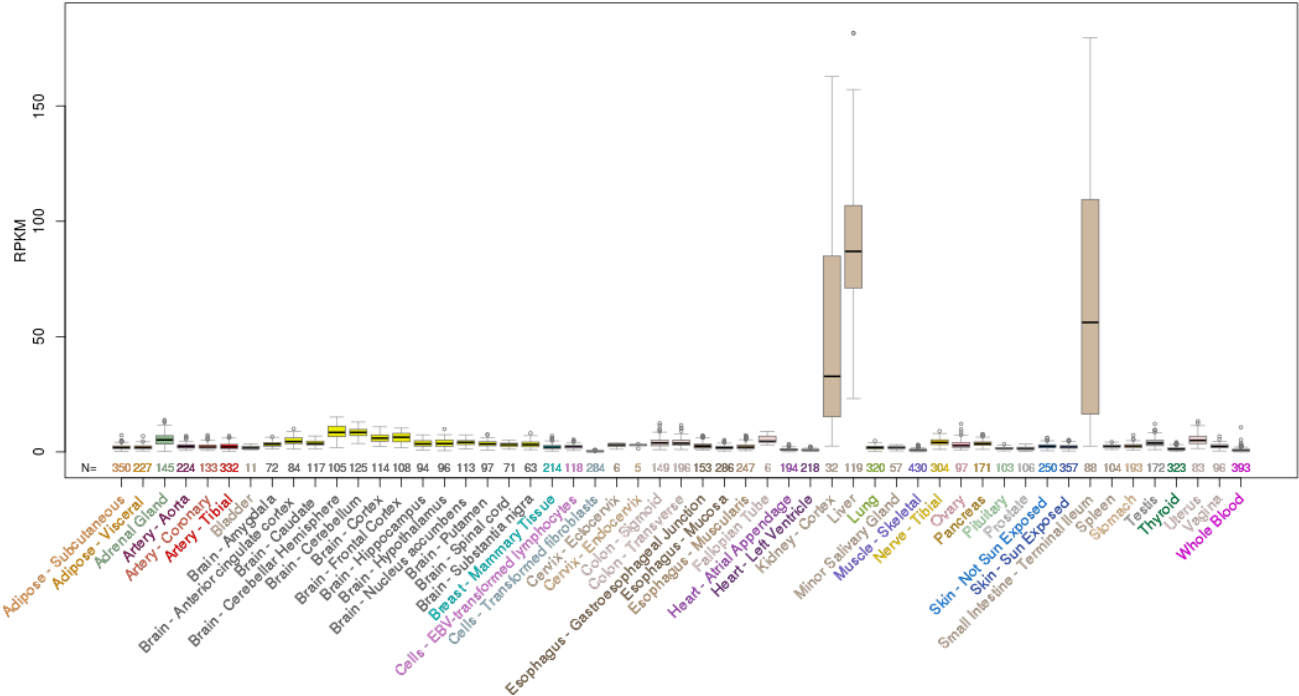
Analysis of 15 μM solutions of glucose 6-phosphate, fructose 6-phosphate, glucose 1-phosphate, or fructose 1-phosphate standards on a HILICpak VT 50-2D column. Each is chromatographically resolved from one another.



Extended figure 3.11. Transformed and proliferative cell lines produce fructose 1-phosphate.

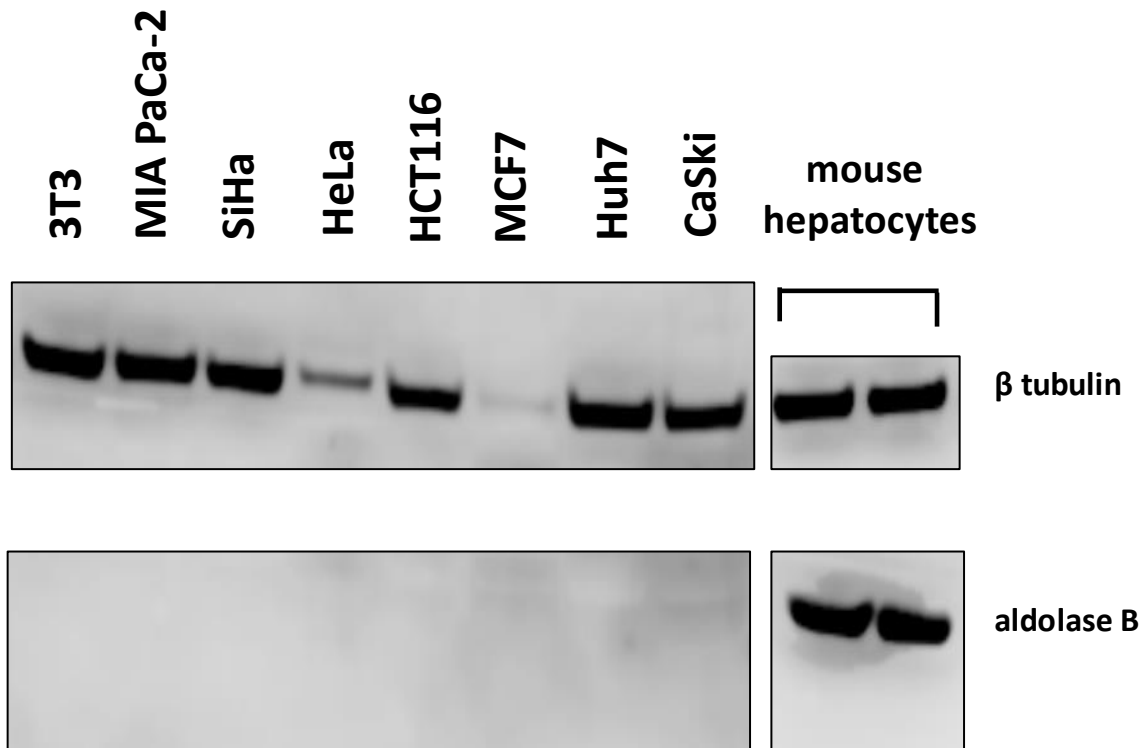
(A to F) Enrichment of fructose 1-phosphate in the indicated cell lines after labeling with [U-¹³C] fructose for 4 hours (n=3). Labeled fructose 1-phosphate indicates KHK expression. All data represent means ± standard deviation.

Gene Expression from GTEx



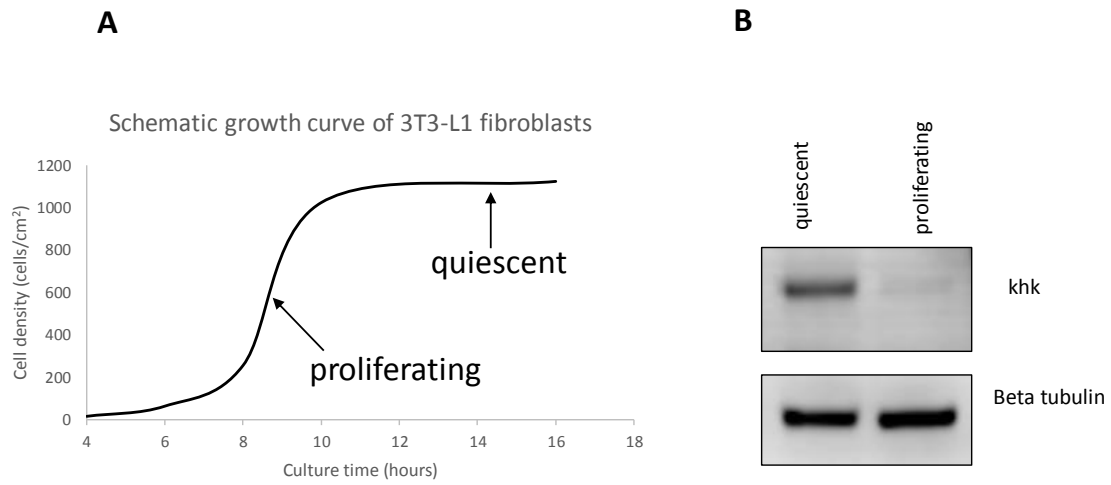
Extended figure 3.12. The *KHK* gene is expressed in common human tissues.

KHK is shown to be expressed in common human tissues from analyzing the Genotype-Tissue Expression (GTEx) data. Kidney, liver, and intestine have the highest *KHK* gene expression compared to other tissue types.



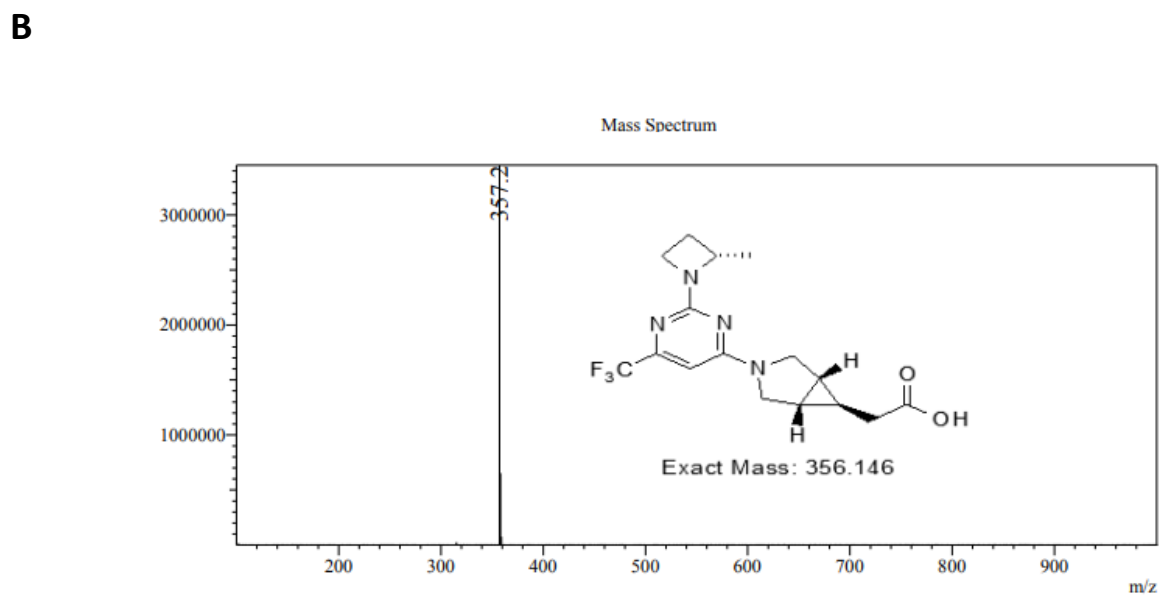
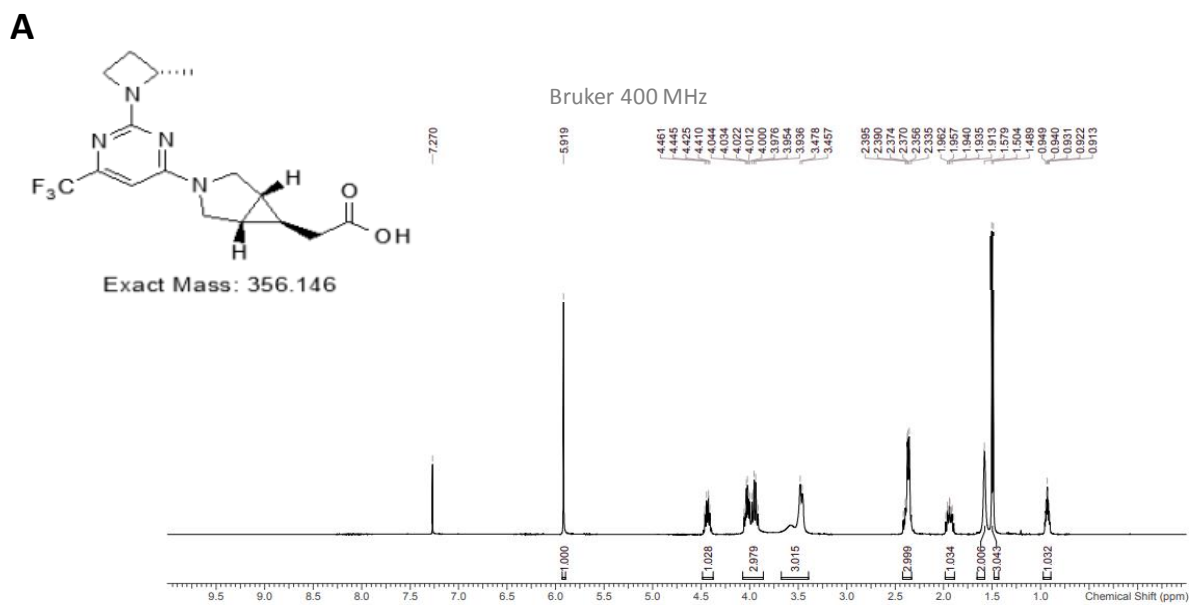
Extended figure 3.13. No tested cell lines express aldolase B.

Western blot against aldolase B in the indicated cell lines or mouse hepatocytes.



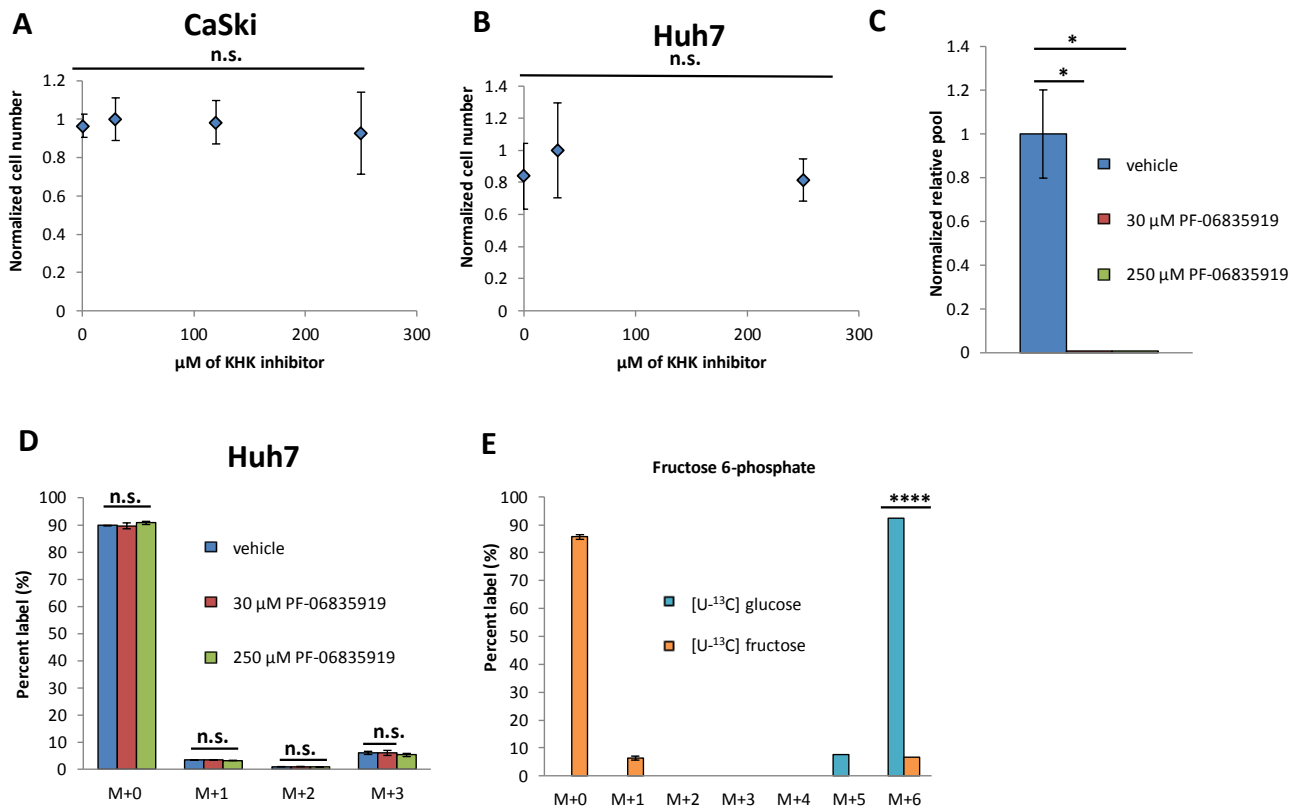
Extended figure 3.14. Proliferating 3T3-L1 cells decrease expression of KHK relative to quiescent state.

(A) Schematic to illustrate that proliferation of 3T3-L1 cells is contact inhibited when cells become confluent. 3T3-L1 cells were harvested at the points indicated to obtain cells in the proliferative or quiescent state. (B) Western blot against KHK in either quiescent or proliferating 3T3-L1 cells. The antibody used did not distinguish KHK isoforms.



Extended figure 3.15. Characterization of PF-06835919.

(A) Proton NMR and (B) mass spectrum of PF-06835919.



Extended figure 3.16. KHK-A is not important for growth of CaSki or Huh7 cells.

(A) Dose-response for PF-06835919 in CaSki cells. Response is measured as CaSki cell number ($n=3$ at each dose). (B) Dose-response for PF-06835919 in Huh7 cells. Response is measured as Huh7 cell number ($n=3$ at each dose). (C) Relative pool size of fructose 1-phosphate in Huh7 cells after treatment with vehicle ($n=3$), 30 μM PF-06835919 ($n=3$), or 250 μM PF-06835919 ($n=3$). Cells were cultured with 10 mM glucose and 10 mM fructose in the media. (D) ¹³C enrichment of lactate from Huh7 cells labeled with 5 mM [U-¹³C] fructose in the presence of vehicle ($n=3$), 30 μM PF-06835919 ($n=3$), or 250 μM PF-06835919 ($n=3$). (E) ¹³C enrichment of fructose 6-phosphate from CaSki cells after labeling with [U-¹³C] fructose ($n=3$) or [U-¹³C] glucose ($n=3$). * $P < 0.05$, ** $P < 0.01$, *** $P < 0.001$, **** $P < 0.0001$, and n.s. is not significant using an unpaired, two-tailed Student's t test. All data represent means \pm standard deviation.

Chapter 4: Organismal metabolism of fructose drives tumor growth

4.1 Introduction

In chapter 2, we observed that high fructose diets could increase tumor growth. In chapter 3, we established that the cancer cell lines do not metabolize fructose directly but co-culture of CaSki cells with hepatocytes were sufficient to transform fructose carbons into those useable for tumor growth. Therefore, in this chapter, we wish to consider how fructose is metabolized *in vivo* to produce tumor growth rate enhancement. It has been reported that fructose is robustly metabolized *in vivo* via organs such as the small intestine, liver, and kidney⁷⁴. Those organs express ketohexokinase-C and aldolase B. In the liver specifically, chronic high fructose consumption has been shown to be a significant contributor to fatty liver^{39,78–81}. However, since our tumors are distal to the liver, liver fat may not have a direct contribution to their growth. Fatty liver has been shown to contribute to insulin resistance^{82,83}. But in our nude mouse model over the timescale of our tumor growth assay, we show in chapter 2 that these mice are not insulin-resistant. Therefore, in this chapter, we assessed the metabolites that were produced from fructolysis and entered the general circulation where they would be available for tumor utilization. Using this approach, we showed that glucose is produced significantly from gluconeogenesis of the fructose label. We showed via administration of a high glucose diet that glucose can increase CaSki tumor growth. Furthermore, the growth-enhancing effects of fructose were blocked via administration of a ketohexokinase inhibitor on a high fructose diet. Administration of the inhibitor on a control diet had no effect. We then recapitulated most of these observations in a different cancer model: that *BRAF*^{V600E}-mutant; *p53*-deficient zebrafish melanomas. Thus, we show that organismal metabolism of fructose can drive tumor growth in the absence of tumor cell autonomous metabolism of fructose

4.2 Results

Fructose requires organismal metabolism to promote the growth of mouse cervical xenografts

Based on the results of our *in vitro* experiments, we speculated that the effect of fructose on tumor growth *in vivo* was not due to utilization of fructose in CaSki cells directly but rather a consequence of fructose first being converted into other nutrients by KHK-C expressing tissues. To assess the metabolism of fructose *in vivo*, mice were administered a 1:1 mixture of unlabeled glucose to [U-¹³C] fructose or mice were administered a 1:1 mixture of [U-¹³C] glucose to unlabeled fructose. First, we directly injected each 1:1 mixture into the tumors of different animals. After 20 minutes, we harvested the tumors and analyzed them by metabolomics for isotopic labeling. Similar to our results from cell culture, we observed extensive utilization of the glucose label but only minimal utilization of the fructose label (figure 4.1A). These differences in the extent of labeling reflect differences in the efficiency of glucose and fructose utilization by the tumor. We also noted that there was no evidence for intratumoral gluconeogenesis from the fructose label (extended data figure 4.1A).

In a second experiment, we administered each 1:1 mixture to separate mice by oral gavage. In contrast to the first set of injections described above, oral gavage resulted in similar labeling of metabolites within tumors irrespective of whether [U-¹³C] glucose or [U-¹³C] fructose was used (figure 4.1B). Additionally, we found substantial labeling of intratumoral glucose from [U-¹³C] fructose, suggesting that [U-¹³C] fructose was used as a substrate for gluconeogenesis in non-tumor tissues (figure 4.1C). An analysis of [U-¹³C] glucose in the serum as a function of time after oral gavage with either [U-¹³C] glucose or [U-¹³C] fructose revealed similar kinetic curves, indicating that fructose is readily transformed into glucose (figure 4.1D). It is interesting that

fructose contributes to gluconeogenesis even when co-administered with stoichiometric amounts of glucose. The result is consistent with previous work showing that fructose activates the carbohydrate-response element-binding protein (ChREBP), which overrides the ability of insulin to suppress gluconeogenesis from fructose^{74,84}. After oral gavage of either [U-¹³C] glucose or [U-¹³C] fructose, labeling of lactate and alanine in the serum were also similar (extended data figure 4.1B,C). These data further highlight that [U-¹³C] fructose is readily transformed in non-tumor tissues. Finally, given that much of the gavaged fructose was rapidly converted into glucose, we wished to determine whether a high-glucose diet itself would promote the growth of CaSki tumors. Similar to high-fructose diets, we found this to be the case (figure 4.1E).

Administration of clinical candidate PF-06835919 impairs fructose-mediated growth

Our results indicate that fructose-derived nutrients such as glucose promote tumor growth and are produced by KHK-C activity in distal, non-cancer tissues. Thus, we sought to evaluate the effect of systemic KHK-C inhibition on tumor growth. For inhibition, we used the KHK inhibitor PF-06835919, which we already established had no direct effect on the proliferation of CaSki cells themselves (extended data figure 3.16A). We found that intraperitoneal administration of increasing concentrations of PF-06835919 led to a dose-dependent increase in mouse serum fructose, suggesting that utilization of fructose declined upon addition of the inhibitor (figure 4.1F). At a drug dose of 50 mg/kg, we also found that label from a large bolus of 1.5g/kg [U-¹³C] fructose was not readily utilized (figure 4.1G). We note that PF-06835919 was still detected in the serum 25 hours after a single 50 mg/kg dose (extended data figure 4.2). Accordingly, we administered a daily 50 mg/kg dose of PF-06835919 to mice on a control diet. As expected, the drug had no effect on tumor growth (figure 4.1H). Administration of the drug to mice on a high-fructose diet, however, significantly decreased tumor growth (figure 4.1I). Collectively, these data show that while fructose carbon cannot be readily utilized by the tumor directly, tumor

growth can still be mediated by the KHK-C dependent transformation of fructose into other nutrients, such as glucose. Furthermore, we provide evidence that administration of a clinical candidate, PF-06835919, can curtail fructose-mediated tumor growth.

Fructose requires organismal metabolism to promote the growth of melanoma tumors in zebrafish

Our mouse cervical xenograft model revealed that metabolism of fructose carbons by the animal is sufficient to promote cervical tumor growth. To begin to explore the applicability of our results beyond this model, we wished to use not only a different cancer model but also a different organism. Previous studies have shown that *BRAF*^{V600E}-mutant; *p53*-deficient zebrafish melanomas are responsive to insulin and high-fat/ketogenic diets and that the onset of tumors is sensitive to the amount of feeding^{10,85-87}. Furthermore, several studies in juvenile or adult zebrafish have shown that fructose administration can induce fatty liver, changes in metabolic gene expression, and changes in serum metabolite levels⁸⁸⁻⁹⁰. Thus, we chose to investigate the effect of fructose on the *BRAF*^{V600E}-mutant; *p53*-deficient zebrafish melanoma model (hereafter referred to as *BRAF/p53* fish), in which *BRAF*^{V600E} is under the control of the melanocyte-specific *mitfa* promoter.

The effects of fructose on tumor growth were evaluated by performing a tumor-regrowth assay (extended data figure 4.3A). Here, we first amputated the *BRAF/p53* melanomas of a cohort of fish so that the tumor surface was flush with the surface of the skin. For every resected-tumor fish, however, tumor tissue remained under the surface of the skin to allow for tumor regrowth. We then randomly transferred the resected-tumor fish to either normal water as a control or water containing 100 mM fructose. After 2 weeks, there was significant regrowth of the tumors in fructose water, while there was only minimal regrowth of tumors in control water (extended data figure 4.3B). Although fish were immersed in a relatively high concentration of fructose,

their serum fructose was only 4 mM, most likely because they do not efficiently take up fructose from the water (extended data figure 4.3C).

To determine whether fructose is metabolized directly by these melanoma tumors, we amputated a tumor from *BRAF/p53* fish, formed a single-cell suspension, and plated the cells *ex vivo* for cell-culture analysis. We then labeled the cells with either [U-¹³C] glucose or [U-¹³C] fructose. Even though the melanoma cells in each condition were viable at the end of the experiment, ¹³C-label from glucose was efficiently incorporated into metabolites whereas ¹³C-label from fructose was not (extended data figure 4.4A,B). These data are consistent with those from all of the cell lines we tested and suggest that melanoma tumors in zebrafish can efficiently use glucose as a substrate, but not fructose. Similarly, as observed for other cell lines, *ex vivo* melanomas produced fructose endogenously from glucose and can transform fructose into fructose 1-phosphate (extended data figure 4.5A,B).

Next, we aimed to compare glucose and fructose metabolism in the tumors of the *BRAF/p53* fish. To accomplish this, we transferred fish to water containing either 50 mM [U-¹³C] glucose or 50 mM [U-¹³C] fructose. Fish were kept in the ¹³C-labeled water for 30 hours prior to analysis to achieve isotopic steady state. We measured comparable labeling in intratumor glucose, lactate, and several TCA cycle intermediates from both [U-¹³C] glucose and [U-¹³C] fructose, suggesting gluconeogenesis of the fructose label as we observed in mice bearing CaSki tumors (extended data figure 14A-D). Indeed, serum metabolites were also similarly labeled by [U-¹³C] glucose and [U-¹³C] fructose (extended data figure 4.6). To assess whether fructose utilization was KHK dependent, we administered a 50 mg/kg intraperitoneal injection of PF-06835919 prior to soaking animals in 50 mM [U-¹³C] fructose for 12 hours. With PF-06835919 treatment, we observed an increase in total serum fructose and a decrease in M+3 glucose (which is a signature

for gluconeogenesis) relative to control animals given a vehicle injection (extended data figure 4.7A,B). These results indicate that [U-¹³C] fructose is primarily metabolized by KHK in zebrafish. Protein analysis also revealed expression of aldolase B (extended data figure 4.7C) in the livers of zebrafish, which is required to transform fructose carbon into glycolytic intermediates (figure 3.2A). We conclude that fructose increases the rate of tumor growth in *BRAF/p53* zebrafish but, like we found for a xenograft model of cervical cancer in mice, fructose cannot be efficiently used by the tumor directly. Rather, it is fructose-derived nutrients produced by non-cancerous tissues that promote tumor growth.

4.3 Discussion

In this chapter, we show that while CaSki tumors don't metabolize fructose directly, ketohexokinase-dependent conversion of ingested fructose to other metabolites results in tumor growth. This is supported by the observation that daily administration of a ketohexokinase inhibitor blocks the effects of fructose mediated growth on the CaSki tumor. One of the most ¹³C- enriched serum metabolites resulting from administration of ¹³C-labeled fructose to mice is glucose. Gluconeogenesis from fructose in the post-prandial period results in glucose carbons which enter the circulation, raising serum glucose levels. That glucose can be metabolized to other secondary metabolites or feed the tumor directly. Administration of a high glucose diet is sufficient to increase the growth of CaSki xenografts. Therefore, we provide evidence that increased glucose availability in an organism can enhance the growth of some tumors. We also show that *BRAF*^{V600E}-mutant; *p53*-deficient zebrafish melanomas regrow faster in the presence of either glucose or fructose, while the melanomas themselves do not metabolize fructose well *ex vivo*. Like in the nude mice, zebrafish also metabolize a significant portion of their carbons to

forming new glucose molecules in the serum. Thus, we have discovered at least one metabolite from organismal fructose metabolism that can support tumor growth.

Like mice and zebrafish, humans also can also form new glucose molecules from fructose^{91,92}. Reports of the efficiency of gluconeogenesis from fructose in humans are varied, however, with most studies indicating that less glucose is made from a fructose bolus than the resulting glucose load from an equivalent glucose bolus. However, most of these studies administer glucose and fructose separately⁹²⁻⁹⁴. It is well-described that fructose is not absorbed as well as glucose when each sugar is administered alone^{46,74,95,96}. This difference in intestinal absorption of each sugar may contribute to why there is less glycemic change with fructose ingestion vs glucose ingestion. Co-administration of fructose with glucose results in much greater absorption of fructose^{95,97}. But few studies have assessed glucose production from fructose with glucose co-administration in humans as we did in this chapter in mice; notwithstanding, fructose is almost always consumed in the human diet along with glucose in the form of sucrose or high fructose corn syrup and is almost never consumed as the sole sugar. Furthermore, fructose is one of the only nutrients that can still undergo robust gluconeogenesis in the presence of glucose. In response to a postprandial insulin spike, especially with a high sugar meal, gluconeogenesis from most nutrient sources is shut off. However, fructose is unique in its ability to produce glucose even in the presence of raised levels of insulin and glucose. This is due to its potent activation of the carbohydrate-response element-binding protein (ChREBP), which overrides insulin signaling in regulating fructose metabolism⁸⁴. This allows fructose to contribute to gluconeogenesis even in a postprandial state. Certain tumors maybe be able to capitalize on this increased glucose availability to promote tumor replication.

Figures

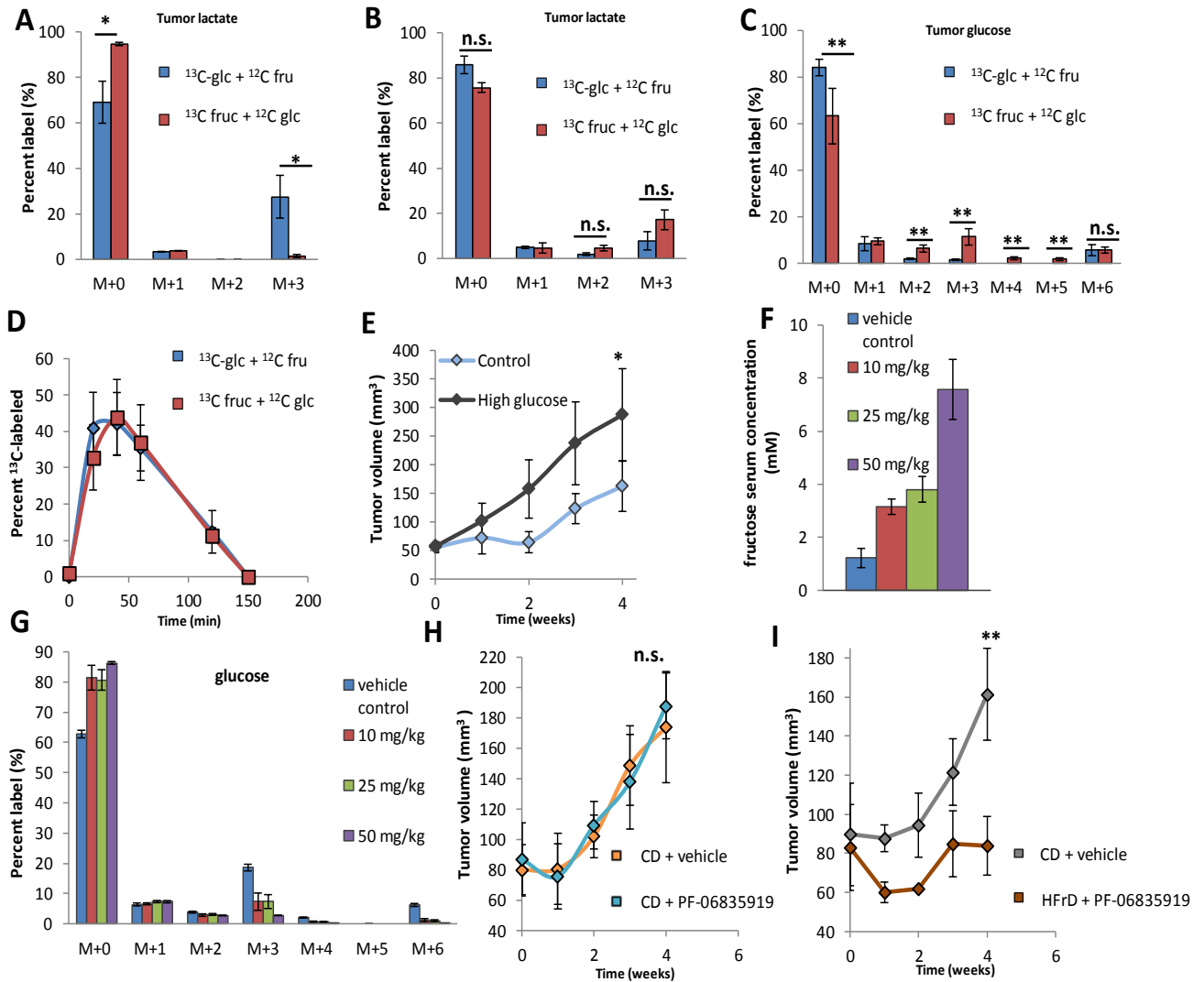
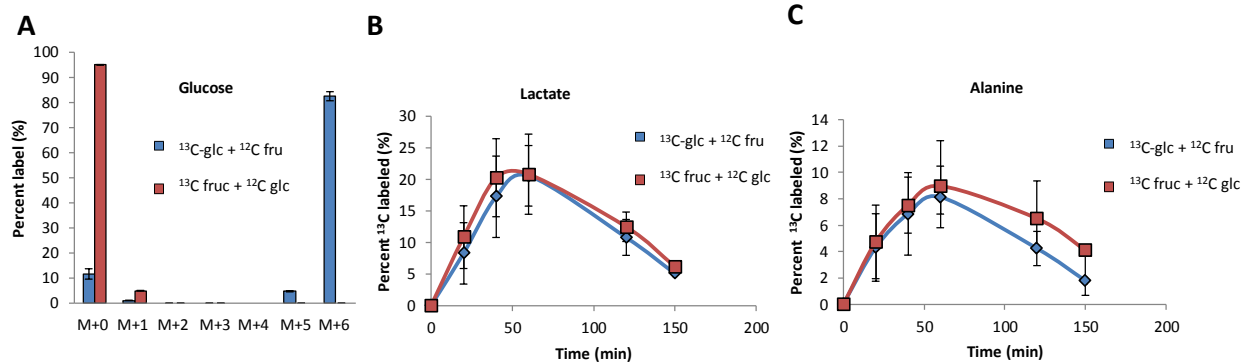


Figure 4.1. Organismal metabolism of fructose drives tumor growth.

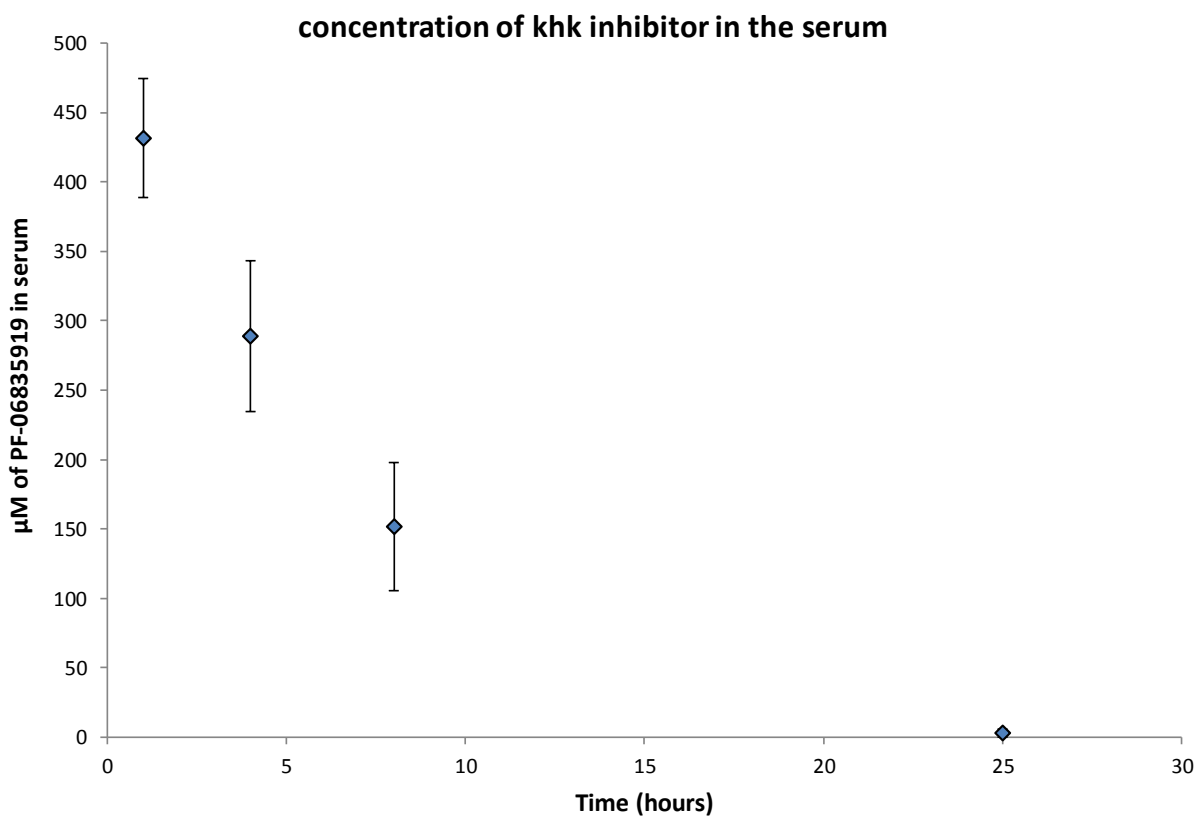
(A) ^{13}C labeling of intratumor lactate from a CaSki xenograft after either direct intratumor injection of 1:1 [^{13}C] glucose : ^{12}C fructose (n=3) or 1:1 [^{13}C] fructose : ^{12}C glucose (n=3). (B) ^{13}C labeling of intratumor lactate from a CaSki xenograft after oral gavage with 1:1 [^{13}C] glucose : ^{12}C fructose (n=4) or 1:1 [^{13}C] fructose : ^{12}C glucose (n=4). (C) ^{13}C labeling of intratumor glucose from a CaSki xenograft after oral gavage with 1:1 [^{13}C] glucose : ^{12}C fructose (n=4) or 1:1 [^{13}C] fructose : ^{12}C glucose (n=4). (D) Time course of total ^{13}C enrichment in serum glucose after oral gavage with either 1:1 [^{13}C] glucose : ^{12}C fructose (n=4) or 1:1 [^{13}C] fructose : ^{12}C glucose (n=4). (E) Relative growth of CaSki xenografts from mice fed either a high glucose diet (n=7) or a control diet (n=5). (F) Concentration of fructose in the serum of mice 30 minutes after administration of [^{13}C] fructose and 75 minutes after the indicated doses of PF-06835919 (n=3-4, per dose). (G) Labeling of serum glucose 30 minutes after administration of [^{13}C] fructose and 75 minutes after the indicated doses of PF-06835919 (n=3-4, per dose). (H) Relative growth of CaSki xenografts in response to daily IP injection of vehicle (n=4) or 50 mg/kg PF-06835919 (n=4) on a control diet (CD). (I) Relative growth of CaSki xenografts in response to daily IP injection of vehicle (n=4) or 50 mg/kg PF-06835919 (n=4) on a control diet (CD) or high fructose diet (HFrD). * $P < 0.05$, ** $P < 0.01$, *** $P < 0.001$, **** $P < 0.0001$, and n.s. is not significant using an unpaired, two-tailed Student's t test. All data represent means \pm standard deviation.

Extended Data Figures



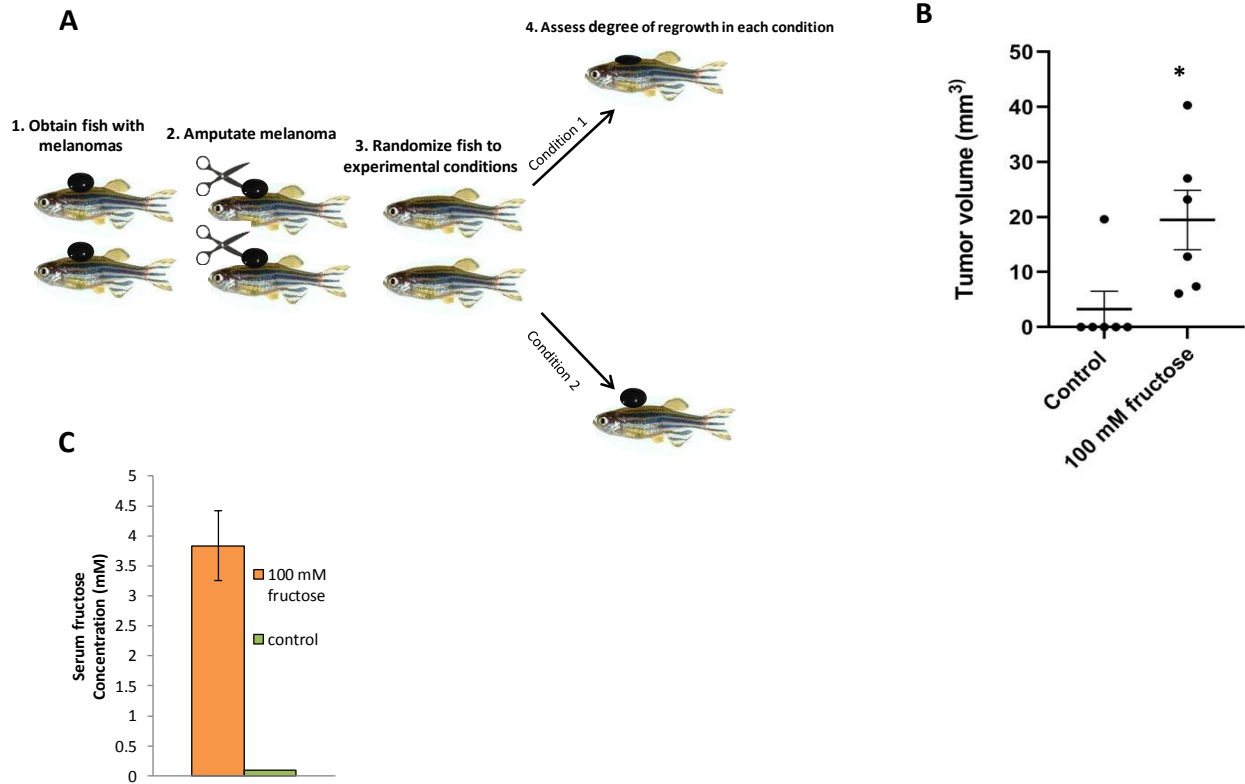
Extended figure 4.1. Fructose is not in metabolized CaSki tumors directly but is readily metabolized by the organism.

(A) ^{13}C enrichment of intratumor glucose from CaSki xenografts 20 minutes after injection of either [U- ^{13}C] glucose (n=4) or [U- ^{13}C] fructose (n=4) into the tumor. Time course of total ^{13}C enrichment in (B) serum lactate or (C) serum alanine after oral gavage with either 1:1 [U- ^{13}C] glucose : ^{12}C fructose (n=4) or 1:1 [U- ^{13}C] fructose : ^{12}C glucose (n=4). * $P < 0.05$, ** $P < 0.01$, *** $P < 0.001$, **** $P < 0.0001$, and n.s. is not significant using an unpaired, two-tailed Student's t test. All data represent means \pm standard deviation



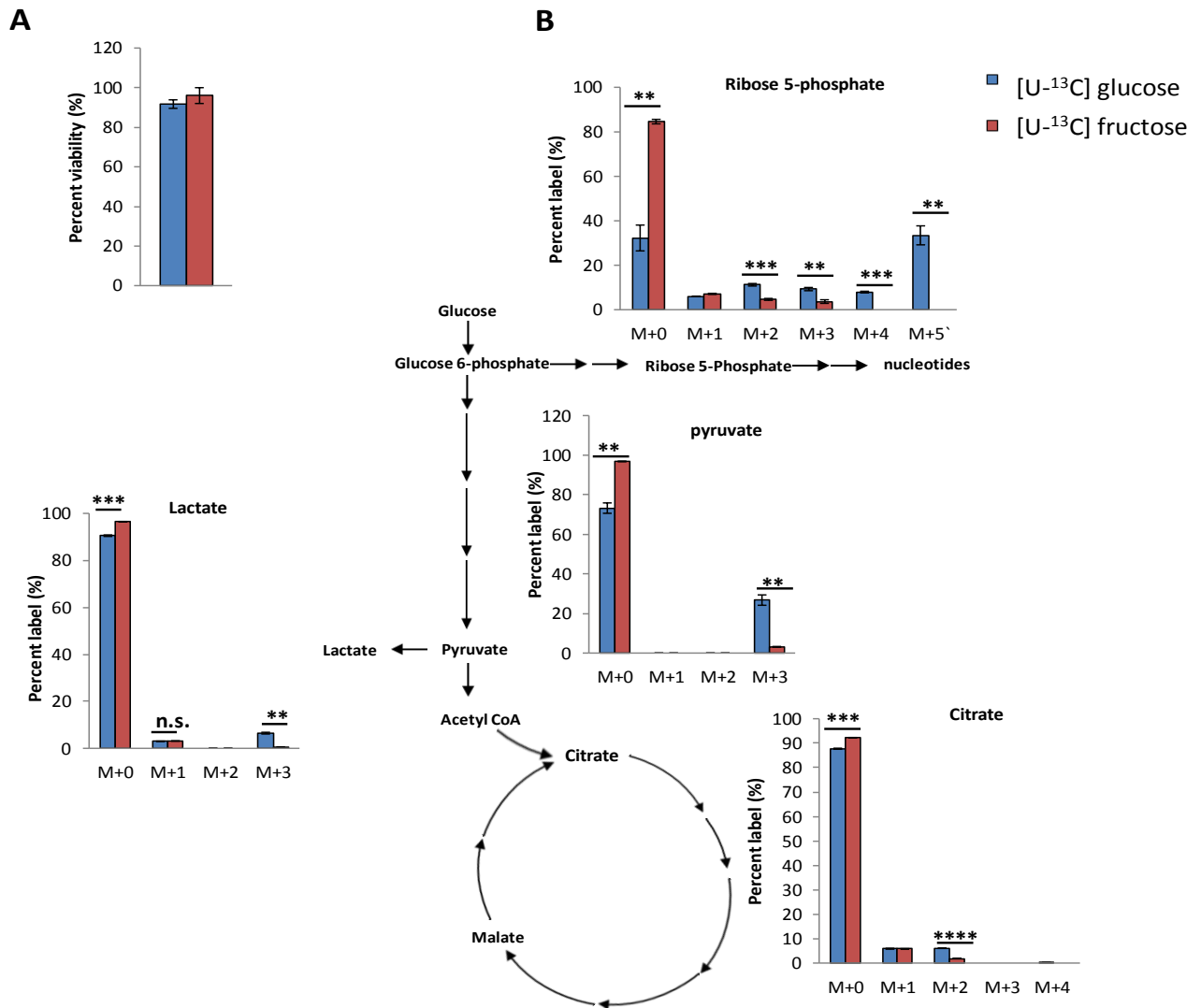
Extended figure 4.2 Single 50 mg/kg dose of PF-06835919 remains in mouse serum for over 24 hours.

Concentration of PF-06835919 in nude mouse serum after an IP-injection at a dose of 50 mg/kg. Measurements were made at 1 hour, 4 hours, 8 hours, and 25 hours post-injection (n=4 mice per data point). All data represent means \pm standard deviation.



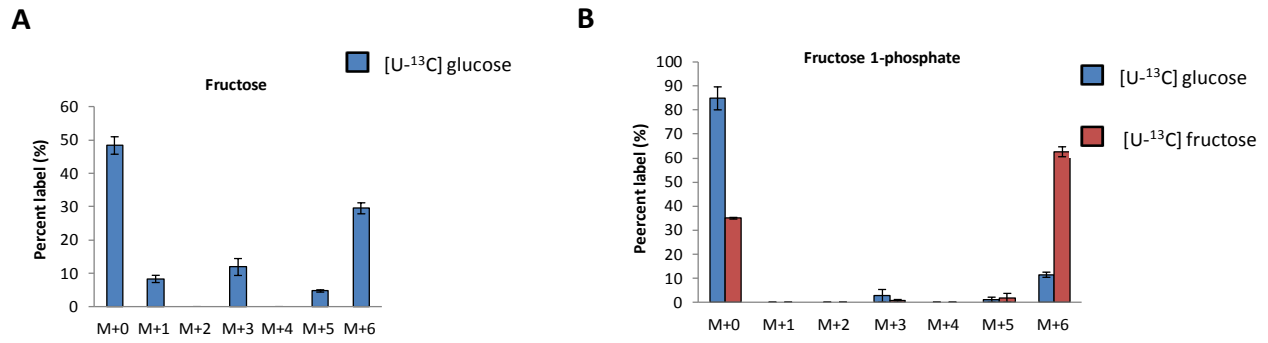
Extended figure 4.3. BRAF/p53 melanoma regrows faster in the presence of fructose.

(A) Schematic illustrating the tumor-regrowth assay. (B) Tumor-regrowth assay from *BRAF/p53* zebrafish in control water (n=6) or water containing 100 mM fructose (n=6). Data represent means \pm SEM. (C) Serum fructose concentration after soaking fish in 100 mM fructose for 30 hours (n=4). Data represent means \pm standard deviation.



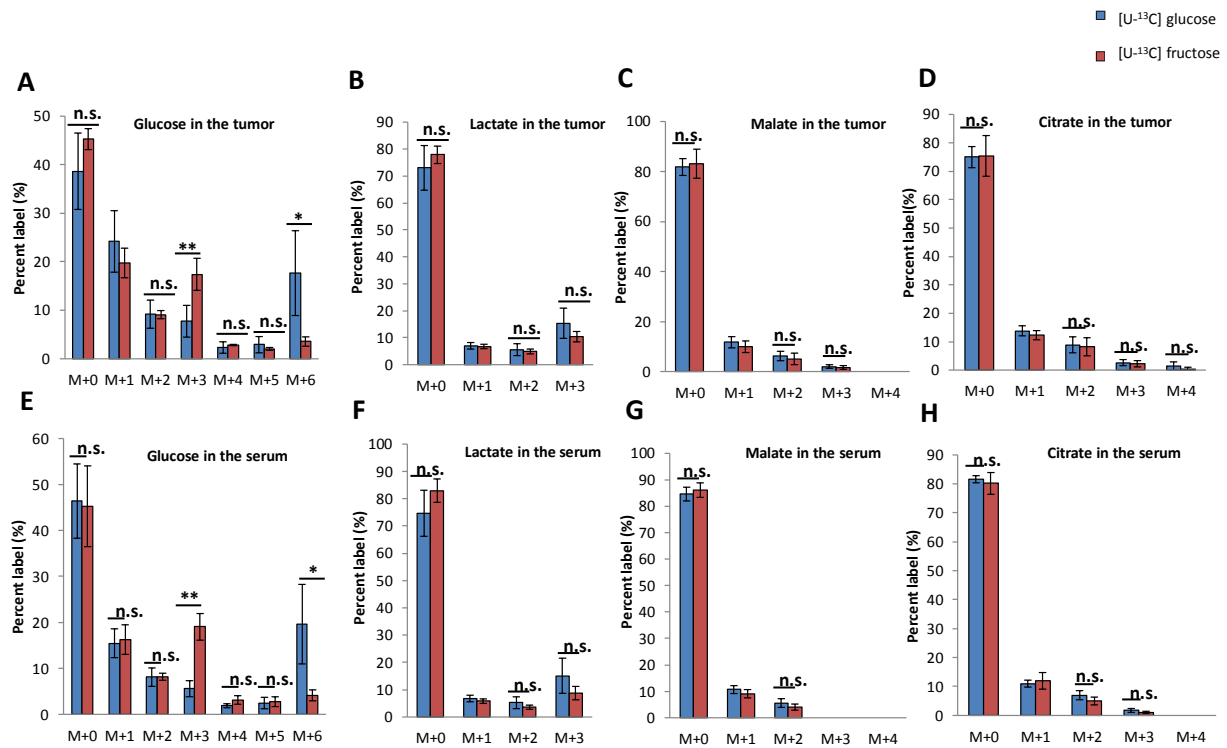
Extended figure 4.4. *BRAF/p53* melanoma plated *ex vivo* do not efficiently metabolize fructose.

(A) Viability of zebrafish melanoma after 4 hours of *ex vivo* culture in media containing either [U-¹³C] glucose (n=3) or [U-¹³C] fructose (n=3) as the only sugar source in the DMEM. (B) ¹³C enrichment of various metabolites from central carbon metabolism after 4 hours of labeling zebrafish *BRAF/p53* melanoma tumors plated *ex vivo* with either [U-¹³C] glucose (n=3) or [U-¹³C] fructose (n=3). *P < 0.05, **P < 0.01, ***P < 0.001, ****P < 0.0001, and n.s. is not significant using an unpaired, two-tailed Student's *t* test. All data represent means ± standard deviation.



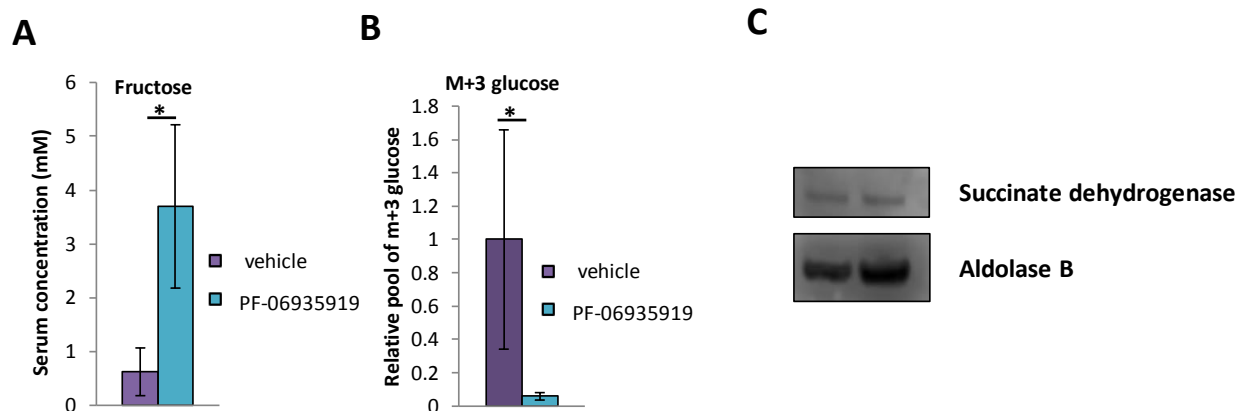
Extended figure 4.5. *Ex vivo* BRAF/p53 zebrafish melanomas produce endogenous fructose and fructose 1-phosphate.

(A) ¹³C enrichment of fructose after labeling *ex vivo* zebrafish melanomas with [U-¹³C] glucose for 4 hours (n=3). (B) ¹³C enrichment of fructose 1-phosphate after labeling *ex vivo* zebrafish melanoma with either [U-¹³C] glucose (n=3) or [U-¹³C] fructose (n=3) for 3 hours. All data represent means ± standard deviation.



Extended figure 4.6. Fructose carbons enter *BRAF/p53* zebrafish melanoma via metabolite exchange.

^{13}C enrichment of (A) intratumor glucose, (B) intratumor lactate, (C) intratumor malate, (D) intratumor citrate, (E) serum glucose, (F) serum lactate, (G) serum malate, or (H) serum citrate after soaking fish in either 50 mM $[\text{U-}^{13}\text{C}]$ glucose (n=6) or 50 mM $[\text{U-}^{13}\text{C}]$ fructose (n=4) for 30 hours. * $P < 0.05$, ** $P < 0.01$, *** $P < 0.001$, **** $P < 0.0001$, and n.s. is not significant using an unpaired, two-tailed Student's t test. All data represent means \pm standard deviation



Extended figure 4.7. *BRAF/p53* Zebrafish metabolize fructose via KHK and aldolase B.

Relative pool size of (A) ^{13}C -fructose and (B) M+3 glucose in zebrafish serum after soaking fish in 20 mM $[\text{U}-^{13}\text{C}]$ fructose water following IP injection of vehicle (c, n=5) or after soaking fish in 20 mM $[\text{U}-^{13}\text{C}]$ fructose and 190 μM PF-06835919 water following an IP injection of 50 mg/kg PF-06835919 (drug, n=4). Fish in each experimental condition were placed in their respective fructose-labeled water conditions an hour after IP injection of PF-06835919 or vehicle. They were then soaked in fructose-labeled water for 12 hours. (C) Western blot from two zebrafish livers against aldolase B. * $P < 0.05$, ** $P < 0.01$, *** $P < 0.001$, **** $P < 0.0001$, and n.s. is not significant using an unpaired, two-tailed Student's t test. All data represent means \pm standard deviation.

Chapter 5: Conclusions

In this study, we have shown that high-fructose diets promote the growth of cervical cancer tumors in mice and melanoma tumors in zebrafish. Interestingly, however, fructose itself does not support the growth of any cancer cell line that we tested *in vitro*, even though these cell lines also produce fructose endogenously. By tracking isotopic labels on fructose, we demonstrated that tumors of cervical cancer from mice and melanoma tumors from zebrafish cannot efficiently use fructose carbon directly because they do not express KHK-C. These results were conserved in every transformed and proliferative cell line that we tested. Although the cells do express hexokinase and KHK-A, both enzymes have only a limited capacity to support fructolysis under physiological conditions. The tumor-enhancing effects of dietary fructose are therefore not cell autonomous. Rather, *in vivo*, fructose is readily metabolized by non-cancerous tissues expressing KHK-C in both mice and zebrafish. Notably, even when fructose and glucose are co-administered, these tissues use gluconeogenesis to transform fructose into glucose, which we showed is sufficient in itself to enhance the growth of cervical cancer tumors in mice. Together, our results support a mechanism where fructose promotes tumor growth through metabolite exchange with otherwise healthy (i.e., non-malignant) tissues expressing KHK-C.

As we show in extended data figure 3.12, expression of KHK is not limited to the liver. Actually, most tissues in the human body express low levels of KHK. When evaluating fructose metabolism, it is important to distinguish between KHK-A and KHK-C. The liver, small intestine, and kidney express high levels of KHK-C, which enables efficient fructolysis. Aldolase B expression is also restricted to these same organs^{74,98}. Most other tissues, in contrast, only express KHK-A. Although the function of KHK-A is still incompletely understood, we have shown that KHK-A does not support efficient utilization of fructose carbon in the context of

cancer. Consequently, detection of fructose 1-phosphate or KHK in a tissue without isoform discrimination is not a sufficient indicator of fructose metabolism by that tissue.

To begin to extend the applicability of our mechanism beyond animal models, we analyzed tumors from 99 patients with cervical cancer. These tumors expressed KHK-A, but not KHK-C. Such an expression pattern may be applicable to other human cancers as well, even those derived from liver and kidney. Although healthy liver and kidney tissue express high levels of KHK-C and aldolase B, liver and kidney tumors have been shown to decrease expression of these enzymes^{99,100}. Even cancers of the liver and kidney may therefore depend upon cell non-autonomous metabolism of fructose in their surrounding organ microenvironments for fructose-induced growth.

Historically, chemotherapies inhibiting metabolism have mostly focused on targeting the tumor itself¹⁰¹. Here, we offer support for an alternative therapeutic paradigm where the metabolism of otherwise healthy tissues is targeted. PF-06835919, an inhibitor of KHK-A and KHK-C, did not affect the growth of CaSki cells *in vitro*. This result is consistent with KHK-A, which is expressed in CaSki cells, not having an important role in cancer cell growth. Yet, when PF-06835919 was administered to mice bearing tumors, the drug inhibited the growth-promoting effects of dietary fructose by preventing metabolite exchange with non-malignant tissues expressing KHK-C. KHK is an attractive drug target because it is a non-essential metabolic enzyme whose loss is not harmful to the organism^{65,102,103}. Indeed, essential fructosuria is a benign, asymptomatic condition in which individuals have a deficiency in KHK. In these patients, fructose is wasted in the urine¹⁰³. Our data reveal that there may be a role for using a KHK inhibitor as a treatment for some cancer patients, particularly those with high sugar intake. There may be complementary benefits of KHK inhibition in the treatment of cancer as well,

independent of fructose metabolite exchange. Fructose comprises a significant portion of the daily caloric intake in the United States^{32,34}. KHK inhibition could therefore lead to caloric restriction, which has been shown to curtail the growth of several types of cancers^{104,105}. Additionally, KHK has been shown to have a role in mediating the effects of high glucose consumption, with loss of KHK rescuing high glucose-induced weight gain and metabolic syndrome¹⁰⁶. KHK inhibition in the setting of high glucose consumption might thus also have an impact on tumors that respond to high dietary glucose.

Chapter 6: Future directions for completed work

Colon cancer metastases express KHK-C

One of the key results of this manuscript is that most cancerous tissue types express KHK-A.

Furthermore, we show that for several cancer cell lines, inhibition of intratumor KHK-A with PF-06835919 does not reduce growth of tested cancer cell lines. KHK-A expression is also not correlated with tumor stage, tumor recurrence, or patient survival in patients with cervical cancer. KHK-A metabolizes fructose very poorly, as the enzyme has a high k_m for fructose. Its primary function remains unknown. KHK-C, on the other hand, robustly metabolizes both endogenous and exogenous sources of fructose. Thus, the expression of KHK-C in a cancer cell would profoundly alter its metabolism. Therefore, we sought to identify any contexts under which a tumor might express KHK-C.

We thought it highly likely that primary colon tumors express KHK-A, as we and others have shown that the normal colon tissue primary expresses KHK-A⁶⁴. Furthermore, HCT116 cells, derived from human colon cancer, express KHK-A and don't metabolize fructose (figure 3.2D and extended figure 3.2E). A significant fraction of primary colon tumors metastasize to the liver, with up to 25% of all patients who present with colon cancer already having liver metastases at the time of tumor detection^{107,108}. We hypothesized that colon tumors that metastasize to the liver may begin to express KHK-C, as colon tumors that metastasize to the liver express higher levels of aldolase B than primary colon tumors⁴⁷

To investigate the expression of different KHK isoforms (figure 6.1A) in colon cancer and associated liver metastasis, we used Cufflinks¹⁰⁹ to calculate the isoform expression using RNA-seq data from a colorectal cancer (CRC) cohort (N=18) with matched adjacent normal and liver-metastatic samples. Overall, we observed an upregulation of the KHK gene in the primary tumor

and metastatic samples comparing to the adjacent normal samples (6.1 figure B,C,D). However, different isoforms (KHK-A, KHK-C, and KHK-203) showed different patterns in their changes in expression during tumor progression. KHK-A has low expression (FPKM = 4.31 ± 2.57) in the normal samples, which only increases to 8.78 ± 5.71 in the primary cancer samples, while shows no further significant increase in the metastatic samples (10.74 ± 6.56) (figure 7C,D). Expression levels of KHK-203 are similar to KHK-A in the adjacent normal and primary cancer samples, but show a significant increase in the metastatic samples (figure 6.1C,D). While 0% of patients have KHK-A with FPKM larger than 25, 55.56% (i.e. 10 out of 18) have KHK-203 with FPKM larger than 25 in metastatic samples (figure 7D) (Fisher's exact test, $p = 0.000344$). KHK-C shows virtually no expression (FPKM = 0.67 ± 0.49) in the adjacent normal samples (figure 6.1C,D). In contrast to KHK-A and KHK-203's upregulation in the primary cancer samples, KHK-C still shows very low expression levels in the primary cancer samples (figure 6.1C,D). However, the expression of KHK-C is greatly upregulated in the metastatic samples (figure 6.1C,D). The upregulation of KHK-203 (FPKM from ~ 8.42 in the primary samples to ~ 31.97 in the metastatic samples; with both Exons 3A and 3C) and especially KHK-C (FPKM from ~ 0.71 in the primary samples to ~ 24.06 in the metastatic samples; only with Exon 3C), represents a selection for the specific Exon 3C of the KHK gene in tumor metastasis. These patterns are also validated by counting isoform specific junction reads (figure 6.1E) and evaluating normalized expression of junction reads (figure 6.1F).

These data reveal that human colon cancer liver metastases begin expressing KHK-C upon metastases to the liver, while the primary colon tumors express KHK-A. This observation implicates PF-06835919, a potent KHK inhibitor, as a therapeutic to slow the growth of colon liver metastases, which already also express aldolase B. The expression of both KHK-C and

aldolase B not only confers an ability for the metastasized tumors to robustly metabolize dietary fructose but also enables a profound rewiring of glucose metabolism as a result of endogenous fructose production (figure 6.2). In every tested cancer line or tumor type, we see evidence of endogenous fructose production via the polyol pathway (figure 3.1G, extended data figure 3.7 B-G, extended figure 4.5B). Expression of KHK-C and aldolase B in a cancer cell can allow for this endogenously-produced fructose to enter glycolysis downstream of the rate-limiting step of glycolysis, phosphofructokinase-1 (PFK-1) (figure 6.2). Thus, the glucose that enters the intrahepatic metastatic colon cancer cell can be metabolized to fructose which is then metabolized via KHK-C and aldolase B to enter glycolysis as phosphorylated trioses (figure 6.2). By bypassing PFK1, a major bottleneck of glycolytic flux, this process could greatly increase the rate of glucose metabolism and thus the growth rate of the tumor. Generation of mouse models to study colon cancer and associated liver metastases could be initiated to investigate these hypotheses and gain more insight into the mechanism behind this KHK isoform switch observed in human colon cancer patients.

The role of fructose metabolism in intrahepatic tumors

Fructose is a major contributor to liver fat and non-alcoholic fatty liver disease. This is achieved via 1) direct fructose carbon contribution to triglyceride and fatty acid production and 2) fructose-dependent activation of carbohydrate-response element-binding protein (ChREBP) to rewire liver metabolism, enhancing hepatic *de novo* lipogenesis. In terms of direct carbon contribution to the liver, fructose can contribute carbons in two ways: 1) direct metabolism of fructose in a KHK-C-dependent manner 2) metabolism of microbiota-derived metabolites. KHK-C-dependent metabolism of fructose has been discussed elsewhere in this dissertation and is the

predominant mechanism by which fructose is metabolized by the body. However, compared with glucose, fructose is rather poorly absorbed from the gut. This is due in part to glucose being absorbed via active transport and fructose being absorbed by passive transport mechanisms⁴⁶. Therefore, while a glucose bolus is completely absorbed by the small intestine, a fructose bolus may not be fully absorbed. This is especially likely when larger quantities of fructose are consumed. Unabsorbed fructose can then enter the colon and be metabolized by the microbiota. These metabolites then go via the portal circulation directly to the liver. One of the primary metabolites that the microbiota can form from fructose carbons is acetate¹¹⁰. When this acetate reaches the liver, it can directly fuel *de novo* lipogenesis after forming acetyl coA via acetyl-coA synthetase (figure 6.3). This acetyl coA can then enter the first committed step of *de novo* lipogenesis by transformation to malonyl coA by acetyl-coA carboxylase (figure 6.3). Therefore, fructose can contribute carbons to *de novo* lipogenesis via both KHK-C-dependent metabolism and microbiota-derived acetate.

Many tumor cell types have been shown to use acetate as a fuel to help them produce lipids. Thus an intrahepatic tumor within the liver may benefit from an acetate bolus that comes from the microbiota after fructose ingestion. Furthermore, development of fatty liver has been shown to increase growth of intrahepatic tumors, via increased availability of exogenous fatty acids for tumor growth¹¹¹. Thus, intrahepatic tumors, based on their location, are uniquely poised for fructose-stimulated growth from KHK-C metabolite exchange, development of fatty liver, and large amounts of fructose-derived acetate from the microbiota.

Currently in clinical trials is a ketohexokinase inhibitor, PF-06835919, and acetyl coA carboxylase inhibitor, PF-05221304. Both drugs are being tested as therapeutics for the amelioration of fatty liver. Use of both PF-06835919 and PF-05221304 as a combination therapy

to patients with intrahepatic tumors would result in concurrent ketohexokinase and acetyl coA carboxylase inhibition. This combination of drugs could be used to 1) decrease fructose-dependent fatty liver and the 2) utilization of fructose carbons from KHK-C dependent metabolism and microbiota-derived acetate.

Figures

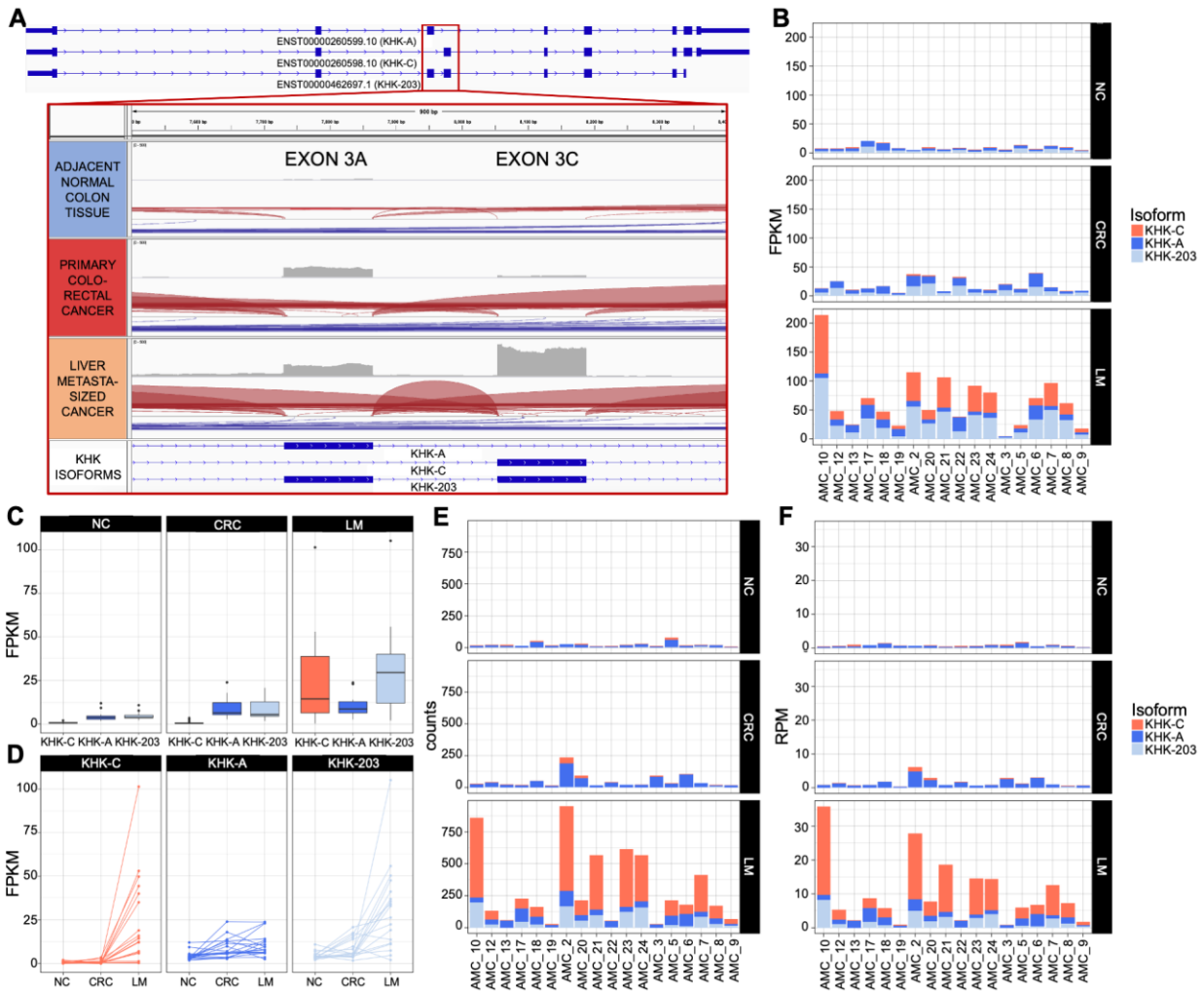


Figure 6.1. Human colon cancers that metastasize to the liver express KHK-C.

(A): IGV view of KHK expression for a matched set of tissues at Exons 3A and 3C. Exon 3 is upregulated in the metastatic sample. Reads spanning the specific junctions are also shown using red lines. (B): Stacked bar plot of KHK isoform expression calculated by Cufflinks. (C): Box plots showing the distribution of KHK isoforms in normal colon tissue (NC), primary colorectal cancer (CRC) and liver-metastasized cancer (LM). (D): Line plots showing the expression of KHK isoforms in normal colon tissue (NC), primary colorectal cancer (CRC) and liver-metastasized cancer (LM). (E): Stacked bar plot of KHK isoform expression as measured by unique junction counts (raw read count). (F): Stacked bar plot of KHK isoform expression as measured by unique junction counts (RPM)

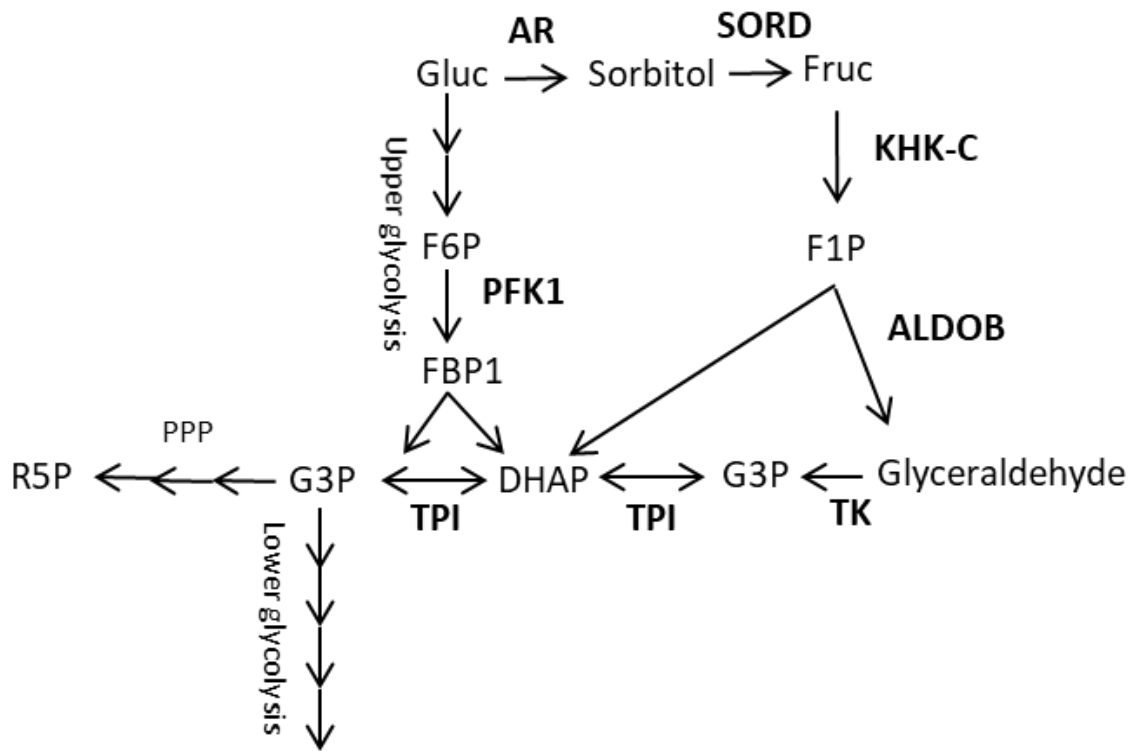


Figure 6.2. KHK-C rewires glucose metabolism via endogenous fructose.

(A) Schematic showing how presence of KHK-C and aldolase B allow for metabolism of endogenous fructose. gluc, glucose; F6P, fructose 6-phosphate; PFK1, phosphofruktokinase-1; FBP1, fructose 1,6-bisphosphate; AR, aldose reductase ; Fruc, fructose; KHK-C, ketohexokinase-C; F1P, fructose 1-phosphate; ALDOB, aldolase B; G3P, glyceraldehyde 3-phosphate; DHAP, dihydroxyacetone phosphate; TK, triokinase; TPI, triose phosphate isomerase; ppp, pentose phosphate pathway; R5P, ribose 5-phosphate

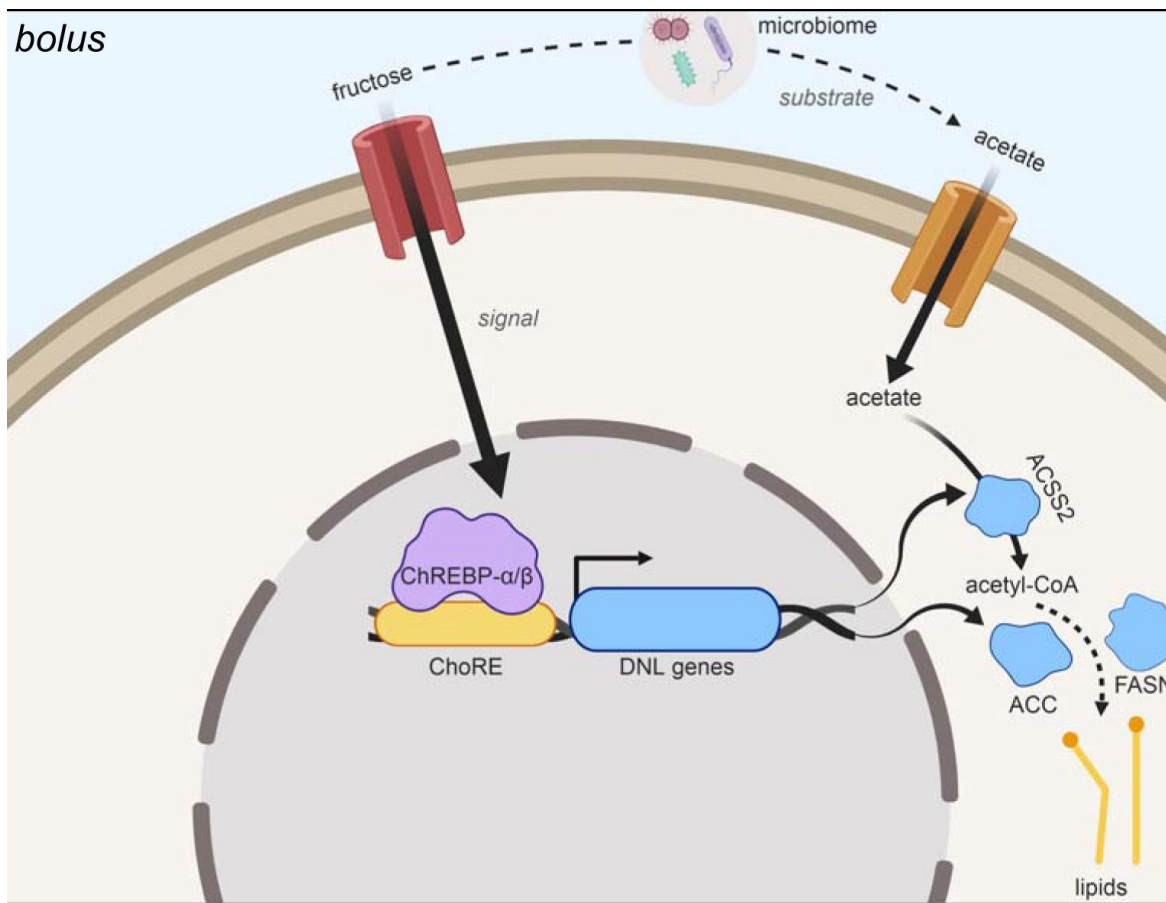


Figure 6.3. Schematic showing contribution of fructose and fructose-derived acetate to *de novo* lipogenesis in a hepatocyte. Shown cell is a hepatocyte. ACS2, acetyl coA synthetase. ACC, acetyl coA carboxylase. FASN, fatty acid synthase. DNL, de novo lipogenesis. choRE, carbohydrate response element. ChREBP carbohydrate-response element-binding protein .

Figure obtained from Zhao et al. *Nature* 2020¹¹⁰.

Chapter 7: Materials and Methods

Mouse xenograft model

All mouse procedures were approved by the Washington University Institutional Animal Care and Use Committee. The number of mice used in each experiment is reported in the associated figure legends. To form xenografts, 3 million cells in 1:1 DMEM: matrigel were injected into the left flank of female nude mice. A week post-injection, tumors were measured with calipers to assess initial tumor volume. Tumor size was then assessed once per week with calipers and volume was calculated by using the formula $V = (1/2) (L * W^2)$, where L and W are length and width respectively. Mice were fed a control diet (Envigo TD.05075), a high fructose diet (Envigo TD.89247), a high sucrose diet (Envigo TD.06685), or a high glucose diet (Envigo TD.05256) *ad lib*. Mice were fed a high fructose corn syrup (HFCS) diet by providing normal chow and *ad lib* access to 10% HFCS water. Average caloric consumption was assessed over a 24 hour period. For the four mice in each of the diet conditions, 65 grams of a given diet were provided. To determine the amount of diet consumed, the weight of diet remaining after 24 hours was recorded. The consumed weight was then converted to calories consumed on the basis of calories/gram of each diet. This value was divided by the number of mice in the cage to get the average caloric consumption per mouse. Each 24-hour measurement was repeated 5 times for each diet, and the average of each trial is reported. All isotopic labels were purchased from Cambridge Isotope Labs. Stock solutions of ^{13}C -labeled nutrients were made for injection into mouse tumors by suspending 200 mg ^{13}C -labeled nutrient per mL of normal saline. The amount of labeled stock solution injected into each mouse tumor was normalized by tumor volume ($40 \mu\text{L}$ of stock solution/ 200 mm^3 CaSki tumor volume). The same stock solution of 200 mg ^{13}C -

labeled nutrient per mL of normal saline was used for oral gavage. When introducing ^{13}C -labeled nutrients by gavage, a feeding needle was used to introduce 5 μL of labeled stock solution per g of mouse weight. PF-06835919 (Wuxi, for chemical structure see fig S15) was administered via intraperitoneal injection in 10% DMSO and 10% tween-80 in normal saline at the doses indicated in figure 5. In experiments where mice were given PF-06835919 via intraperitoneal injection and $[\text{U}-^{13}\text{C}]$ fructose via gavage, a feeding needle was used to introduce 1.5 g of $[\text{U}-^{13}\text{C}]$ fructose stock solution per kg of mouse weight. In all isotope-tracer experiments, mice were fasted for 4 hours prior to the administration of label. Mouse whole-blood samples (approximately 25 μL) were collected via tail snip. Mouse xenograft tumors were collected via rapid manual dissection with a scalpel and flash frozen in liquid nitrogen. Tissues were stored at $-80\text{ }^{\circ}\text{C}$ until extraction for liquid chromatography/mass spectrometry (LC/MS) analysis.

Zebrafish

All zebrafish procedures were approved by the Washington University Institutional Animal Care and Use Committee. The number of *Tg(mitfa:BRAF^{V600E}); p53^{-/-}* fish ¹¹² used in each experiment is reported in the associated figure legends. Fish used were reared according to standard laboratory procedures. Fish were kept in an indoor environment at a temperature of $28 \pm 1\text{ }^{\circ}\text{C}$ with a 14:10-hr light:dark circadian cycle. Fish were euthanized with an ice bath. Euthanization was deemed complete 1 minute after cessation of opercular movement in an ice water slurry.

To perform *in vivo* ^{13}C -labeling of *Tg(mitfa:BRAF^{V600E}); p53^{-/-}* zebrafish (referred to as *BRAF/p53* fish), 50 mM of either $[\text{U}-^{13}\text{C}]$ glucose or $[\text{U}-^{13}\text{C}]$ fructose was dissolved directly into zebrafish tank water containing 3% penicillin/streptomycin (Life Technologies), 5 $\mu\text{g}/\text{mL}$ kanamycin (MilliporeSigma), and 100 $\mu\text{g}/\text{mL}$ ampicillin (MilliporeSigma) to prevent bacterial

contamination. Fish were maintained at a density of 1 fish/100 mL ¹³C-labeled water. Fish were maintained in labeled water for 30 hours prior to euthanization. Melanomas were rapidly harvested from the surface of the body, snap frozen in liquid nitrogen, and stored at -80 °C until LC/MS analysis. Serum and tissues were harvested as described below.

To perform the tumor regrowth assay, *BRAF/p53* zebrafish were anesthetized in tricaine and a scalpel was used to amputate their tumors to be flush with the surface of the skin. Every fish had tumor tissue that extended beneath the surface of the skin, and this portion of the tumor remained after dissection. Fish were then randomized to the fructose-treated group or the control group. In the fructose-treated group, fish were placed in normal zebrafish water containing 100 mM fructose, 3% penicillin/streptomycin, 5 µg/mL kanamycin, and 100 µg/mL ampicillin. In the control group, fish were in the same water conditions without fructose. The water in both conditions was changed every other day to prevent bacterial contamination. Fish were maintained at a density of 1 fish / 333 mL of water in each condition. Fish were fed brine shrimp once a day in each condition. After two weeks in each condition, tumor regrowth was assessed with calipers. Tumor volume above the surface of the skin was calculated with the formula $V = (W * L * H) * 0.5236$, where W, L, and H are width, length, and height respectively.

To administer PF-06835919 or vehicle control (DMSO) to *BRAF/p53* zebrafish, a 10 µL nanofil syringe (WPI) was used to inject 50 mg / kg of PF-06835919. PF-06835919 was dissolved in DMSO and the injection volume was 2 µL drug solution / gram zebrafish weight. Fish were injected with PF-06835919. An hour later, fish were then placed in zebrafish water containing 25 mM [U-¹³C] fructose, 190 µM PF-06835919, 3% penicillin/streptomycin, 5 µg/mL kanamycin, and 100 µg/mL ampicillin. Fish that were injected with vehicle were placed in the same water

conditions, except without PF-06835919. After 12 hours, fish in both conditions were euthanized and serum was collected as described below.

To collect *BRAF/p53* zebrafish serum for LC/MS analysis, the following method was used. A simple blood collection device was constructed by forming a small hole in the bottom of a microcentrifuge tube (the holding tube) with a razor blade. The hole was approximately the diameter of the cross section created through distal amputation of a given fish. This holding tube was then fit into another microcentrifuge tube (the collection tube), and the connection was secured with tape. To begin the blood-collection process, fish were euthanized in ice water as described above. Fish were then removed from ice water and dried thoroughly with a kimwipe. A razor blade was used to amputate the caudal fin and some associated distal tissue by making a transverse cross section midway between the anal and caudal fin. The amputated fish were immediately placed into the holding tube (with the wound end nearest the hole). The holding tube was then placed into the collection tube, securing the connection with tape. We placed the entire collection device containing the amputated fish into a microcentrifuge and spun at 100 xg at 28 °C for 1 minute. Tissues were anatomically dissected, snap frozen in liquid nitrogen, and stored at -80 °C until extraction for LC/MS analysis.

Preparation of mouse and zebrafish serum

Mouse and zebrafish blood samples were placed on ice without anticoagulant for 20 minutes. The samples were subsequently centrifuged at 6000 rpm for 10 minutes. Serum was then collected and stored at -80 °C until extraction for LC/MS analysis.

Cell culture

Cell lines were maintained in high glucose DMEM (Life Technologies) containing 10% FBS (Life Technologies) and 1% penicillin/streptomycin (Life Technologies). For all monoculture growth studies, cells were maintained at the indicated conditions for 4 days. For the co-culture growth study, CaSki cells and hepatocytes were maintained at the indicated conditions for 48 hours. For evaluating cell number, all cells were trypsinized and stained with trypan blue. For isotope-tracer experiments with [U-¹³C] glucose or [U-¹³C] fructose, labels were administered in no glucose DMEM with 10% FBS and 1% penicillin/streptomycin in 100 mm cell culture plates. Except where indicated, 5 mM of each label was administered. Unless specified otherwise, cells were harvested after 4 hours of labeling. Harvesting was performed after washing cells once with PBS and then water. Cells were quenched with 1 mL of methanol per 100 mm plate (TPP), and cells were collected into a microcentrifuge tube via scraping. Methanol was removed from cells with a nitrogen evaporator. Samples were then lyophilized for 12 hours. Dried samples were weighed and extracted by using the metabolite extraction protocol below. PF-06835919 was administered to cells in DMSO for a final concentration of 30 μM or 250 μM in the culture media. These cell culture PF-06835919 experiments were done in DMEM containing 10 mM glucose and 10 mM fructose with 10% FBS and 1% penicillin/streptomycin. NBDG (Caymen) and NBDF (Caymen) uptake studies were performed based on previous work¹¹³. In summary, media was aspirated from cells plated in a 96-well plate at a uniform density. Cells were then incubated in PBS for 30 minutes and subsequently incubated in glucose-free DMEM and 10% dialyzed FBS with 100 μM NBDG or NBDF for 30 minutes. After media removal and PBS rinsing, fluorescence was read on a Cytation 5 microplate reader (Biotek) with an excitation of 475 nm and an emission of 550 nm while cells were in PBS.

Primary hepatocytes were isolated as described previously¹¹⁴. The hepatocytes were plated on a collagen-coated transwell (Corning). When co-cultured with CaSki cells, 1×10^5 CaSki cells were plated on the upper insert of the transwell containing hepatocytes. In the control conditions, 1×10^5 CaSki cells were plated on both the insert and the bottom well. CaSki cells were harvested from the upper inserts of both conditions for LC/MS analysis or determination of relative cell number via trypan blue staining.

Ex vivo culture of *BRAF/p53* zebrafish melanoma was performed via amputation of a melanoma from a euthanized fish, based on a previously applied protocol¹¹⁵. A single-cell suspension of the isolated tumor was formed via incubation of the tumor at room temperature in a 0.075 mg/mL solution of liberase (Sigma) for 30 minutes. Disintegration of the tumor was encouraged via periodic pipetting. The suspension was filtered through a 40 μ m filter (MidSci) to remove any aggregates of tumor and then centrifuged at 1000 rpm for 5 minutes. The pellet was resuspended in DMEM containing 10% FBS, 1% penicillin/streptomycin, 1% glutamax, and no pyruvate prior to being plated on fibronectin-coated plates (Corning) and cultured at 28.5 °C and 5% CO₂.

Metabolite extraction

For mouse serum and cell culture media extractions, 90 μ L of 2:2:1 methanol:acetonitrile:water (M:A:W) was added to 10 μ L of sample. For zebrafish serum extraction, 36 μ L of M:A:W was added to 4 μ L of sample. The samples were vortexed and placed at -20 °C for an hour. The samples then were centrifuged at 4 °C for 10 minutes. The supernatant was removed and analyzed by LC/MS. For tissue, frozen samples were first ground into a fine powder with a mortar and pestle in the presence of liquid nitrogen. The powder was weighed and 1 mL M:A:W

was added per 5 mg of tissue weight. For tumors, the entire sample was extracted. For cell-culture samples, 1 mL of M:A:W was added per 1 mg of lyophilized cell pellet. Tissue and cell-culture samples were then vortexed for 30 seconds, placed in liquid nitrogen for 1 minute, and sonicated for 10 minutes. This cycle was repeated 3 times. The samples were subsequently maintained at -20 °C for an hour, centrifuged at 14,000 rpm for 10 minutes, and then the supernatants were transferred to new microcentrifuge tubes. The M:A:W solvent was evaporated under nitrogen, and samples were resuspended in 60:40 acetonitrile:water with a normalization of 40 µL per milligram of initial lyophilized cell pellet or tissue weight.

Western blots

Cells or tissues were harvested in RIPA buffer (Thermo Fisher Scientific) with a protease inhibitor cocktail (Thermo Fisher Scientific). Each sample was sonicated for 30 seconds, and the resulting lysates were separated on SDS-PAGE under reducing conditions. Protein bands were transferred to a PVDF membrane. Immunoblotting was performed with anti-ketohexokinase (Santa Cruz), anti-ketohexokinase-C (Signalway), anti-ketohexokinase-A (Signalway), anti-sorbitol dehydrogenase (Santa Cruz), or anti-aldolase B (Santa Cruz). Anti-beta tubulin (Cell Signaling) or anti-succinate dehydrogenase (Cell Signaling) was used as a loading control. Anti-rabbit and anti-mouse secondary antibodies were from Cell Signaling. Blots were imaged on a LI-COR C Digit blot scanner (LICOR).

Silencing of sorbitol dehydrogenase

Sorbitol dehydrogenase was silenced in various cell lines by using a collection of siRNA duplexes targeting human *SORD* (TriFECTa, IDT; Design ID hs.Ri.SORD.13). Lipofectamine

RNAiMAX Transfection Reagent (Invitrogen) was used for the transfection according to the manufacturer's instructions. Scrambled siRNA (TriFECTa, IDT) was used as a negative control. The knockdown efficiency was assessed via western blotting.

LC/MS

LC/MS was performed by using a SeQuant ZIC-PHILIC column (EMD Millipore) interfaced with an Agilent 6540 Q-TOF. Unless otherwise indicated, a 150 × 2.1 mm, 5 μm SeQuant ZIC-PHILIC column was used with an Agilent 1290 Infinity II LC system, applying methods established previously¹¹⁶. Mobile-phase solvents had the following composition: A = 20 mM ammonium acetate in water:acetonitrile (95:5) and B = 100% acetonitrile. The following linear gradient was used: 0–0.5 min, 90% B; 0.5–30 min, 90–30% B; 30–31 min, 30% B. Injection volumes were 2 μL for all experiments. The column compartment was maintained at 45 °C. Mass range was set to 50 to 1500 m/z. MS parameters were as follows: gas, 200 °C at 4 L/min; nebulizer, 44 psi at 2000 V; sheath gas, 300 °C at 12 L/min, capillary, 3000 V; fragmentor, 100 V; skimmer, 65 V; and scan rate, 3 scans/second. The MS was operated in negative ionization mode for all samples analyzed. Isotopologues were generated from analysis of the raw data. Isotopologues are not natural-abundance corrected.

To separate fructose 1-phosphate from other hexose phosphates, a 2 mm x 150 mm HILICpak VD 50-2D column (Shodex) was used with an isocratic flow of 80% acetonitrile, 20% water with 25 mM formic acid. The flow rate was 0.150 mL/min. All other experimental conditions were kept as above.

Analysis of human cervical cancer patient data

Cervical cancer patients included in this study ($N=99$) were enrolled in a prospective tumor banking study with written informed consent (201105374), and data were analyzed with institutional review board (IRB) approval with waiver of consent. All patients in this cohort were uniformly treated with curative-intent chemoradiation and clinical data were prospectively collected, including outcome data and FIGO stage. Primary cervical cancer samples with sufficient high-quality RNA, as defined by the criteria utilized for TCGA ¹¹⁷, were included in this study for whole transcriptome sequencing (RNA-seq). PolyA-selection and multiplexed sequencing (Illumina HiSeq 2500, 1×50 nt, ~40 million reads per sample) were performed at the Genome Technology Access Center (GTAC) at Washington University School of Medicine. RNA-seq reads were aligned to the Genome Reference Consortium Human Build 38 (GRCh38) using STAR2 with Ensembl genes for homo sapiens version 90. Isoform expression levels for KHK-A and KHK-C were calculated and normalized as Fragments Per Kilobase per Million reads (FPKM) using Cufflinks with default parameters ^{118,119}. Integrative genomics viewer (IGV) was used to visualize and manually inspect sequencing reads from isoform specific exons ¹²⁰. The Kaplan–Meier estimator is used to estimate recurrent-free survival and overall survival based on KHK-A expression levels, and significance levels from log rank test were reported.

Statistics

Data are reported as means \pm SD. Comparisons of the means of different experimental conditions were performed with a Student's unpaired, two-tailed t test. Statistical significance is designated according to the following convention: * $P < 0.05$, ** $P < 0.01$, *** $P < 0.001$, **** $P < 0.0001$.

Except where indicated, all data represent means \pm standard deviation.

References:

1. Draper, C. F. *et al.* Menstrual cycle rhythmicity: metabolic patterns in healthy women. *Sci. Rep.* **8**, 1–15 (2018).
2. Bisdee, J. T., Garlick, P. J. & James, W. P. T. Metabolic changes during the menstrual cycle. *Br. J. Nutr.* **61**, 641–650 (1989).
3. Dupont, J. & Scaramuzzi, R. J. Insulin signalling and glucose transport in the ovary and ovarian function during the ovarian cycle. *Biochemical Journal* vol. 473 1483–1501 (2016).
4. Shortt, J. & Johnstone, R. W. Oncogenes in cell survival and cell death. *Cold Spring Harb. Perspect. Biol.* **4**, (2012).
5. Hanahan, D. & Weinberg, R. A. Hallmarks of cancer: The next generation. *Cell* vol. 144 646–674 (2011).
6. Bardelli, A. & Velculescu, V. E. Mutational analysis of gene families in human cancer. *Current Opinion in Genetics and Development* vol. 15 5–12 (2005).
7. Mardis, E. R. & Wilson, R. K. Cancer genome sequencing: A review. *Hum. Mol. Genet.* **18**, R163 (2009).
8. Commisso, C. *et al.* Macropinocytosis of protein is an amino acid supply route in Ras-transformed cells. *Nature* **497**, 633–637 (2013).
9. Kimmelman, A. C. Metabolic dependencies in RAS-driven cancers. *Clin. Cancer Res.* **21**, 1828–1834 (2015).
10. Xia, S. *et al.* Prevention of Dietary-Fat-Fueled Ketogenesis Attenuates BRAF V600E Tumor Growth. *Cell Metab.* **25**, 358–373 (2017).
11. Dong, Y., Tu, R., Liu, H. & Qing, G. Regulation of cancer cell metabolism: oncogenic MYC in the driver’s seat. *Signal Transduction and Targeted Therapy* vol. 5 1–11 (2020).
12. Yao, C. H. *et al.* Exogenous Fatty Acids Are the Preferred Source of Membrane Lipids in Proliferating Fibroblasts. *Cell Chem. Biol.* **23**, 483–493 (2016).
13. Lin, X., Xiao, Z., Chen, T., Liang, S. H. & Guo, H. Glucose Metabolism on Tumor Plasticity, Diagnosis, and Treatment. *Frontiers in Oncology* vol. 10 317 (2020).
14. Adekola, K., Rosen, S. T. & Shanmugam, M. Glucose transporters in cancer metabolism. *Current Opinion in Oncology* vol. 24 650–654 (2012).
15. Witney, T. H. & Lewis, D. Y. Imaging cancer metabolism with positron emission tomography (PET). in *Methods in Molecular Biology* vol. 1928 29–44 (Humana Press Inc., 2019).

16. Zhu, A., Lee, D. & Shim, H. Metabolic positron emission tomography imaging in cancer detection and therapy response. *Semin. Oncol.* **38**, 55–69 (2011).
17. Ancey, P., Contat, C. & Meylan, E. Glucose transporters in cancer – from tumor cells to the tumor microenvironment. *FEBS J.* **285**, 2926–2943 (2018).
18. Liberti, M. V. & Locasale, J. W. The Warburg Effect: How Does it Benefit Cancer Cells? *Trends in Biochemical Sciences* vol. 41 211–218 (2016).
19. Jiang, B. Aerobic glycolysis and high level of lactate in cancer metabolism and microenvironment. *Genes and Diseases* vol. 4 25–27 (2017).
20. Yu, L., Chen, X., Sun, X., Wang, L. & Chen, S. The glycolytic switch in tumors: How many players are involved? *Journal of Cancer* vol. 8 3430–3440 (2017).
21. Törnroth-Horsefield, S. & Neutze, R. Opening and closing the metabolite gate. *Proceedings of the National Academy of Sciences of the United States of America* vol. 105 19565–19566 (2008).
22. Heiden, M. G. V., Cantley, L. C. & Thompson, C. B. Understanding the warburg effect: The metabolic requirements of cell proliferation. *Science* vol. 324 1029–1033 (2009).
23. Moreno-Sánchez, R. *et al.* Who controls the ATP supply in cancer cells? Biochemistry lessons to understand cancer energy metabolism. *Int. J. Biochem. Cell Biol.* **50**, 10–23 (2014).
24. Yao, C. H. *et al.* Mitochondrial fusion supports increased oxidative phosphorylation during cell proliferation. *Elife* **8**, (2019).
25. Wallace, D. C. Mitochondria and cancer. *Nature Reviews Cancer* vol. 12 685–698 (2012).
26. Luengo, A. *et al.* Increased demand for NAD⁺ relative to ATP drives aerobic glycolysis. *Mol. Cell* **81**, 691-707.e6 (2021).
27. Akella, N. M., Ciraku, L. & Reginato, M. J. Fueling the fire: Emerging role of the hexosamine biosynthetic pathway in cancer. *BMC Biology* vol. 17 1–14 (2019).
28. Leithner, K. *et al.* The glycerol backbone of phospholipids derives from noncarbohydrate precursors in starved lung cancer cells. *Proc. Natl. Acad. Sci. U. S. A.* **115**, 6225–6230 (2018).
29. Geeraerts, S. L., Heylen, E., De Keersmaecker, K. & Kampen, K. R. The ins and outs of serine and glycine metabolism in cancer. *Nature Metabolism* vol. 3 131–141 (2021).
30. Chen, L. *et al.* NADPH production by the oxidative pentose-phosphate pathway supports folate metabolism. *Nat. Metab.* **1**, 404–415 (2019).
31. Laughlin, M. R. Normal roles for dietary fructose in carbohydrate metabolism. *Nutrients* **6**, 3117–29 (2014).
32. Vos, M. B., Kimmons, J. E., Gillespie, C., Welsh, J. & Blank, H. M. Dietary fructose

- consumption among US children and adults: The Third National Health and Nutrition Examination Survey CME. *MedGenMed Medscape Gen. Med.* **10**, 160 (2008).
33. Rendeiro, C. *et al.* Fructose decreases physical activity and increases body fat without affecting hippocampal neurogenesis and learning relative to an isocaloric glucose diet. *Sci. Rep.* **5**, (2015).
 34. Sun, S. Z., Anderson, G. H., Flickinger, B. D., Williamson-Hughes, P. S. & Empie, M. W. Fructose and non-fructose sugar intakes in the US population and their associations with indicators of metabolic syndrome. *Food Chem. Toxicol.* **49**, 2875–2882 (2011).
 35. Vos, M. B., Kimmons, J. E., Gillespie, C., Welsh, J. & Blank, H. M. Dietary fructose consumption among US children and adults: The Third National Health and Nutrition Examination Survey CME. *MedGenMed Medscape Gen. Med.* **10**, 160 (2008).
 36. Lustig, R. H. *et al.* Isocaloric fructose restriction and metabolic improvement in children with obesity and metabolic syndrome. *Obesity* **24**, 453–460 (2016).
 37. Abdelmalek, M. F. *et al.* Increased fructose consumption is associated with fibrosis severity in patients with nonalcoholic fatty liver disease. *Hepatology* **51**, 1961–1971 (2010).
 38. Lim, J. S., Mietus-Snyder, M., Valente, A., Schwarz, J. M. & Lustig, R. H. The role of fructose in the pathogenesis of NAFLD and the metabolic syndrome. *Nature Reviews Gastroenterology and Hepatology* vol. 7 251–264 (2010).
 39. Stanhope, K. L. *et al.* Consuming fructose-sweetened, not glucose-sweetened, beverages increases visceral adiposity and lipids and decreases insulin sensitivity in overweight/obese humans. *J. Clin. Invest.* **119**, 1322–1334 (2009).
 40. Khitan, Z. & Kim, D. H. Fructose: A key factor in the development of metabolic syndrome and hypertension. *Journal of Nutrition and Metabolism* vol. 2013 (2013).
 41. Liu, L. *et al.* Triose Kinase Controls the Lipogenic Potential of Fructose and Dietary Tolerance. *Cell Metab.* **32**, 605-618.e7 (2020).
 42. Xu, D. *et al.* The protein kinase activity of fructokinase A specifies the antioxidant responses of tumor cells by phosphorylating p62. *Sci. Adv.* **5**, 4570–4594 (2019).
 43. Kim, J. *et al.* Ketohexokinase-A acts as a nuclear protein kinase that mediates fructose-induced metastasis in breast cancer. *Nat. Commun.* **11**, 1–20 (2020).
 44. Li, X. *et al.* A splicing switch from ketohexokinase-C to ketohexokinase-A drives hepatocellular carcinoma formation. *Nat. Cell Biol.* **18**, 561–571 (2016).
 45. Goncalves, M. D. *et al.* High-fructose corn syrup enhances intestinal tumor growth in mice. <http://science.sciencemag.org/>.
 46. Goncalves, M. D. *et al.* High-fructose corn syrup enhances intestinal tumor growth in mice. *Science (80-.)*. **363**, 1345–1349 (2019).

47. Bu, P. *et al.* Aldolase B-Mediated Fructose Metabolism Drives Metabolic Reprogramming of Colon Cancer Liver Metastasis. *Cell Metab.* **27**, 1249-1262.e4 (2018).
48. Liu, H. *et al.* Fructose Induces Transketolase Flux to Promote Pancreatic Cancer Growth. *Cancer Res.* **70**, 6368–6376 (2010).
49. Jeong, S. *et al.* High Fructose Drives the Serine Synthesis Pathway in Acute Myeloid Leukemic Cells. *Cell Metab.* **33**, 145-159.e6 (2021).
50. Chen, W. L. *et al.* GLUT5-mediated fructose utilization drives lung cancer growth by stimulating fatty acid synthesis and AMPK/mTORC1 signaling. *JCI Insight* **5**, (2020).
51. You, L., Zhang, B. & Tang, Y. Application of Stable Isotope-Assisted Metabolomics for Cell Metabolism Studies. *Metabolites* **4**, 142–165 (2014).
52. Van der Linden, P. J. Q., Kets, M., Gimpel, J. A. & Wiegerinck, M. A. H. M. Cyclic changes in the concentration of glucose and fructose in human cervical mucus. *Fertil. Steril.* **57**, 573–577 (1992).
53. Zaviačič, M. *et al.* Concentrations of Fructose in Female Ejaculate and Urine: A Comparative Biochemical Study. *J. Sex Res.* **24**, 319-325 CR-Copyright © 1988 Taylor & Franc (1988).
54. Berger, N. A. Obesity and cancer pathogenesis. *Ann. N. Y. Acad. Sci.* **1311**, 57–76 (2014).
55. De Pergola, G. & Silvestris, F. Obesity as a major risk factor for cancer. *Journal of Obesity* vol. 2013 (2013).
56. Hodge, A. M., Bassett, J. K., Milne, R. L., English, D. R. & Giles, G. G. Consumption of sugar-sweetened and artificially sweetened soft drinks and risk of obesity-related cancers. *Public Health Nutr.* **21**, 1618–1626 (2018).
57. Gallagher, E. J. & LeRoith, D. Obesity and diabetes: The increased risk of cancer and cancer-related mortality. *Physiol. Rev.* **95**, 727–748 (2015).
58. Softic, S. *et al.* Fructose and hepatic insulin resistance. *Critical Reviews in Clinical Laboratory Sciences* vol. 57 308–322 (2020).
59. Basciano, H., Federico, L. & Adeli, K. Fructose, insulin resistance, and metabolic dyslipidemia. *Nutrition and Metabolism* vol. 2 5 (2005).
60. Elliott, S. S., Keim, N. L., Stern, J. S., Teff, K. & Havel, P. J. Fructose, weight gain, and the insulin resistance syndrome. *Am. J. Clin. Nutr.* **76**, 911–922 (2002).
61. Liu, H. *et al.* Fructose induces transketolase flux to promote pancreatic cancer growth. *Cancer Res.* **70**, 6368–6376 (2010).
62. Vander Jagt, D. L. *et al.* Substrate specificity of human aldose reductase: identification of 4-hydroxynonenal as an endogenous substrate. *Biochim. Biophys. Acta* **1249**, 117–26 (1995).

63. Borhani, D. W., Harter, T. M. & Petrash, J. M. The crystal structure of the aldose reductase.NADPH binary complex. *J. Biol. Chem.* **267**, 24841–7 (1992).
64. Diggle, C. P. *et al.* Ketoheokinase: Expression and localization of the principal fructose-metabolizing enzyme. *J. Histochem. Cytochem.* **57**, 763–774 (2009).
65. Ishimoto, T. *et al.* Opposing effects of fructokinase C and A isoforms on fructose-induced metabolic syndrome in mice. *Proc. Natl. Acad. Sci. U. S. A.* **109**, 4320–4325 (2012).
66. Mirtschink, P. *et al.* HIF-driven SF3B1 induces KHK-C to enforce fructolysis and heart disease. *Nature* **522**, 444–449 (2015).
67. Park, T. J. *et al.* Fructose-driven glycolysis supports anoxia resistance in the naked mole-rat. *Science (80-.).* **356**, 307–311 (2017).
68. Daniels, L. B., Perkins, J. L., Krieder, D., Tugwell, D. & Carpenter, D. Blood Glucose and Fructose in the Newborn Ruminant. *J. Dairy Sci.* **57**, 1196–1200 (1974).
69. Kurz, M. M. & Willett, L. B. Carbohydrate, Enzyme, and Hematology Dynamics in Newborn Calves. *J. Dairy Sci.* **74**, 2109–2118 (1991).
70. Calle, R., Bergman, A., Somayaji, V., Chidsey, K. & Kazierad, D. PS-110-Ketoheokinase inhibitor PF-06835919 administered for 6 weeks reduces whole liver fat as measured by magnetic resonance imaging-proton density fat fraction in subjects with non-alcoholic fatty liver disease. *J. Hepatol.* **70**, e69–e70 (2019).
71. US20170183328A1 - Substituted 3-azabicyclo[3.1.0]hexanes as ketoheokinase inhibitors - Google Patents. <https://patents.google.com/patent/US20170183328A1/en>.
72. Rikmenspoel, R. & Caputo, R. The Michaelis-Menten constant for fructose and for glucose of hexokinase in bull spermatozoa. *J. Reprod. Fertil.* **12**, 437–444 (1966).
73. SOLS, A. & CRANE, R. K. Substrate specificity of brain hexokinase. *J. Biol. Chem.* **210**, 581–595 (1954).
74. Jang, C. *et al.* The Small Intestine Converts Dietary Fructose into Glucose and Organic Acids. *Cell Metab.* **27**, 351-361.e3 (2018).
75. Levi, J. *et al.* Fluorescent fructose derivatives for imaging breast cancer cells. *Bioconjug. Chem.* **18**, 628–634 (2007).
76. Chen, W.-L. *et al.* Enhanced Fructose Utilization Mediated by SLC2A5 Is a Unique Metabolic Feature of Acute Myeloid Leukemia with Therapeutic Potential. *Cancer Cell* **30**, 779–791 (2016).
77. Zamora-León, S. P. *et al.* Expression of the fructose transporter GLUT5 in human breast cancer. *Proc. Natl. Acad. Sci. U. S. A.* **93**, 1847–52 (1996).
78. Scholarlycommons, S. & Zhao, S. *From Sugar To Acetate-The Origins Of Acetyl-Coa Dictate Its Use From Sugar To Acetate-The Origins Of Acetyl-Coa Dictate Its Use In Cells And In Mice In Cells And In Mice*. <https://repository.upenn.edu/edissertations>.

79. Jang, C. *et al.* The small intestine shields the liver from fructose-induced steatosis. *Nat. Metab.* **2**, 586–593 (2020).
80. Schwarz, J. M. *et al.* Effects of Dietary Fructose Restriction on Liver Fat, De Novo Lipogenesis, and Insulin Kinetics in Children With Obesity. *Gastroenterology* **153**, 743–752 (2017).
81. Jensen, T. *et al.* Fructose and sugar: A major mediator of non-alcoholic fatty liver disease. *Journal of Hepatology* vol. 68 1063–1075 (2018).
82. Park, J. H. Insulin resistance in non-alcoholic fatty liver disease. *The Korean journal of hepatology* vol. 12 16–30 (2006).
83. Kitade, H., Chen, G., Ni, Y. & Ota, T. Nonalcoholic fatty liver disease and insulin resistance: New insights and potential new treatments. *Nutrients* vol. 9 (2017).
84. Kim, M. S. *et al.* ChREBP regulates fructose-induced glucose production independently of insulin signaling. *J. Clin. Invest.* **126**, 4372–4386 (2016).
85. Zhang, Y. M. *et al.* Distant Insulin Signaling Regulates Vertebrate Pigmentation through the Sheddase Bace2. *Dev. Cell* **45**, 580-594.e7 (2018).
86. Zhang, M. *et al.* Adipocyte-derived lipids mediate melanoma progression via FATP proteins. *Cancer Discov.* **8**, 1006–1025 (2018).
87. Grigura, V., Barbier, M., Zarov, A. P. & Kaufman, C. K. Feeding amount significantly alters overt tumor onset rate in a zebrafish melanoma model. *Biol. Open* **7**, (2018).
88. Yadav, D., Kim, S.-J., Bae, M. A., Kim, J.-R. & Cho, K.-H. The Ability of Different Ketoheptoses to Alter Apo-A-I Structure and Function In Vitro and to Induce Hepatosteatosis, Oxidative Stress, and Impaired Plasma Lipid Profile in Hyperlipidemic Zebrafish. (2018) doi:10.1155/2018/3124364.
89. Sapp, V., Gaffney, L., EauClaire, S. F. & Matthews, R. P. Fructose leads to hepatic steatosis in zebrafish that is reversed by mechanistic target of rapamycin (mTOR) inhibition. *Hepatology* **60**, 1581–1592 (2014).
90. Chen, B., Zheng, Y.-M. & Zhang, J.-P. Comparative Study of Different Diets-Induced NAFLD Models of Zebrafish. *Front. Endocrinol. (Lausanne)*. **9**, 366 (2018).
91. Sun, S. Z. & Empie, M. W. Fructose metabolism in humans - what isotopic tracer studies tell us. *Nutr. Metab. (Lond)*. **9**, 89 (2012).
92. Jandrain, B. J. *et al.* Fructose utilization during exercise in men: Rapid conversion of ingested fructose to circulating glucose. *J. Appl. Physiol.* **74**, 2146–2154 (1993).
93. Tran, C. *et al.* Sex differences in lipid and glucose kinetics after ingestion of an acute oral fructose load. *Br. J. Nutr.* **104**, 1139–1147 (2010).
94. Delarue, J. *et al.* The contribution of naturally labelled ¹³C fructose to glucose appearance in humans. *Diabetologia* vol. 36 (1993).

95. *Incomplete absorption of pure fructose in healthy subjects.*
<https://academic.oup.com/ajcn/article/48/6/1424/4716115> (1988).
96. Zhao, S. *et al.* Dietary fructose feeds hepatic lipogenesis via microbiota-derived acetate. *Nature* **579**, 586–591 (2020).
97. Fujisawa, T. *et al.* The effect of exercise on fructose absorption. *Am. J. Clin. Nutr.* **58**, 75–79 (1993).
98. Lebherz, H. G. & Rutter, W. J. Distribution of Fructose Diphosphate Aldolase Variants in Biological Systems. *Biochemistry* **8**, 109–121 (1969).
99. Li, X. *et al.* A splicing switch from ketohexokinase-C to ketohexokinase-A drives hepatocellular carcinoma formation. *Nat. Cell Biol.* **18**, 561–571 (2016).
100. Hwa, J. S. *et al.* The expression of ketohexokinase is diminished in human clear cell type of renal cell carcinoma. *Proteomics* **6**, 1077–1084 (2006).
101. Luengo, A., Gui, D. Y. & Vander Heiden, M. G. Targeting Metabolism for Cancer Therapy. *Cell Chemical Biology* vol. 24 1161–1180 (2017).
102. Diggle, C. P. *et al.* Both isoforms of ketohexokinase are dispensable for normal growth and development. *Physiol Genomics* **42**, 235–243 (2010).
103. Miller, C. O. *et al.* Ketohexokinase knockout mice, a model for essential fructosuria, exhibit altered fructose metabolism and are protected from diet-induced metabolic defects. *Am. J. Physiol. - Endocrinol. Metab.* **315**, E386–E393 (2018).
104. Kalaany, N. Y. & Sabatini, D. M. Tumours with PI3K activation are resistant to dietary restriction. *Nature* **458**, 725–731 (2009).
105. Ruggeri, B. A., Klurfeld, D. M., Kritchevsky, D. & Furlanetto, R. W. Caloric Restriction and 7,12-Dimethylbenz(a)anthracene-induced Mammary Tumor Growth in Rats: Alterations in Circulating Insulin, Insulin-like Growth Factors I and II, and Epidermal Growth Factor. *Cancer Res.* **49**, 4130–4134 (1989).
106. Lanaspá, M. A. *et al.* Endogenous Fructose Production and Metabolism in the Liver Contributes to the Development of Metabolic Syndrome. *Nat. Commun.* **4**, 1–8 (2013).
107. Sheth, K. R. & Clary, B. M. Management of hepatic metastases from colorectal cancer. *Clinics in Colon and Rectal Surgery* vol. 18 215–223 (2005).
108. Adloff, M., Arnaud, J. P., Thebault, Y., Ollier, J. C. & Schloegel, M. Hepatic metastases from colorectal cancers. *Chir. - Mem. l'Academie Chir.* **116**, 144–149 (1990).
109. Trapnell, C. *et al.* Differential gene and transcript expression analysis of RNA-seq experiments with TopHat and Cufflinks. *Nat. Protoc.* **7**, 562–578 (2012).
110. Zhao, S. *et al.* Dietary fructose feeds hepatic lipogenesis via microbiota-derived acetate. *Nature* **579**, 586–591 (2020).

111. Li, Y. *et al.* Hepatic lipids promote liver metastasis. *JCI Insight* **5**, (2020).
112. Kaufman, C. K. *et al.* A zebrafish melanoma model reveals emergence of neural crest identity during melanoma initiation. *Science (80-.)*. **351**, (2016).
113. Levi, J. *et al.* Fluorescent Fructose Derivatives for Imaging Breast Cancer Cells. *Bioconjug. Chem.* **18**, 628–634 (2007).
114. Mccommis, K. S. *et al.* Loss of Mitochondrial Pyruvate Carrier 2 in Liver Leads to Defects in Gluconeogenesis and Compensation via Pyruvate-Alanine Cycling HHS Public Access. *Cell Metab* **22**, 682–694 (2015).
115. Heilmann, S. *et al.* A quantitative system for studying metastasis using transparent zebrafish. *Cancer Res.* **75**, 4272–4282 (2015).
116. Spalding, J. L., Naser, F. J., Mahieu, N. G., Johnson, S. L. & Patti, G. J. Trace Phosphate Improves ZIC-pHILIC Peak Shape, Sensitivity, and Coverage for Untargeted Metabolomics. *J. Proteome Res.* **17**, 3537–3546 (2018).
117. Burk, R. D. *et al.* Integrated genomic and molecular characterization of cervical cancer. *Nature* **543**, 378–384 (2017).
118. Liao, Y., Smyth, G. K. & Shi, W. FeatureCounts: An efficient general purpose program for assigning sequence reads to genomic features. *Bioinformatics* **30**, 923–930 (2014).
119. Trapnell, C. *et al.* Transcript assembly and quantification by RNA-Seq reveals unannotated transcripts and isoform switching during cell differentiation. *Nat. Biotechnol.* **28**, 511–515 (2010).
120. Robinson, J. T. *et al.* Integrative genomics viewer. *Nature Biotechnology* vol. 29 24–26 (2011).

